UNIVERSITY OF OKLAHOMA

GRADUATE COLLEGE

QUANTIFICATION OF CHLOROPHYLL IN SMALL RESERVOIRS USING AIRBORNE VIDEO IMAGERY

A Dissertation

SUBMITTED TO THE GRADUATE FACULTY

in partial fulfillment of the requirements for the

degree of

Doctor of Philosophy

By

MARGARET AVARD
Norman, Oklahoma
1998

UMI Number: 9839788

UMI
300 North Zeeb Road
Ann Arbor, MI 48103

QUANTIFICATION OF CHLOROPHYLL IN SMALL RESERVOIRS USING AIRBORNE VIDEO IMAGERY

A Dissertation APPROVED FOR THE
SCHOOL OF CIVIL ENGINEERING AND ENVIRONMENTAL SCIENCE

BY

ACKNOWLEDGEMENTS

This research has been funded by the Oklahoma EPSCoR grant as part of a National Science Foundation Cooperative Agreement with the State of Oklahoma. Sincere thanks go to the U. S. Department of Agriculture Agricultural Research Service for the use of data collected in the Little Washita River Watershed.

My experience at the University of Oklahoma has been a wonderful one, and there are many people I would like to thank. Since I was somewhat of a non-traditional student, "the system" was gratefully adapted to my circumstances. Thanks go to Dr. Canter for agreeing to be my advisor, Dr. Schiebe for directing my research, and Dr. Kolar for all his editorial advice and grant administration. Also, thanks to Dr. Knox for finding a means of financial support and to Dr. Williams for grant advice. I was very fortunate in that I am now able to call several of my mentors friends. Also, on a personal note, thanks to Eric for supporting my endeavor, my friends at Southeastern for providing motivation, to Mamie and Papa for tolerating my strange hours, and to Steve and Jeannie for giving me that swift kick whenever I needed it (even when I didn't know it). Most of all, thanks to Mom and Dad for teaching me that learning is a never-ending process and always a joy - I am what I am today because of you!

Table of Contents

List of Tables

List of Figures

ABSTRACT

The primary objective of this study was to develop a rapid, economic method of assessing water quality and productivity in surface impoundments. Airborne video cameras equipped with narrow band filters were used to assess chlorophyll-a concentration in flood retention reservoirs of the Little Washita River Watershed in central Oklahoma. The video data was calibrated by converting raw data (digital numbers) into radiance values ($uW/cm^2/sr$) and further processed into reflectance values by the incorporation of solar irradiance data. Results indicate that chlorophyll-a concentration in reservoirs may be approximated using airborne video imagery and that this relationship is best described by the model $y = a_0(1-e^{-x/40})$. Studies utilizing aerial videography may be performed more quickly and are less expensive than traditional field-based studies.

CHAPTER 1. INTRODUCTION

In order to effectively utilize surface water resources, methods to assess the quality of water in impoundments in relation to their intended use need to become more rapid and economical. Traditionally, surface water quality has been assessed using various limnological methods and laboratory analyses. This is time consuming, requires field sampling by trained personnel, and is expensive. The purpose of this project was to develop a rapid, economic method of determining surface water quality using advanced technology and limited resources.

The main objective of this research was to develop a convenient mathematical method based on aerial remote sensing to assess water quality and productivity in surface impoundments. Useful indicators include any constituents visible to the human eye or to optical instruments sensitive to electromagnetic regions outside the human visible range. The most likely candidates include suspended inorganic particles, phytoplankton, organic detritus, dyes, and animal life. This study includes a discussion of suspended sediments but will concentrate on remote sensing of phytoplankton.

Suspended solids can be detected using practical satellite technology. Infrared wavelengths have been the most successful in tracking changes in suspended sediment levels within lakes and reservoirs. It is more difficult to assess the presence of phytoplankton because the available wavelength bands on satellites are too wide (100 nm). Recent research indicates that very narrow bands (10 nm) in the near-infrared portion of the spectrum, centered at 670 nm and 700 nm, can be used to quantify chlorophyll concentration, even in the presence of high concentrations of suspended solids. A band at 800 nm can also be used to quantify inorganic suspended solids. This study utilized airborne video cameras equipped with narrow band filters to assess chlorophyll-a concentration in flood control reservoirs of the Little Washita River Watershed in west central Oklahoma. The ultimate goal was to determine the relationship between narrow band absorption/reflectance and chlorophyll-a concentration for these reservoirs.

This dissertation is written in a traditional format with chapters describing work previously performed in relevant fields, methods used during research and analysis, results, applications of the technology, and summary and conclusions.

As a result of this research, four papers will be submitted to journals for publication. "Quantification of chlorophyll in small agricultural impoundments using airborne video" was presented in May, 1997, at a remote sensing conference and has been published in the "Proceedings of the 16th Biennial Workshop on Videography and Color Photography in Resource Assessment", Weslaco, TX, November 1997. It provides a detailed description of the methodology and reports preliminary results. A follow-up paper, "Quantification of chlorophyll in reservoirs of the Little Washita watershed using airborne video" will be submitted to the journal "Photogrammetric Engineering and Remote Sensing" for publication. It also describes the methodology in detail but includes the final results of the study. "Remote sensing of chlorophyll in water quality assessment" will be submitted to the journal "Lake and Reservoir Management"; this paper addresses possible uses of the technology with respect to lake management strategies. "Remote sensing of chlorophyll concentration in water impoundments - a tool for retrospective and prospective impact analysis" will focus on the numerous potential applications of the technology developed in this study and their use in environmental impact assessment. This paper will be submitted to the "International Journal of Environmental Studies".

CHAPTER 2. REMOTE SENSING FACTORS

INTRODUCTION

In order to fully understand this research project, it is important to have some background knowledge on the fundamentals of remote sensing. When processing and/or interpreting any remotely sensed data, all factors affecting that data must be considered. The type of remote sensing platform will govern which factors need to be addressed. Factors specifically affecting airborne video imaging are discussed here. Each section consists of a short description of each topic and its relevance to this study.

GAIN

Gain describes the relationship between radiation and the sensor output of the charged coupled detector (CCD) array sensor of the video camera. Ordinarily, video cameras have automatic gain controls (AGC) which continuously adjust the electronic gain. For this study, the AGC was turned off and the f-stop was used to limit the light on the sensors such that they were operating in their linear ranges (i.e., below the saturation values). This ensured that the cameras were responding linearly to the received light. The f-stop was set at 5.6 for both the 665-675 nm and 695-705 nm video cameras.

SUNGLINT

Sunglint is the bright reflection of the sun off of water resulting from specular reflection and causing sensor saturation. The result is unusable video data.

Sun angle/ Time of day

The angle that the sun forms with the horizon. which is directly related to the time of day and time of year. is an important aspect in airborne remote sensing. Reflections from target objects on the surface may vary. There are three types of reflections: specular. Lambertian. and a combination of the two.

A specular. or perfect. reflector will produce a "mirror image" of an object. Examples of specular reflectors include mirrors and calm waters. In physics. the law of reflection states that the angle of incidence is equal to the angle of reflection. When radiation from the sun strikes a smooth surface, the ray paths are parallel both when they strike the surface and when they are reflected from the surface producing a "mirror image" (Figure 2.1). It is this type of reflection that is the primary concern in remote sensing. If specular reflection is received by an airborne sensor. the result is sunglint.

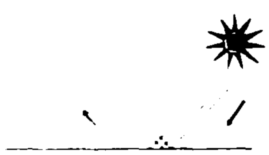

Figure 2.1. Specular reflectance.

Lambertian, or diffuse, reflectors have uneven surfaces and include almost all surfaces that are not specular reflectors. When radiation from the sun strikes an uneven surface, the incoming rays are parallel to each other but are reflected from the surface in every direction (Figure 2.2).

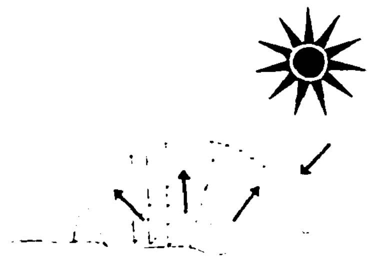

Figure 2.2. Diffuse reflectance.

A lake is a good example of a combination reflector. When radiation strikes the surface of a lake, a diffuse component scatters it in all directions and a specular component concentrates a large portion of the reflections in one direction (Figure 2.3).

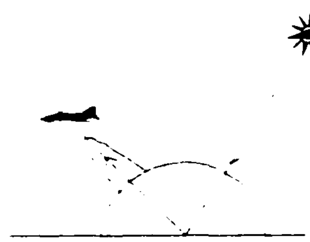

Figure 2.3. Combination reflectance.

If an airplane flies over a body of water during late morning or early afternoon, the chance of sunglint occurring is very high because the sun is at a high angle to the horizon and so is the airplane (Figure 2.3). Therefore, the best time to gather airborne video imagery is early in the morning when the sun is at a low angle.

In addition, wind speed is generally at a daily minimum and there is little dust in the atmosphere in the morning.

Wind speed

Sunglint may also be related to wind speed. As increased wind speed causes the surface of the water to ripple, the water begins to act more like a diffuse reflector and scatters light strongly in every direction. This may also cause sunglint and ineffectual data. In general, wind speeds increase in the afternoon, so airborne video imaging is most effective in the morning when wind speeds are slower. The study described herein was limited by airplane availability, thus ideal imaging times for each flight were not possible. Most of the data was collected mid-morning. Some of the afternoon data was discarded because of the presence of sunglint and was not part of the final 33 reservoirs analyzed.

DIRECT VS. DIFFUSE RADIATION

There are two types of radiation present in the atmosphere: direct and diffuse. The amount of total radiation present is the sum of direct and diffuse radiation. Direct radiation is representative of the beam of radiation coming directly from the sun, while diffuse radiation represents atmospheric scattering of radiation. The amount of diffuse radiation present is dependent on the amount of particulate matter in the atmosphere, primarily water and dust. As the number of particles in the atmosphere increases, scattering is also increased, resulting in higher diffuse radiation.

Path transmittance/Path radiance

The amount of radiation reaching an airborne sensor (L_R) is the sum of the diffuse radiation reaching the sensor as a result of atmospheric scattering (L_p) and the radiance being radiated from the target (l) modulated by attenuation (τ_p):

$$L_R = L_p + I\tau_p \qquad (1)$$

Both signals are received by the sensors and are not distinguishable from one another. τ_p varies between 0-1 and is indicative of the ability of radiance from the target to penetrate the atmosphere.

Path transmittance, or atmospheric attenuation (τ_p), and path radiance (L_p) approximate an inversely proportional relationship. On clear days, τ_p is high while L_p is very low, and on hazy days, τ_p is very low while L_p is high. As τ_p approaches zero, conditions are hazy and little of a target's signal will reach an airborne sensor, therefore $L_R = L_p$, or the radiance received by the sensor is compiled entirely of atmospheric scattering. In this case, path radiance accounts for all of the radiance received by the sensor. If the atmosphere is clear (i.e., little dust or water), τ_p approaches 1 and L_p approaches 0, so the signal received by airborne sensors is mostly from the target. Conditions during flights of this study were hazy, so the amount of radiance received by the airborne sensors was most likely a combination of diffuse radiation and radiance from the target. Since path transmittance cannot be determined from existing data, images have not been corrected for τ_p. If a dark ground target had been available, path transmittance could have been estimated.

Atmospheric dust

Atmospheric dust may include dust, ash, smoke, pollen, or any other form of small particulate matter. Most atmospheric dust is located within one kilometer of the earth's surface and will contribute to diffuse radiation picked up by airborne sensors. Atmospheric scattering is wavelength dependent.

If the wavelength of radiation is greater than the particle size, Rayleigh scattering occurs. Rayleigh scattering tends to affect shorter wavelengths (i.e., blue). The scattering of radiation off of gas molecules in the atmosphere is the cause of "blue sky". Rayleigh scattering is the primary cause of haze in hazy images but can be corrected with the use of filters.

If the wavelength of radiation is approximately equal to the particle size, Mie scattering occurs. Mie scattering affects longer wavelengths than Rayleigh scattering and is particularly important in the red and near-infrared ranges of the spectrum. Water vapor and dust promote Mie scattering, so Mie scattering is particularly significant in overcast conditions.

If the wavelength of radiation is smaller than the particle size, non-selective scattering occurs. In this case, all wavelengths are scattered equally (non-selectively) so objects appear white. Water droplets scatter non-selectively which is why clouds and fog appear white. All of these types of scattering increase the overall amount of atmospheric scattering which contributes to diffuse radiation. In this study, since conditions were overcast on flight days, Mie and non-selective scattering were probably most prevalent.

Atmospheric water

Water droplets in the atmosphere are also a source of atmospheric scattering and their formation depends both on the amount of water vapor in the air (humidity) and the temperature. As the temperature increases, air is capable of holding more water. As a warm air mass near the earth's surface rises, it expands and cools. Since the air is cooler, it cannot hold as much moisture and the water vapor will condense to form water droplets (clouds). This occurs at the dew point temperature. The dew point at any given time or location will vary as a function of humidity and the rate of atmospheric cooling with altitude. Generally, the higher the humidity at the surface, the lower the altitude at which the dew point will be reached. Humid locations will often have low clouds or haze, while more arid regions tend to have clouds forming at much higher altitudes. Both atmospheric water and dust scatter radiation in the atmosphere creating "noise" in remotely sensed data. Conditions during the flights were hazy, so atmospheric water probably contributes significantly to atmospheric scattering.

RADIATION IN THE UNDERWATER LIGHT FIELD

The absorption of radiation in the water column varies with the wavelength of radiation and the turbidity of the water body. For pure water, absorption is least in the blue range of the spectrum (450 - 520 nm) and increases slightly for shorter and exponentially for longer wavelengths (Smith and Baker, 1981; Palmer and Williams, 1974). This is also true for clear ocean waters. For inland waters, however, blue wavelengths attenuate very rapidly, and the yellow/green wavelengths generally exhibit the least absorption (Kirk, 1983; Pickard and Emery, 1982). This is believed to be the result of the presence of higher concentrations of yellow substance in inland waters than in ocean waters (Kirk, 1983). This explains why, in clear ocean waters, most objects appear blue in color while in inland waters objects appear yellowish/green. In inland waters, blue wavelengths may only penetrate 0 - 5 m into the water column while green may penetrate 0.5 - 15 m. The longer wavelengths of red and near-infrared may penetrate 2 - 9 m and less than 3 m, respectively (Pickard and Emery, 1982). In summary, for inland waters, longer wavelengths of visible light generally attenuate less rapidly than the shorter wavelengths, but in the near-infrared portion of the spectrum, attenuation is very rapid. The relevant wavelengths of this research fall into the near-infrared portion of the spectrum so they attenuate rapidly with depth into the water column.

OFF-NADIR DIFFICULTIES

Nadir is a term meaning "straight down". It is desirable to perform imaging from the nadir position to minimize atmospheric corrections for sunglint and distance (the longer the ray path, the more atmospheric scattering). Only nadir images were used in this study.

CALIBRATION

Calibration of the video imaging system corrects for any influences the system itself may have on data collection. This includes the video cameras, magnetic video tapes, video cassette recorder, filter, and electrical system.

CHAPTER 3. LITERATURE REVIEW

INTRODUCTION

Fresh water resources are critical to the survival of many species, so it is imperative that they be protected. Water quality studies have been conducted for decades, but with the implementation of new technologies, field studies are giving way to more economical, less time-consuming, remote sensing techniques. These techniques are also potentially superior as they provide more complete spatial, temporal, and/or synoptic information.

A review of the literature reveals the long history of attempts made to determine water quality using remotely sensed data. Landsat images were compared to field data to determine whether or not any variations or changes in water quality could be detected from space. As space-borne instruments became better understood, interpretation of resulting data revealed better, more accurate information.

FIELD STUDIES

Standard water quality tests may include such parameters as turbidity, primary productivity (chlorophyll-a), dissolved oxygen, nutrients such as nitrogen and phosphorus, pH, temperature, salinity, dissolved and suspended solids. Traditionally, a sample of water is collected and taken to a laboratory for analysis. In-situ methods of data collection exist for temperature, pH, salinity, and dissolved oxygen so these parameters may be determined quickly with only minimal effort. These parameters may also be evaluated continuously with such instruments as hydrolabs and data loggers. The remaining parameters, however, must be determined in the laboratory often utilizing tedious and time-consuming methods. This is currently both the most accurate and the most time-consuming method for determination of water quality.

Use of computer models for scientific studies has become a popular means of simulating environmental conditions. DeCoursey and Snyder (1969) attempted some of the first computer modeling of hydrologic parameters. As computer modeling technology was in its infancy at this time, these models were only marginally successful. Since that time, technologies have greatly improved, and computer modeling using field-gathered information has become a solid method of data analysis. It can be difficult to analyze field data because of various physical restraints. Computer modeling enables the user to overcome physical restrictions and predict what may not be physically constructed. For example, a model of the earth's interior temperatures and pressures cannot be physically duplicated but, using computer models and available physical data, the interior's thermodynamic structure and motions may be envisioned.

LANDSAT APPLICATIONS

In 1967 a program called ERTS (Earth Resources Technology Satellites) was designed to study the earth from space. Six satellites were to eventually be launched into orbit around the earth primarily for geologic research. ERTS I was launched in 1972 and operated until 1978. In 1975, the program was renamed LANDSAT, so ERTS I was retroactively named LANDSAT I. Five LANDSAT satellites have been in use: I 1972 - 1978, II 1975 - 1982, III 1978 - 1983, IV 1982 - present, and V 1984 - present. LANDSAT I, II, and III were very similar as were LANDSAT IV and V.

LANDSAT I, II, and III were set into orbit at an altitude of 900 km above the earth's surface. They made one revolution around the earth every 103 min, or 14 times per day. The main sensors onboard were part of the multispectral scanner system (MSS) which collected data in a digital format usable for computer analysis. Each picture covers a 185 km swath with 56 m ground spacing between readings. The wavelengths in which data was gathered included

Band 4	500 - 600 nm
Band 5	600 - 700 nm
Band 6	700 - 800 nm
Band 7	800 - 1100 nm.

Bands 4 and 5 best identified cultural uses, bands 6 and 7 distinguished water bodies, and bands 6 and 7 were most useful for examining geological features (Lillesand and Kiefer, 1987). Information included on each LANDSAT image was comprehensive:

date
latitude/longitude for center of image and nadir
sensor and band
direct or recorded reception mode
sun elevation and azimuth
orbital and processing parameters
LANDSAT identification
scene identification number.

LANDSAT IV and V included several modifications. They were put into orbit at an altitude of 705 km so the space shuttle would potentially be able to reach them if necessary. Their orbital period is 98.9 minutes. For these satellites, MSS bands 4 - 7 were renamed 1 - 4 and, in addition to MSS, they also carry the thematic mapper (TM) system. This system consists of seven nominal bands:

Band	Wavelength	Spectrum Range	Uses
Band 1	450 - 520 nm	Blue	water
Band 2	520 - 600 nm	Green	vegetation
Band 3	630 - 690 nm	Red	chlorophyll absorption
Band 4	760 - 900 nm	Near-Infrared	vegetation, soil moisture
Band 5	1550 - 1750 nm	Mid-Infrared	soil moisture
Band 6	10400 - 12500 nm	Thermal-Infrared	vegetation stress, soil moisture
Band 7	2080 - 2350 nm	Mid-Infrared	rocks, vegetation, soil moisture

As a result of Landsat technology, many scientists realized that a basic water quality parameter, suspended sediment concentration, might be detected from satellite sensors (McHenry, et al., 1977; Ritchie, et al., 1976; Ritchie, et al., 1978; Scarpace, et al., 1979). Further, some believed that the trophic class of a water body could actually be determined from Landsat data (Meinert, et al., 1978).

As technology onboard Landsat satellites improved, many agreed that suspended sediment concentration could readily be examined from space, but the methodology for extracting this information from remotely sensed data was uncertain.

Analyzing Landsat data was new territory in the 1970s and research continues to improve data collection and interpretation primarily with regard to effects of the atmosphere on imaging and its correction.

Early successes of Landsat imaging included the ability to isolate and determine the size of water bodies, the ability to assess the moisture content of surface soils, and estimation of Secchi depth. Early analyses revealed that land reflected more light than water, so Landsat data was useful in determining where bodies of water were located and their surface areas (Boland, 1976). It was also determined that soils holding moisture appeared darker since water absorbs rather than reflects light (Wiesnet, 1976).

The simplest and most economic procedure used in the 1970s to examine Landsat MSS data made use of a microdensitometer. A negative transparency was obtained for the desired Landsat photograph. A light beam of known intensity was passed through the transparency and the change in intensity was measured with a microdensitometer. This was reported as percent transmission or optical density (Boland, 1976). Tonal characteristics were then evaluated to determine surface features. Known problems at the time included the inability to analyze a time-series of photographs, the rarity of microdensitometers, model correlation over time, and the presence of atmospheric interferences (clouds, haze, scattering). It soon became possible to determine land cover types (Robinove, 1982) and estimate suspended sediment loads (McHenry, et al., 1977; Ritchie, et al., 1976; Ritchie, et al., 1978; Scarpace, et al., 1979; Whitlock, et al., 1981). Later, land resource assessments would be conducted (Burrough, 1988) and algal reflectance examined (Lin, et al., 1984; Vos, et al., 1986) from Landsat data.

In the 1980s, the RIPS (Remote Image Processing System) computer software was used to obtain digital counts from MSS computer compatible tapes (CCTs). It provided an inexpensive method of obtaining numerical data without the necessity of using microdensitometer techniques. Linear regression was performed to determine the quality of densitometer measurements as estimates of digital counts (Schiebe et al., 1992). The results were good ($r^2 = 0.98$) (Figure 3.1), so many subsequent studies were based on RIPS data conversion. Digital counts were obtained using RIPS and then converted into radiance and reflectance values (Robinove, 1982; Markham and Barker, 1986).

An important part of analyzing satellite imagery is the correlation of results with field data. This procedure is known as ground truthing. Laboratory experiments also provide valuable supporting evidence for data accuracy. Relevant studies in the 1980s included the determination of underwater scattering using irradiance measurements (Kirk, 1981), solar radiance measurements (Iqbal, 1983), and radiance and irradiance values in the field (Duggin, 1980). Studies were also conducted concerning sensor accuracy and other questions that had arisen about Landsat data acquisition:

determination of physical values from Landsat data (Robinove, 1982)
satellite radiometer calibration (Price, 1987)
comparison of results after correcting data for atmospheric effects
(Verdin, 1983, 1985)
image interpretation (Lillesand and Kiefer, 1987)
noise removal (Crippen, 1989)
TM and MSS calibrations (Markham and Barker, 1986)

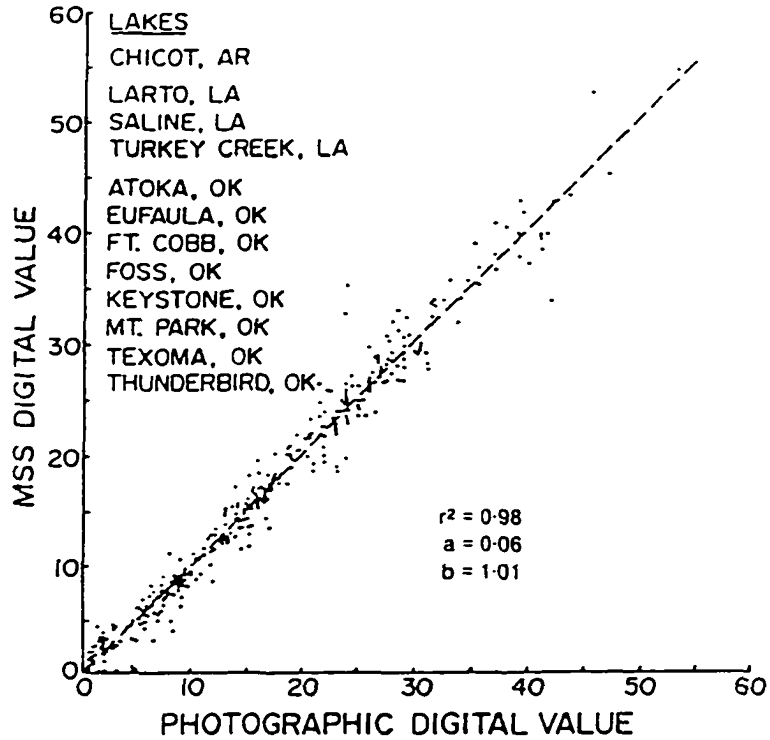

Figure 3.1. Relationship between MSS values determined by densiometry of transparencies and corresponding MSS values extracted from CCTs (after Schiebe, et al., 1992).

effective band widths for TM and MSS (Palmer, 1984)

solar constants (Thekaekara, 1970)

atmospheric effects and corrections (Turner and Spencer, 1972)

These studies greatly improved Landsat image interpretation.

Today, research is focused on accurate calibration methods for instrumentation aboard satellites, detailed laboratory studies designed to accurately quantify radiance and irradiance measurements, image processing using geographic information systems (GIS), and ways to further clarify image interpretation. All of these techniques are correlated with, and verified by, actual field data.

SUSPENDED SEDIMENT CONCENTRATION

Early attempts to establish a universal algorithm for determining suspended sediment concentration in water bodies (Holyer, 1978) were not successful, but efforts continued with moderate success (Schiebe, et al., 1987; Curran and Novo, 1988; Topliss, et al., 1990; Hinton, 1991; Ritchie and Cooper, 1991; Ross, et al., 1991; Lathrop, 1992). Early studies of determining suspended sediment concentration from space involved the use of hand-held spectroradiometers. These instruments were tested both in the field and in laboratory settings in order to establish guidelines for evaluating water reflectance. One such study was conducted at Lake Chicot, Arkansas. Water samples were taken and evaluated in the laboratory where it was concluded that the most effective wavelength for evaluating suspended sediment concentration was 700 - 800 nm (Witte, et al., 1981). Using a portable spectroradiometer, Ritchie, et al. (1983) determined that as suspended sediment concentration (SSC) increased, reflectance increased and determined that the best wavelengths for examining suspended sediment concentration were 700 - 900 nm.

As Landsat images were first examined, interpretation was based on field data as well as spectroradiometer readings. A series of Landsat images taken between 1972 and 1979 was analyzed, and it was evident that suspended sediment patterns were detectable in MSS Band 7 (800 - 1100 nm) but only when sediment concentrations were greater than 100 mg/L (LeCroy, 1982). Further studies revealed that MSS Band 3 (near-infrared, 700 - 800 nm) had the greatest potential for sensing suspended sediment concentration (Ritchie and Schiebe, 1986; Schiebe and Ritchie, 1986) as did TM data from Band 3 (red, 630 - 690 nm) (Schiebe, et al., 1985). It was finally determined that MSS Band 3 is most effective for concentrations greater than 100 mg/L (Schiebe, et al., 1987), while Band 2 (red, 600.1 - 699.0 nm) reflectance is most effective in monitoring SSCs less than 100 mg/L (Ritchie and Cooper, 1991). Since these wavelengths penetrate water to a limited depth, measurements reflect SSC in the surface mixed layer only, which roughly corresponds to the epilimnion. The measured surface SSC must be connected by mathematical modeling to the remainder (hypolimnion) of the water body (Stefan, et al., 1984).

Radiance (upwelling) describes the amount of radiation being reflected by a surface. Irradiance (downwelling) is the amount of incoming radiation from the atmosphere. Reflectance, in general, is determined by dividing radiance by irradiance (Lillesand and Kiefer, 1987):

$$EREF_\lambda = \frac{\pi L_\lambda}{Ecc\, E_\lambda \sin\alpha} \qquad (1)$$

where $EREF_\lambda$ = exoatmospheric reflectance

λ = wavelength band of instrument

E_λ = avg. solar irradiance at top of atmosphere for that wavelength

Ecc = eccentricity correction factor (Iqbal, 1983)

α = elevation angle of sun

L_λ = spectral radiance

A relationship, based on the physics of light scattering from particles suspended in water, between reflectance and SSC was developed by Schiebe (1997, personal communication) and Schiebe, et al. (1987):

$$EREF_\lambda = B(1 - e^{-c/s}) \qquad (2)$$

where $EREF_\lambda$ = exoatmospheric reflectance

c = concentration of suspended sediment (mg/L)

B = constant describing the maximum reflectance

s = concentration constant.

At a concentration equal to s, the model predicts a reflectance of 63% of the asymptotic value (B). This equation describes the relationship between atmospheric reflectance and the reflectance of sediment laden water measured just above the water surface.

In further studies of Lake Chicot water quality was analyzed using remotely sensed data before and after the installation and operation of three hydraulic structures used to control inflow, outflow, and lake level. These controls were utilized to regulate the water and suspended sediment levels in the lake (Harrington and Schiebe, 1989). Landsat MSS images revealed distinct differences in SSC: before the structures were added, water reflectance was much greater than after the structures had been installed. Subsequent to installation of these structures, SSCs were greatly decreased and the water absorbed more light than it reflected. It was concluded that variations in water quality in terms of SSC could easily be determined from remotely sensed data because water reflects light based on the concentration of suspended solids (Harrington, et al., 1992).

Band ratios are often used to reduce atmospheric effects (Curran and Novo, 1988); use of such ratios has the following advantages:

- may classify images by spectral characteristics (Hilton, 1984),
- more information may be obtained about the shape of spectral curves because two band widths are being combined (Lillesand and Kiefer, 1987), and
- variations in irradiance acting equally in all spectral bands are annulled (Dekker, et al., 1991).

Topliss et al. (1990) designed an empirical algorithm for SSC based on data from highly turbid Canadian coastal waters:

$$\mathrm{Log}_e SS = -9.2\, R_{1/2} + 2.8\, R_{1/2}^{\;2} + 9.4 \qquad (3)$$

where SS = surface sediment concentration (mg/L)

$R_{1/2}$ = ratio of reflectance (MSS Band 1 to Band 2).

A similar algorithm was derived by analysis of data from Enid Reservoir, Mississippi (Ritchie and Cooper, 1991). After determining the ratio for all combinations of MSS bands, they found that the ratio of MSS Band 1 to MSS Band 2 yielded the best coefficient of determination (0.59). This was improved (0.80) by taking the log of SSC to determine the best fit equation:

$$Log_e SS = -9.21\ R_{1/2} + 2.71\ R_{1/2}^2 + 8.45 \qquad (4)$$

The similarity of these equations, even though one is for coastal waters and the other for an inland reservoir, suggests that development of a universal algorithm for estimating SSC from Landsat MSS data may be plausible. Lathrop (1992), however, determined that an algorithm developed from TM data for Green Bay and Lake Michigan, Wisconsin (turbid inland waters) could not be used for the oligotrophic waters of Yellowstone or Jackson lakes in Wyoming. In addition, Hinton (1991) believes that algorithms based on regression may not be used universally because of differing water conditions, so a database of algorithms should exist from which one could choose the appropriate equation based on site-specific water conditions. He also suggests that eigenvector analysis of radiance data, which has potential for determining the composition of material in suspension, may be used as a criterion for selecting an appropriate algorithm.

Lake Thunderbird, Oklahoma, as well as 15 other lakes in Oklahoma, were examined over a two year period (Menzel, et al., 1989; Ross, et al., 1991). Land surfaces are more reflective than water surfaces, and water is detected most easily in MSS Band 4 since it absorbs light strongly in this wavelength band. Therefore, water surface maps may be created using this principle (Ross, et al., 1991). In addition, by adding another constant, A, equation 1 may be modified to include energy as a result of light scattering in the air (path radiance) in the direction of the satellite detector:

$$EREF_{\lambda} = A + B(1 - e^{-c/s}) \qquad (5) \qquad \text{(Figure 3.2)}$$

Using this equation, sediment classes could be defined by assigning values of SSC to the various shades of gray in MSS Band 3 images. This concept was used to make seasonal SSC maps of Lake Thunderbird.

A study of Delaware Bay, using data collected from NOAA's AVHRR (Advanced Very High Resolution Radiometer) satellite attempted to relate SSC to the diffuse attenuation coefficient (result of in-situ measurements from an underwater irradiance meter) (Stumpf and Pennock, 1991). A strong linear relationship was found to exist between the red (580 - 680 nm) and near-infrared (720 - 1000 nm) wavelengths and SSC (Figure 3.3), further proof that reflectance increases in certain wavebands as SSC increases.

Eleven years of data from Lake Chicot, Arkansas was examined to determine the best wavelengths for evaluating SSC from exoatmospheric reflectance (EREF). Plotting EREF versus SSC, an increase in SSC resulted in an increase in reflectance. Using regression analysis, the strongest relationship existed for MSS Band 3 (near-infrared, 700 - 800 nm, $r^2 = 0.72$) and is best described by a saturating exponential relationship similar to equation one (Schiebe, et al., 1992). MSS Band 2 (red, 600 - 700 nm, $r^2 = 0.70$) is also good for predicting SSC. These results agreed well with those of previous studies. Since Secchi depth data is readily available in the literature, the Secchi depth versus reflectance relationships were examined. Since Secchi depth decreases and turbidity increases with increasing SSC, reflectance may also be used to predict Secchi depth or turbidity using band 2 or 3 (Harrington, et al., 1992). Generally, red and near-infrared wavelengths are best for evaluating the surface water qualities of SSC and Secchi depth from remotely sensed data.

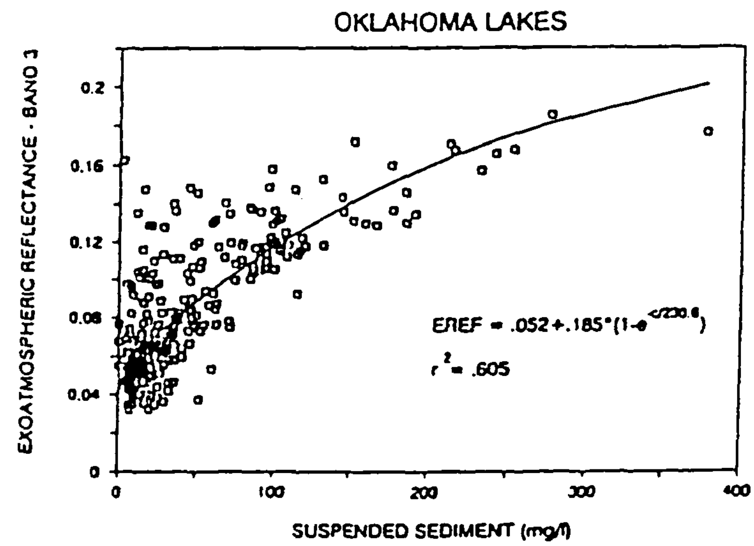

Figure 3.2. Suspended sediment values of water from 16 lakes in south-central Oklahoma compared to exoatmospheric reflectance (after Ross, et al., 1991).

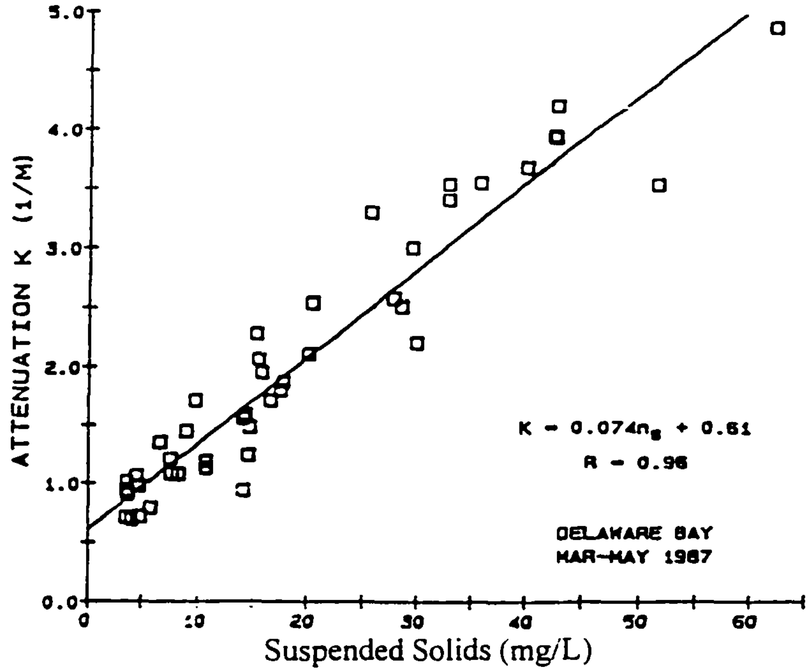

Figure 3.3. Attenuation vs. suspended solid concentration.

(after Stumpf and Pennock, 1991).

It is of significance to note that empirical algorithms are, in general, inferior to those developed from physically-based theoretical models. Physically-based models tend to have wider applicability. Empirical algorithms or algorithms based on statistical methods tend to be limited to the circumstances that were used to develop them. It is unacceptable to use statistical formulation beyond the range of data. For physically-based theoretical models, when the process involved is understood, conclusions can be drawn beyond the range of data.

LABORATORY STUDIES

Chen, et al. (1991) conducted a laboratory study using a spectroradiometer to determine the relationship between SSC in water and reflectance (Figure 3.4). They analyzed 875 wavebands (350 - 2500 nm) for 18 different sediment types/grain sizes at 30 different concentrations (0 - 1300 mg/L). It was concluded that a log-linear relationship existed for wavelengths between 450 and 700 nm, while the relationship for wavelengths 700 - 1050 nm was linear. They then measured spectral radiance, found its derivative with respect to wavelength, determined SSC in both a laboratory setting and at sea (Chen, et al., 1992), and found a strong correlation between SSC and the derivative of spectral radiance in both environments. In general, the derivative increased with SSC on the shorter wavelength side of absorption features and decreased with SSC on the longer wavelength side. Even though relationships were stronger in the laboratory than at sea, they recommended the use of derivatives for evaluating SSC from reflectance. The use of derivatives was also supported in later studies conducted by Han, et al. (1994).

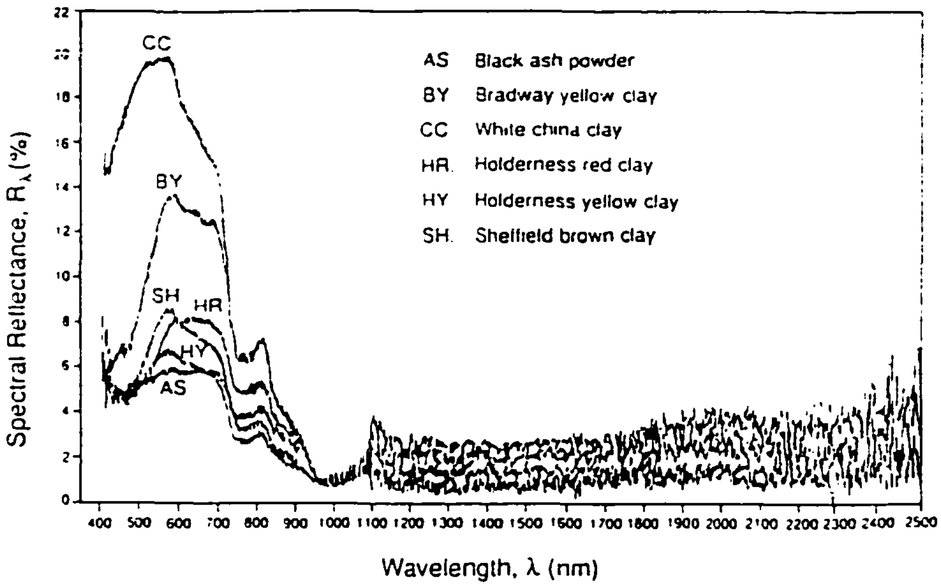

(a)

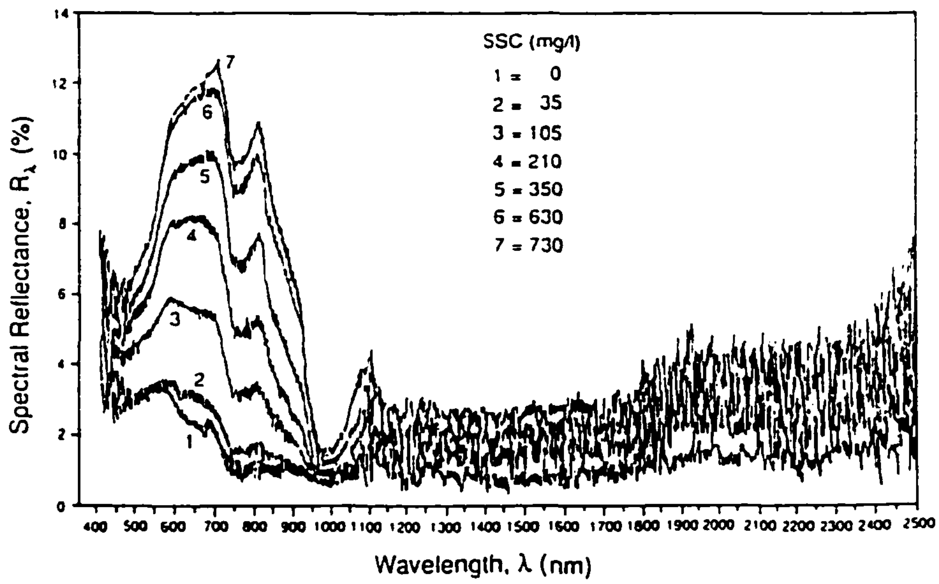

(b)

Figure 3.4. Spectral reflectance as a function of wavelength for (a) six sediment types, SSC = 210 mg/L; (b) Holderness red clay, seven levels of SSC (after Chen, et al.,1991).

SSC AND CHLOROPHYLL-A

Much research has been completed about the relationship between SSC and spectral reflectance. Having a foundation for analyzing data gathered by remote sensing platforms, scientists have begun to expand upon the types of subject matter that may be investigated with this new research tool. Primary productivity, which may be estimated by chlorophyll-a concentration, was a logical step since the necessary technology should presumably be extended from SSC analyses. It was later concluded, however, that analysis may be similar, but behavior in the light field was quite different. Suspended sediments primarily scatter light, while algal cells absorb many wavelengths of radiation.

Both scattering and absorption of underwater light is great in eutrophic lakes. Absorption affects the spectral response of water because it takes place at specific wavelengths. Lathrop, et al. (1991) examined TM data from Green Bay, Wisconsin. This section of Lake Michigan has a variety of trophic states ranging from hypereutrophic at the southern end to oligotrophic in the north. They determined that suspended solids had the most effect on reflectance and saw no evidence of chlorophyll-a absorption in these highly turbid waters. As SSC increased, both backscatter and reflectance increased across all wavelengths. Peak response occurred in the longer red wavelengths with the preferred exponential model utilizing a Band 3 to Band 1 ratio (660 nm / 485 nm) (Figure 3.5):

$$y = ae^{bx} \tag{6}$$

where y = SSC

x = the reflectance ratio

a,b = regression coefficients.

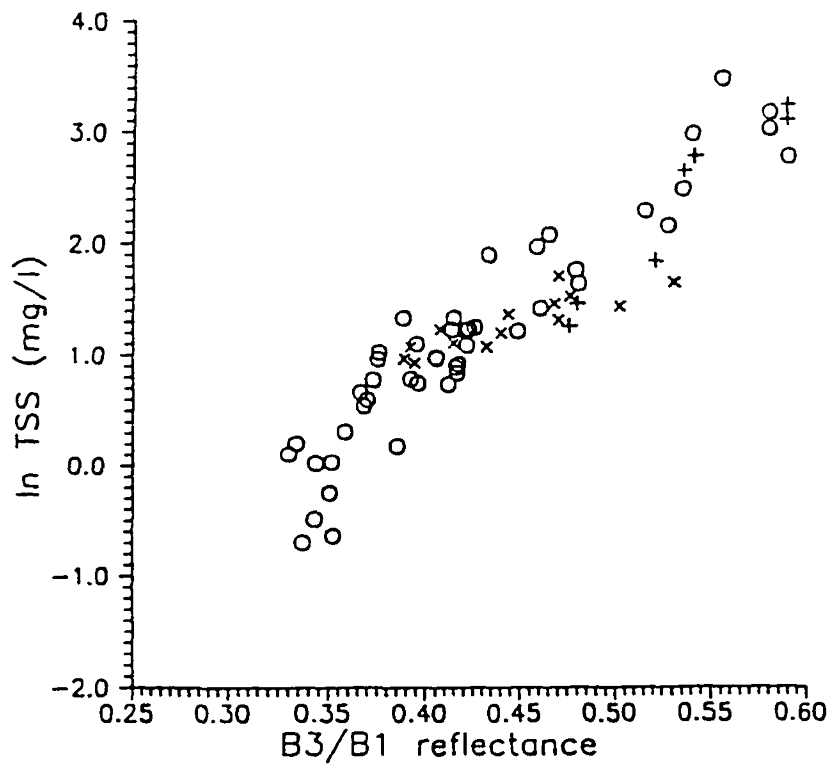

Figure 3.5. Plot of natural-logarithm-transformed total suspended solids (TSS) against TM reflectance; + July 24, 1986, o June 9,1987 (after Lathrop, et al., 1991).

This TM data also correlated well with Secchi depth.

The rivers Don and Severny Donets, the Sea of Azov, and Lake Balatov in Russia were evaluated using portable spectroradiometers at a height of 10 - 15 m. In this study, Gitelson and Kondratyev (1991) noticed that a chlorophyll-a minimum occurred at about 670 nm and a maximum between 685 nm and 700 nm. The maximum, however, shifted towards longer wavelengths as the chlorophyll concentration was increased. As a result, they empirically determined that chlorophyll-a concentration was related to a 700 nm / 675 nm ratio by

$$C_{chl} = az^{b} \qquad (7)$$

$$r^2 = 0.98$$

where C_{chl} = chlorophyll concentration

a = 67.67 mg/m3

b = 2.75

z = ratio (Ex: 700/675)

note: a and b depend on the size and type of suspended sediments, phytoplankton composition, dissolved organic matter, etc.

Radiance and irradiance, measured with a submersible spectroradiometer on the Loosdrecht Lakes, Netherlands, exhibited the following features (Figure 3.6) (Dekker, et al., 1991):

- low values from 400 - 500 nm attributed to absorption by yellow matter and chlorophyll-a,

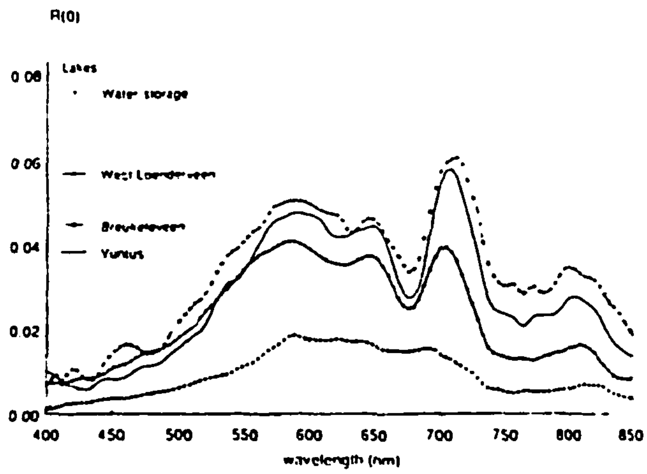

Figure 3.6. Reflectance spectra (R(0)) for four lakes of the Loosdrecht Lakes System (after Dekker, et al., 1991).

- increased values up to 600 nm representative of low absorption and increased scattering with an increase in SSC,
- a minimum at 630 - 640 nm which was probably a result of cyanobacterial absorption,
- chlorophyll-a absorption band at 675 - 680 nm, and
- a peak at 700 - 720 nm.

A PMI (Programmable Multispectral Imager) was also flown over the study area at an altitude of 1000 m and eutrophic plumes were evidenced easily on images by the darker shades of gray.

Analyzing three lakes with high SSCs, Ritchie, et al. (1994) tried to distinguish chlorophyll-a content. They found that, in general, chlorophyll-a concentration was inversely proportional to SSC. For example, chlorophyll-a concentrations greater than 100 mg/m^3 were found in waters having low SSCs (40 - 80 mg/L). This may be a result of the high SSC limiting light and preventing algal growth. They concluded, however, that chlorophyll-a could not be measured by broad band (100 nm) MSS data because its reflectance was masked by the reflectance of the suspended sediments and they recommended the use of narrow band (10 - 15 nm widths) spectral resolution centered at approximately 675 nm and 705 nm. Novo and Shimabukuro (1994) studied waters of the Brazilian Amazon and detected a correlation between reflectance in the 600 to 700 nm spectral region and chlorophyll concentration. Laboratory studies (Dekker, et al., 1991; Quibell, 1992; Gitelson, et al., 1993) have also indicated the existence of a reflectance minimum at 675 nm and a maximum at 705 nm. It is believed that this spectral pattern is due to absorption by chlorophyll. Gitelson (1992) noticed that the minimum does not vary with a change in chlorophyll concentration, but the maximum shifts from 685 nm at very low concentrations to 715 nm at concentrations of 100 mg/m^3.

Quibell (1991) conducted a laboratory study in which chlorophyll was grown in tanks of water having various concentrations (200 - 600 mg/L) of suspended sediment. He concluded that the primary spectral characteristics of chlorophyll in water remained intact: the algal absorption minimum at 660-670 nm and the algal reflectance peak at 700-720 nm. Han, et al. (1994) performed a similar experiment with sediment concentrations ranging between 50 and 1000 mg/L at chlorophyll concentrations of 295 and 718 ug/L. They also noticed the preservation of the chlorophyll signature: a minimum near 675 nm and a peak near 700 nm (Figure 3.7) and concluded that the positions of the minimum and maximum were primarily dependent on the algal chlorophyll in water and not the SSC.

In a related study, Filella and Penuelas (1994) examined various plant types with a hand-held spectroradiometer in order to determine red edge parameters. The red edge is the point of maximum slope in vegetation reflectance spectra occurring between the wavelengths of 680 nm and 750 nm where reflectance varies from very low in the red absorption region to very high in the near-infrared (as a result of scattering). They concluded that chlorophyll content was related to the wavelength of the red edge.

Yacobi et al. (1995), using a portable spectroradiometer fixed 2 m above the surface at various locations on Lake Kinneret, Israel, further examined reflectance in relation to chlorophyll content. They also detected the minimum at 670 nm and the maximum at 700 nm (which shifted to longer wavelengths with increasing amounts of chlorophyll). In an effort to determine a relationship between reflectance and chlorophyll content, they believed that "chlorophyll estimation should depend solely

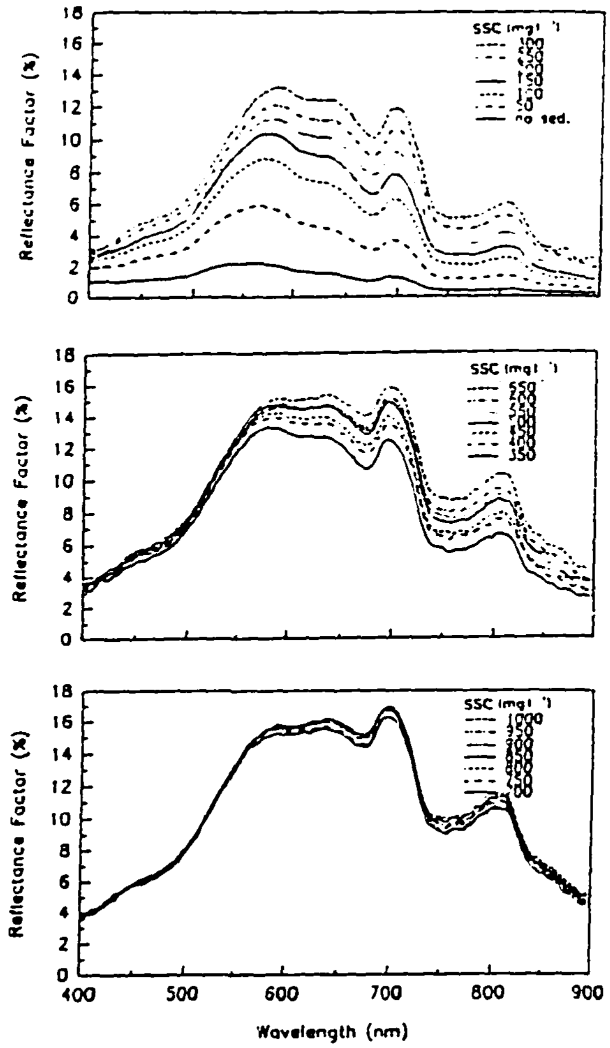

chl-a 295 ug/L

Figure 3.7. Spectral reflectance (after Han, et al., 1994).

Reflectance factor (%) = (L/B) x Cal x 100
L = wavelength-specific target radiance
B = corresponding radiance from reflectance panel
Cal = calibration factor for panel

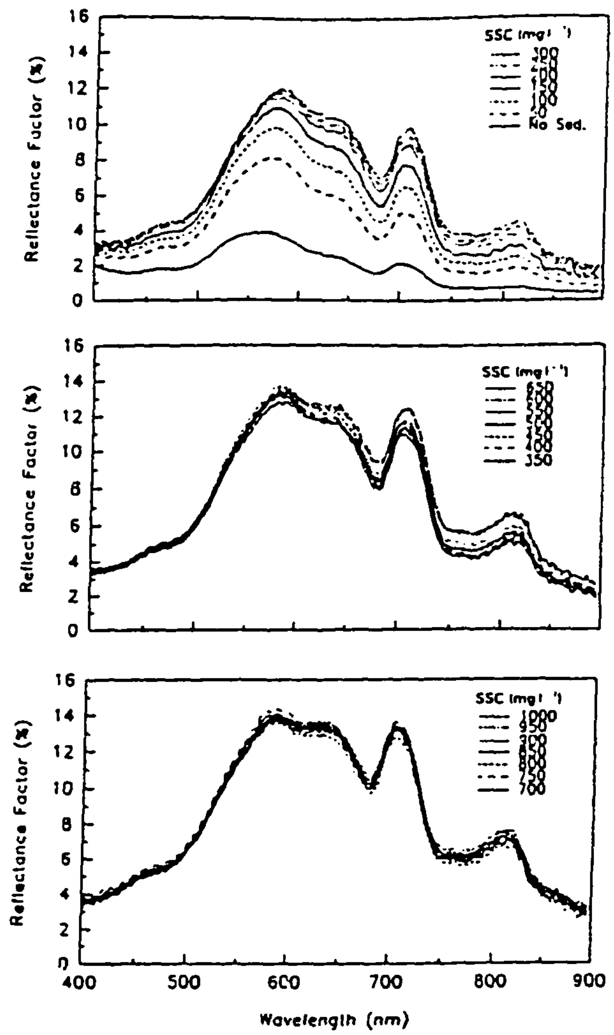

chl-a 718 ug/L

Figure 3.7. Continued.

on chlorophyll and no other water constituents, and should not be influenced by survey conditions." Therefore, since the minimum at 670 nm is insensitive to chlorophyll content and the maximum near 700 nm is distinctly related to chlorophyll, these are the wavelengths that should be used to determine chlorophyll concentration.

In order to analyze reflectance, Yacobi, et al. (1995) created an index: Rmax / R670 and compared calculated values with chlorophyll measured in-situ. This resulted in the following relationship:

$$Chl_{pred} = 5.14 + 0.86\ Chl_{meas} \tag{8}$$

with $r^2 = 0.96$ and an estimated error of less than 9.55 mg/m^3.

Results, however, consistently underestimated chlorophyll content, so they designed two new methods. Both used the concept of a baseline. They chose two reflectance points, 670 nm and 850 nm, drew a straight line between the two and labeled this the baseline. In the first method, reflectance line height (RLH), the distance between the baseline and the reflectance maximum near 700 nm, was calculated and, in the second, the sum of reflectance above the baseline was calculated. Both gave similar results and avoided problems created by variations in peak location and shape; thus the following relationship was proposed:

$$Chl_{pred} = 1.07 + .91\ Chl_{meas} \tag{9}$$

with $r^2 = 0.98$ and an estimated error of less than 6.18 mg/m^3.

The stability of their model depended on the taxonomic composition of phytoplankton, particle size of non-living material, nature of dissolved matter, changes in the underwater light field, technical limitations, and waves. Yacobi, et al. (1995) recommended that chlorophyll assessment from remotely sensed data be performed using three wavebands: 665 - 675 nm, 705 - 715 nm, and 830 - 870 nm.

In 1995, Repic, et al. analyzed data from the Little Washita River watershed. They compared airborne video data and measurements taken with a hand-held spectroradiometer. Using a simple difference relationship between reflectance at 700 nm and at 670 nm, they concluded that chlorophyll content could be estimated from airborne sensors.

SUMMARY

Many studies have been performed examining the nature of the relationships between reflectance, SSC, and chlorophyll-a concentration. Whether performed in the laboratory, in the field, or from remote sensing platforms, the same general conclusions have been reached. Exoatmospheric reflectance of water bodies in the near-infrared wavelength range depends on the amount of suspended solids present: as SSC increases, reflectance increases. This relationship may be detected even by broad band (100 nm width) sensors of the various satellites. Chlorophyll-a concentration, however, is masked by the presence of SSC on these broad band sensors but may be evidenced using narrow band filters (10 nm width) at lower altitudes. Since chlorophyll-a absorbs light strongly at about 670 nm and reflects light near 700 nm, the behavior of reflectance at these two wavebands is examined herein to determine chlorophyll-a concentration.

CHAPTER 4. METHODS

INTRODUCTION

The purpose of this chapter is to describe the methods used during this research project. It will provide a step-by-step description of data collection and analysis so that the study may be reproduced by anyone wishing to perform similar research. The method is then illustrated by stepping through the entire process using one of the reservoirs of the Little Washita River Watershed.

DESCRIPTION OF STEPS

Step 1. Assemble pertinent data.

Compile aerial images, water quality data (chlorophyll concentration), and solar radiation data.

Aerial Images. In August of 1994, three flights were made over reservoirs of the Little Washita River Watershed: the morning and afternoon of the 19th and the morning of the 23rd. Flights were scheduled to accommodate the availability of the Endeavor Space Shuttle whose SIR-C/X-SAR microwave sensors were utilized in other areas of research. The entire project involved personnel from many different agencies and universities including the Oklahoma Conservation Commission, Oklahoma State University, and NASA. The video flights were organized and flown by personnel of the Agricultural Research Service in Durant, OK and Weslaco, TX. The purpose of these flights was to obtain reflectance images from the surface waters of each of the flood control reservoirs within the watershed and use them as indicators of certain water quality/productivity parameters. The dates and times of the aircraft overflights were predetermined by scheduling considerations so, unfortunately, the majority of the data for this study was obtained under overcast conditions.

A twin engine airplane was equipped with three panchromatic video cameras with fixed 12.5 mm focal length lenses. It was flown at an altitude of 6500 ft at an average plane speed of 125 knots. Video cameras are equipped with internal automatic gain controls (AGC) which adjust for variable lighting conditions. This AGC feature was disabled so that camera sensitivity was controlled by f-stop only. Each camera was fitted with a narrow band filter so the camera would record only a small portion of the electromagnetic spectrum as shown in Table 4.1.

Table 4.1. Camera Filters

Filter center wavelength (nm)	F-Stop	Band width (nm)	Effective wavelength band (nm)
670	2.8	10	665 - 675
700	2.8	10	695 - 705
800	5.6	70	765 - 835

Images were obtained by the video camera and recorded on video tape using a video cassette recorder (VCR). Images of each reservoir were "grabbed" from each of the three video tapes providing an image of each reservoir at each of the designated wavelengths: 670 nm, 700 nm, and 800 nm. Since there are several minutes of video for each reservoir, the image that was grabbed was the one located as close to the nadir (straight down) position as possible. This decreases the need for various atmospheric corrections that would be required if an image from another angle was utilized for the study. The images of the reservoirs were imported into the Geographic Information System (GIS) IDRISI for analysis.

Chlorophyll Concentration. Samples were collected by personnel of the Agricultural Research Service (ARS), Oklahoma Conservation Commission, and Oklahoma State University from each reservoir on the same dates that the airborne data was collected. Samples were taken in the middle of the reservoirs near the dams (at the deeper portions of the water bodies) so that samples would be representative of the reservoir rather than the river input or areas having high rates of runoff. Samples of surface water were collected for analysis in the laboratory. Data collected in situ included site depth, Secchi depth, pH, and conductivity. Subsequent laboratory analyses performed at the ARS Water Quality Laboratory in Durant, OK included turbidity, total solids, total dissolved solids, total suspended solids, total nitrogen, ammonia, nitrate, total phosphorus, dissolved phosphorus, and chlorophyll concentration (phaeophytin corrected, trichromatic equations). The focus of this study is the surface chlorophyll concentration.

The chlorophyll concentration was determined using methods from Lind (1979). One liter samples of water were collected at the surface of each reservoir. Samples were kept cool in an ice chest. Samples were filtered through a 0.8 um, 47 mm glass filter until the filtering rate began to decrease. At this time, the filter was placed into a 1-inch test tube and the volume of water filtered was measured. Filters were frozen until being processed. The filter was ground in a tissue grinder with 2 to 3 mL of acetone, transferred to a centrifuge tube, and stoppered for extraction. After remaining overnight in a dark refrigerator, the fluid was centrifuged and decanted into a 10 mL graduated cylinder. Then 10 mL of solution was made by adding 90% alkalized acetone. Using a blank of acetone, absorbance (abs) was measured at 750, 665, 645, and 630 nm. The absorbance at 750 nm was subtracted from each of the other absorbances to correct for turbidity. The following trichromatic equations were then used to determine chlorophyll-a, chlorophyll-b, and chlorophyll-c concentrations:

$$\text{chl-a} = 11.6(\text{abs at } 665 \text{ nm}) - 1.31(\text{abs at } 645 \text{ nm}) - 0.14(\text{abs at } 630 \text{ nm}) \quad (1)$$

$$\text{chl-b} = 20.7(\text{abs at } 645 \text{ nm}) - 4.33(\text{abs at } 665 \text{ nm}) - 4.42(\text{abs at } 630 \text{ nm}) \quad (2)$$

$$\text{chl-c} = 55.0(\text{abs at } 630 \text{ nm}) - 4.64(\text{abs at } 665 \text{ nm}) - 16.3(\text{abs at } 645 \text{ nm}) \quad (3)$$

Samples were also corrected for phaeophytin, which is a product of the degradation of chlorophyll that also absorbs light at chlorophyll wavelengths. After absorbance was determined at 750 and 665 nm, the samples were acidified with one drop of 1.0 N HCl. After one minute, the absorbances were remeasured and corrected for turbidity. The amount of phaeophytin was then subtracted from the chlorophyll measurement.

Solar Radiation Data. The Mesonet is a comprehensive network of 108 weather stations in the state of Oklahoma. There is at least one station in each county which collects data every five minutes and transmits it to the Oklahoma Climatological Survey at the University of Oklahoma every fifteen minutes. The collected data includes air temperature, incoming solar radiation (irradiance), wind speed and direction (at 10 m), rainfall, barometric pressure, relative humidity (at 1.5 m), and soil temperature at a depth of 10 cm under bare soil and natural grass cover.

The Micronet is a component of the Mesonet located within the Little Washita River Watershed (Figure 4.1). There are 45 Micronet stations within and immediately surrounding the watershed that measure the same parameters as the Mesonet stations. The only difference is in the measurement of wind speed and direction. These

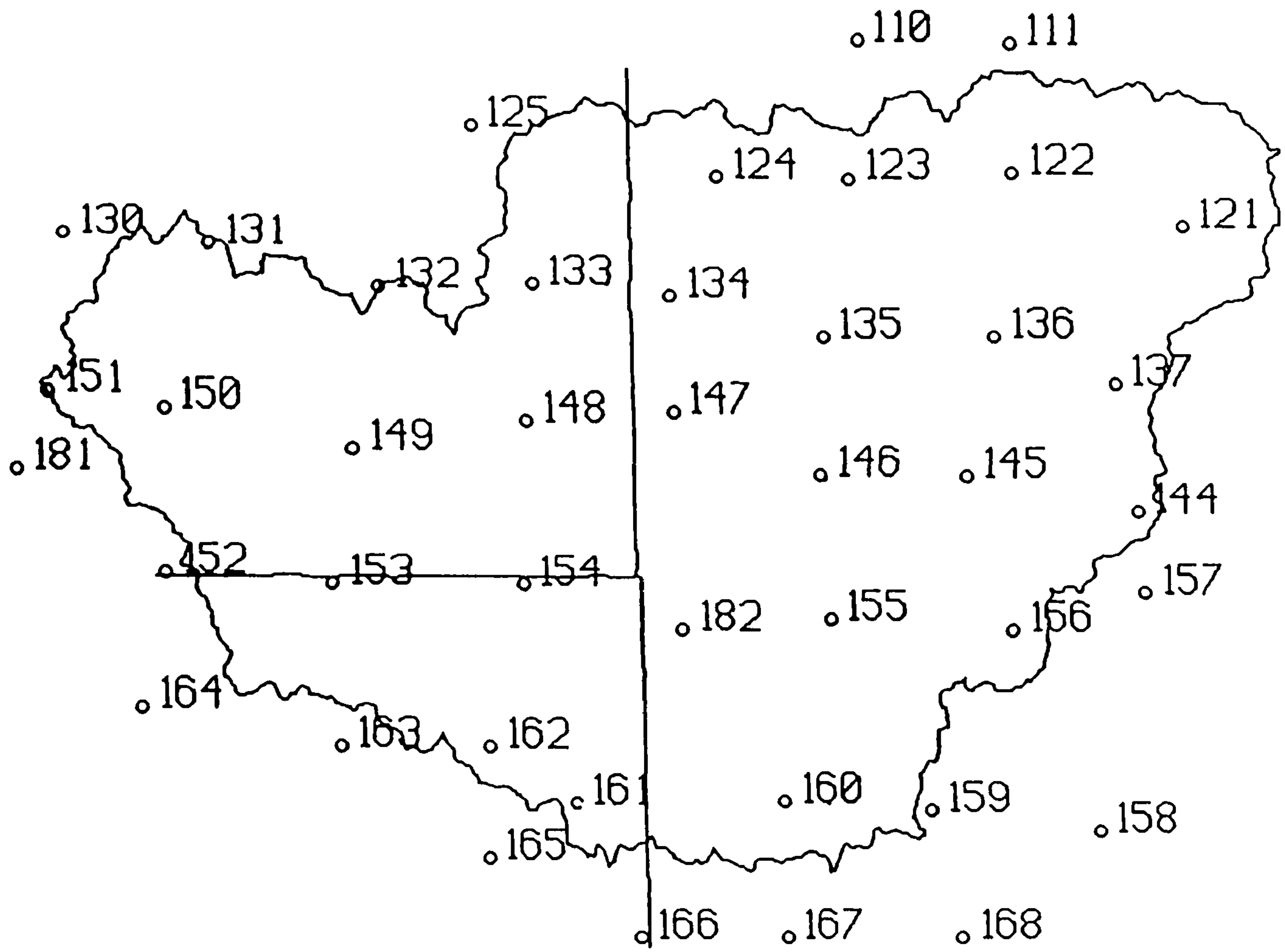

Figure 4.1. Micronet stations of the Little Washita River Watershed.

parameters are measured at a height of 10 m on the Mesonet stations and at 2 m on the Micronet stations. The Micronet was established in order to obtain comprehensive climatological data in a relatively small area in order to observe fine-scale weather events. This study utilizes the solar radiation data collected at the Micronet stations.

Step 2. Select reservoirs for use in study.

There are 45 flood retention reservoirs in the Little Washita River Watershed (Figure 4.2). A complete set of data necessary for this study was available for 33 of the reservoirs. Data sets were incomplete for various reasons including inaccessibility to the reservoirs for sampling and images of poor quality. The 33 reservoirs analyzed varied in chlorophyll-a concentration from 1.18 to 206.28 mg/m^3, and suspended sediment concentration ranged from 0.5 to 21 mg/L as determined in the laboratory (ARS, 1994).

Step 3. Select area of reservoir(s) for analysis.

In order to develop the scale of the maps, it was necessary to determine pixel size. The cameras each had a 2/3 inch CCD (charge coupled detector) array with 640x480 active sensors in the horizontal and vertical directions respectively. Using a COHU Multifunction CCTV Calculator, the field of view was determined to be 4600 ft (38.5°) in the horizontal direction and 3450 ft (29.5°) in the vertical direction. However, since images were recorded on a VCR with only 400 line horizontal resolution, the basic pixel size was reset to 3450 ft /400 = 8.625 ft (2.63 m). Thus, each pixel represented an area of 2.63 m x 2.63 m, or 6.92 m^2, in size.

The next step was to determine an appropriate pixel array size to be analyzed in this study. This was accomplished by comparing pixel array size to radiance for several reservoirs to establish where average radiance values became consistent. The determination of the radiance value from a pixel is described in step four. Four

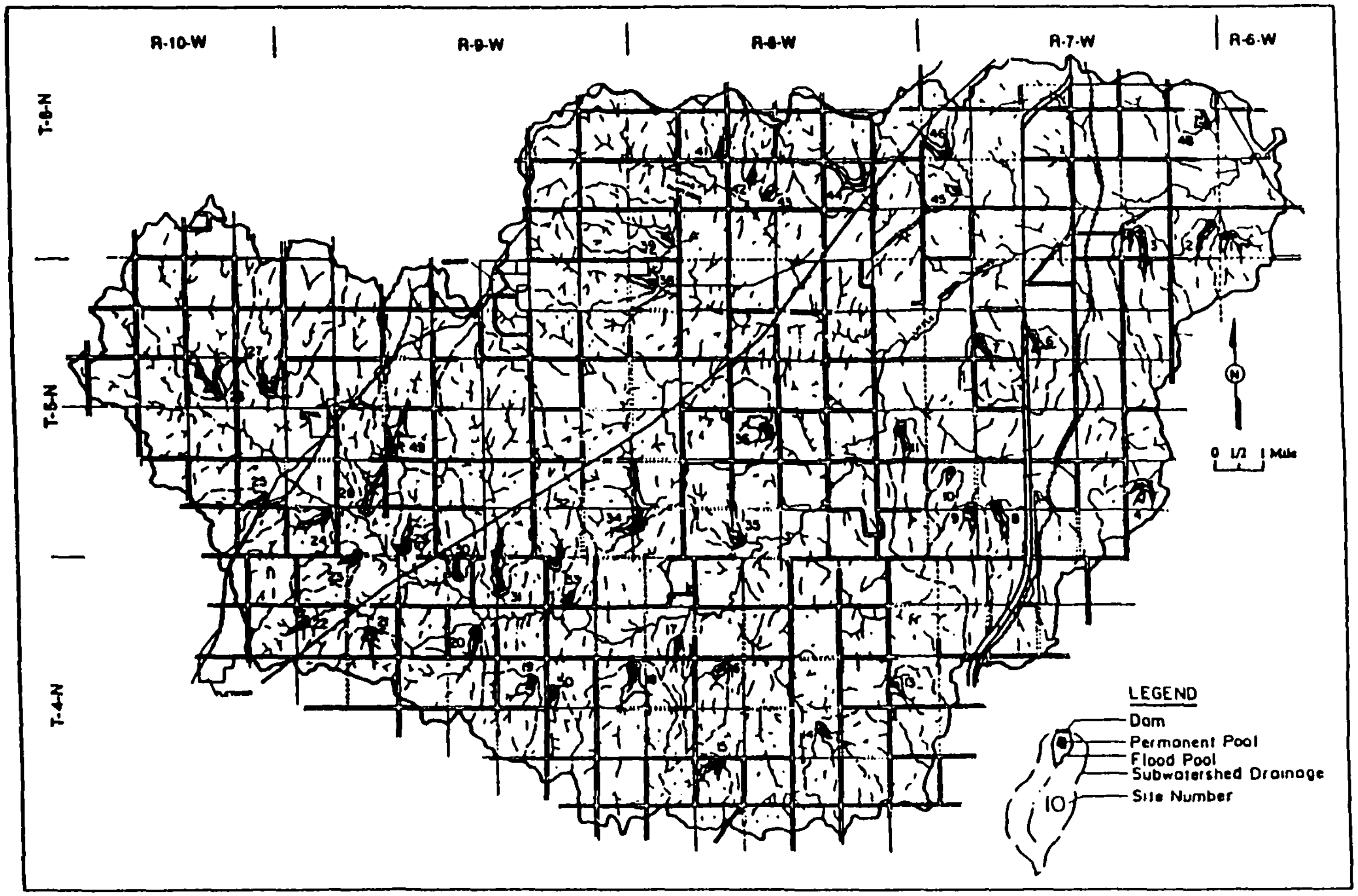

Figure 4.2. Reservoirs of the Little Washita River Watershed

(after Allen and Naney, 1991).

reservoirs were chosen based on their widely varying concentrations of chlorophyll-a and suspended sediment. A 10x10 window of pixels was evaluated for the 700 nm waveband, which was chosen because it has the highest degree of sensitivity to chlorophyll concentration, from these four reservoirs in order to determine a representative average value of radiance (Ritchie and Cooper, 1987). Pixel array sizes from 1x1 to 10x10 were evaluated (Table 4.2). The 1x1 array was located in the upper left-hand corner of the window. Successive pixel arrays were chosen down and to the right of the previous array. Figure 4.3 shows that the average radiance approached a fairly constant value by a 7x7 pixel array size for all of the reservoirs and would therefore be the minimum acceptable size. This study utilized a pixel array size of 10x10 (Appendix A), which corresponds to an area of approximately 692 m^2. Array sizes larger than this become problematic, especially in the smaller reservoirs, as values may become variable as a result of changing surface water conditions (nearshore sediment influx or plant growth) or unintentional incorporation of land surfaces into average water values.

The locations of the arrays were chosen to be as near where the field samples were collected as possible. For each of the 33 reservoirs, an average value for the 10x10 digital number pixel array was determined for each of the relevant wavelengths (670 nm, 700 nm, 800 nm). The data is shown in Appendix B.

Step 4. Convert original imaging data (DN) into radiance (uW/cm^2/sr) based on ground-truthing methods.

The initial images recorded by the cameras are simply digital number images in which each shade of gray is assigned a separate value. These values are scaled numerically from black through gray to white. It is difficult, however, to evaluate these numbers in a physically meaningful way. The cameras, therefore, must be

Table 4.2. Comparison of pixel array size

Reservoir	Pixel Array Size (Radiance uW/cm2/sr)									
	1x1	2x2	3x3	4x4	5x5	6x6	7x7	8x8	9x9	10x10
26	6.33	6.56	6.55	6.58	6.58	6.54	6.60	6.61	6.61	6.63
41	6.79	6.45	6.59	6.57	6.56	6.61	6.58	6.58	6.57	6.56
42	6.79	6.83	6.90	6.92	7.01	7.04	7.02	7.04	7.02	7.03
43	7.41	7.18	7.22	7.27	7.23	7.30	7.31	7.30	7.35	7.32

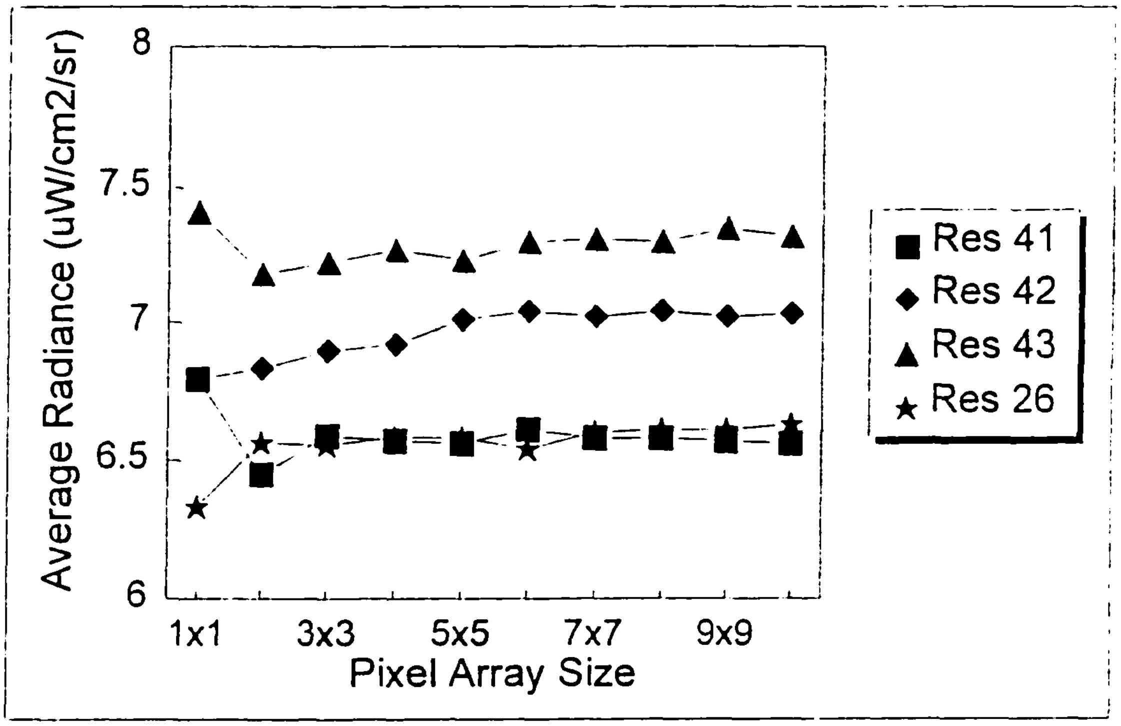

Figure 4.3. Pixel array size.

calibrated to provide physically meaningful data. In order to accomplish this, the plane flew over a series of five panels: white, gray-white, gray, gray-black, and black. As the airborne video cameras recorded the shades of gray, spectroradiometers on the ground were hand-held directly above the panels in order to determine actual radiance values. Three points on each panel were evaluated in order to establish the relationship between digital numbers recorded by the video camera and radiance measured using the spectroradiometer. Saturation was reached when the CCD sensors in the video cameras reached their maximum and did not respond to further increases in radiation. Using regression analysis, the panel data was used to generate a relationship between radiance (L) and digital number (DN) for each camera:

$L(670) = 4.31 + .069\ (DN)$	$DN<172$	(Figure 4.4)	(4)
$L(700) = -3.37 + .154\ (DN)$	$DN<160$	(Figure 4.5)	(5)
$L(800) = 15.2 + 1.59\ (DN)$	$DN<165$		(6)

where the multiplicative coefficients have units of $uW/cm^2/sr$. The average DN value of every reservoir at each of the relevant wavelengths (calculated in step three) was then converted, using the above equations, into radiance values. The results are listed in Appendix B.

Step 5. Convert radiance values into reflectance by incorporating solar irradiance data from the Oklahoma Mesonet/Micronet.

Radiance images are converted into reflectance (R) images by examining the irradiance (I), or incoming solar radiation. This step "normalizes" the data to correct for variable atmospheric conditions such as cloud conditions and sun angle which influence the amount of irradiance illuminating the target reservoirs. The data

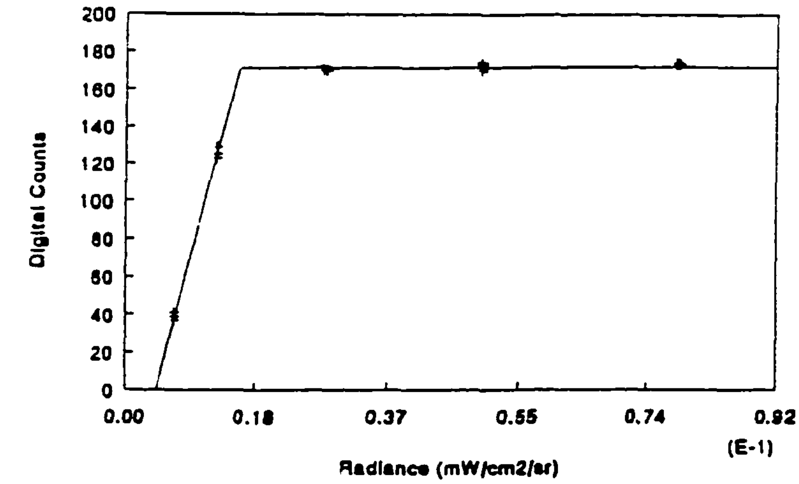

Figure 4.4. Video camera calibration for 670 nm waveband.

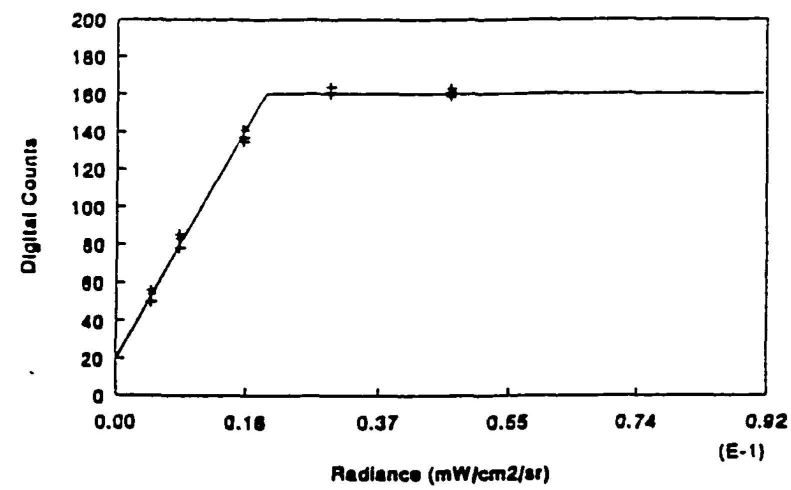

Figure 4.5. Video camera calibration for 700 nm waveband.

obtained from the Micronet stations included the UTM (Universal Transverse Mercator) coordinates for each station and incoming solar radiation values (reported in W/m^2) at each station every five minutes (Table 4.3). It was also necessary to determine the UTM coordinates for each of the reservoirs and to find the Micronet stations located nearest each reservoir. These coordinates were determined, using IDRISI, from a satellite image of the watershed.

In most cases, flight times did not correspond exactly with the times data was reported at the Micronet stations (Table 4.3). A manual interpolation in time was therefore necessary. Using data from the stations nearest to the reservoir, the two times bracketing the flight time were determined, and irradiance values from the stations at those times were recorded. Linear interpolation was then performed for each stations in order to obtain an irradiance value for each of the stations at the actual flight time.

An interpolation in space was also required in order to determine an irradiance value for each reservoir relative to the irradiance values measured at the adjacent Micronet stations. This was achieved using the interpolation package in IDRISI. The UTM coordinates of the Micronet stations and their respective irradiance data were input into IDRISI which generated a "surface" using an inverse distance-squared relationship. This resulted in the generation of an irradiance map around each reservoir at its respective flight time. These contour maps produced smooth surfaces with no noticeable areas of high irradiance concentrations. The UTM coordinates of the reservoirs were then used to determine the approximate irradiance illuminating the reservoir at the actual time of the imaging flight (Table 4.3). This irradiance value, however, is representative of the entire visible and near-infrared spectrum. Only a

Table 4.3. Data for Reservoir and Time Interpolations

Reservoir	Flight time	Mesonet station(s) used	Station time(s) used	Mesonet irradiance for multiple times (W/m^2) (requiring time interpolation)	Station irradiance at time of reservoir flight (W/m^2)	Reservoir irradiance at flight time (W/m^2)
1W	02:34:43 pm	121, 137	02.35 pm		467 59, 717 27	584 11
1E	02:34:43 pm	121, 137	02.35 pm		467.59, 717.27	567 46
2	02:33:31 pm	121, 137	02:30, 02:35 pm	891.98, 681.93; 467.59, 717 27	577, 706	611 40
4	10:44:30 am	144	10.45 am		298 51	298 51
6	10:46:23 am	136	10:40; 10.45 am	244.59, 232 27	238	238 00
7	10:46:55 am	136	10:45; 10:50 am	232.27; 280.28	252	252 00
8	10:14:51 am	145, 156, 144, 157	10:15 am		721 62, 733 20, 736 52, 749	727 20
9	10:15:03 am	145, 156, 144, 157	10:15 am		721 62, 733.20, 736 52, 749	727 20
11	10:17:35 am	145, 146	10:15; 10:20 am	721 62, 721 65, 734.55, 732.97	730, 729	729 40
13	02:28:35 pm	155, 156, 159, 160	02:25; 02:30 pm	869.88, 912 62, 914.52, 814.09; 856.44, 929 71, 863.07, 809.39	860, 925, 880, 810	863 67
16	02:26:35 pm	182, 161, 160, 155	02:25; 02.30 pm	835.64, 679 24, 814.09, 869.88; 861.78, 664.97, 809.39, 856.44	841, 675, 812, 866	802 33
18	10:24:28 am	182, 161, 162, 154	10:25 am		748.51, 610.53, 788 39, 755	693 53
19	10:38:31 am	162	10:35; 10.40 am	304.11; 273 13	282	282 00
20	10:29:52 am	162, 163, 154, 153	10:30 am		799 11, 778.43, 764.28, 752	780 55
21	10:37:17 am	153, 163	10:35; 10:40 am	562.44, 322.5; 922.17, 546.97	702, 414	490 80
22	10:34:56 am	153, 163, 164, 152	10:35 am		562.44, 322.5, 320, 893 02	434 60
23	10:36:14 am	153	10:35; 10:40 am	762.96; 775 57	768	768 00
26	11:04:31 am	150	11:05 am		378 11	378 11
27	11:02:53 am	150, 149	11:00; 11:05 am	417.37, 378.11; 435.63, 458.05	428, 423	427 00
29	02:24:05 pm	153	02.20; 02:25 pm	861.48; 842.56	848	848 00
30	02:24:30 pm	153, 154	02:25 pm		842.56, 837.21	838 28
31	11:11:03 am	154	11:10; 11:15 am	450.08; 370 6	432	432 00
32	10:29:49 am	154	10:30 am		296.41	296 41
33	10:32:40 am	154	10.30; 10:35 am	764.28; 773 21	770	770 00
34	10:27:07 am	154, 182	10.25; 10:30 am	391 67, 529 19; 296.41, 357.7	353, 465	412 73
36	10:22:15 am	147, 146	10:20; 10:25 am	733.20, 732.97; 746.88, 746.03	740, 740	740 00
38	10:58:08 am	134	10.55; 11:00 am	839.79; 782 59	808	808 00
41	10:56:51 am	124	10:55, 11:00 am	736.54; 676 86	715	715 00
42	10:23:53 am	124	10:20; 10:25 am	692.73; 362 46	440	440 00
43	03:04:22 pm	124, 123	03:05 pm		736 54, 715 57	729 55
45	10:52:51 am	123, 122	10:50; 10.55 am	316.74, 290.04; 307.88, 313.04	313, 300	304 33
46	10:53:15 am	123, 122	10:50; 10:55 am	316.74, 290.04; 307.88, 313.04	312, 302	306 67
49	11:01:38 am	149	11.00; 11:05 am	435.63, 458.05	444	444 00
50	10:38:42 am	162	10.35; 10:40 am	304.11; 273 13	280	280 00

small fraction of this in the appropriate wavelength band is required to normalize the measured radiance.

Utilizing spectra collected by Harrington (1996, personal communication) (Figure 4.6) on-site during the flights, the total area under the curve and the area of the relevant wavebands (i.e., 665-675 nm, 695-705 nm) was determined and ratioed. This resulted in the fraction of incoming radiation in these wavebands with respect to incoming total solar radiation measured at the Micronet stations:

$$b = \text{spectral area}_{(\text{waveband})} \, / \, \text{spectral area}_{(\text{total})} \qquad (7)$$

This resulted in b(665-675) = 0.029844 and b(695-705) = 0.02433. Taking this into account, reflectance was calculated using

$$R = \pi L / bI \qquad (8)$$

where I is the irradiance interpolated in space and time from the Micronet data. The results are listed in Appendix B.

Step 6. Develop relationship between DN, radiance, and reflectance difference (700 nm - 670 nm) and chlorophyll-a surface concentration. This will result in the development of a model which best describes chlorophyll-a surface concentration from remotely sensed data.

As previously discussed, the difference between light reflectance, measured at 670 nm and 700 nm, is strongly related to the amount of chlorophyll-a present in a water body. This difference method is related to the first derivative method described by Han, et al. (1994), Rundquist, et al. (1996), and Schalles, et al. (1997).

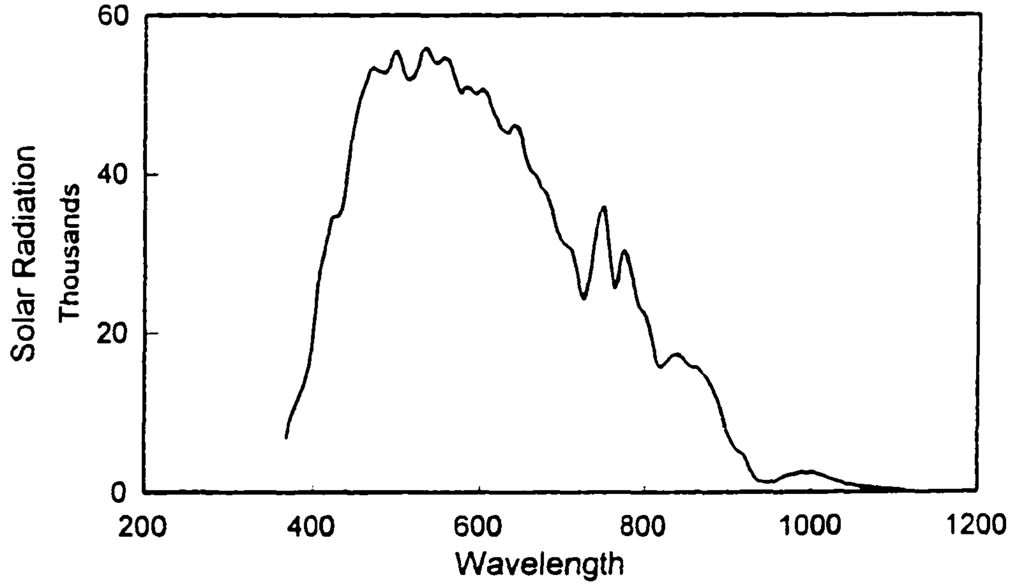

Figure 4.6. Incoming solar radiation (after Harrington, 1996, personal communication).

The initial images imported into IDRISI were simply digital number images in which each shade of gray of the black and white image is assigned a separate, though physically meaningless, value. For each of the 33 reservoirs, an average value for the 10x10 digital number pixel array was determined for each of the relevant wavelengths. The difference between DN at 700 nm and 670 nm was then calculated and compared to chlorophyll concentration for each reservoir (Figure 4.7). This process was also followed after processing the data into radiance and reflectance values (Figures 4.8 and 4.9).

Multiple models were analyzed before one was chosen that most reasonably and accurately described the relationship between chlorophyll-a surface concentration and remotely sensed data.

ILLUSTRATION

In order to illustrate the methods used in this study, the process of obtaining the data for reservoir #2 is described.

Step 1.

Aerial Images. The flight over reservoir #2 occurred on August 19, 1994 at 2:33:31 pm under cloudy conditions.

Chlorophyll Concentration. Water samples were collected and later analyzed in the laboratory with the result being a surface chlorophyll-a concentration of 5.24 mg/m^3.

Solar Radiation Data. Since data is collected every 5 minutes at the Micronet stations, solar irradiance at 2:30 pm and 2:35 pm was used in order to bracket the flight time of approximately 2:33 pm.

Step 2. Reservoir #2 was one of the reservoirs for which all of the data was available.

Figure 4.7. Chlorophyll concentration vs digital number.

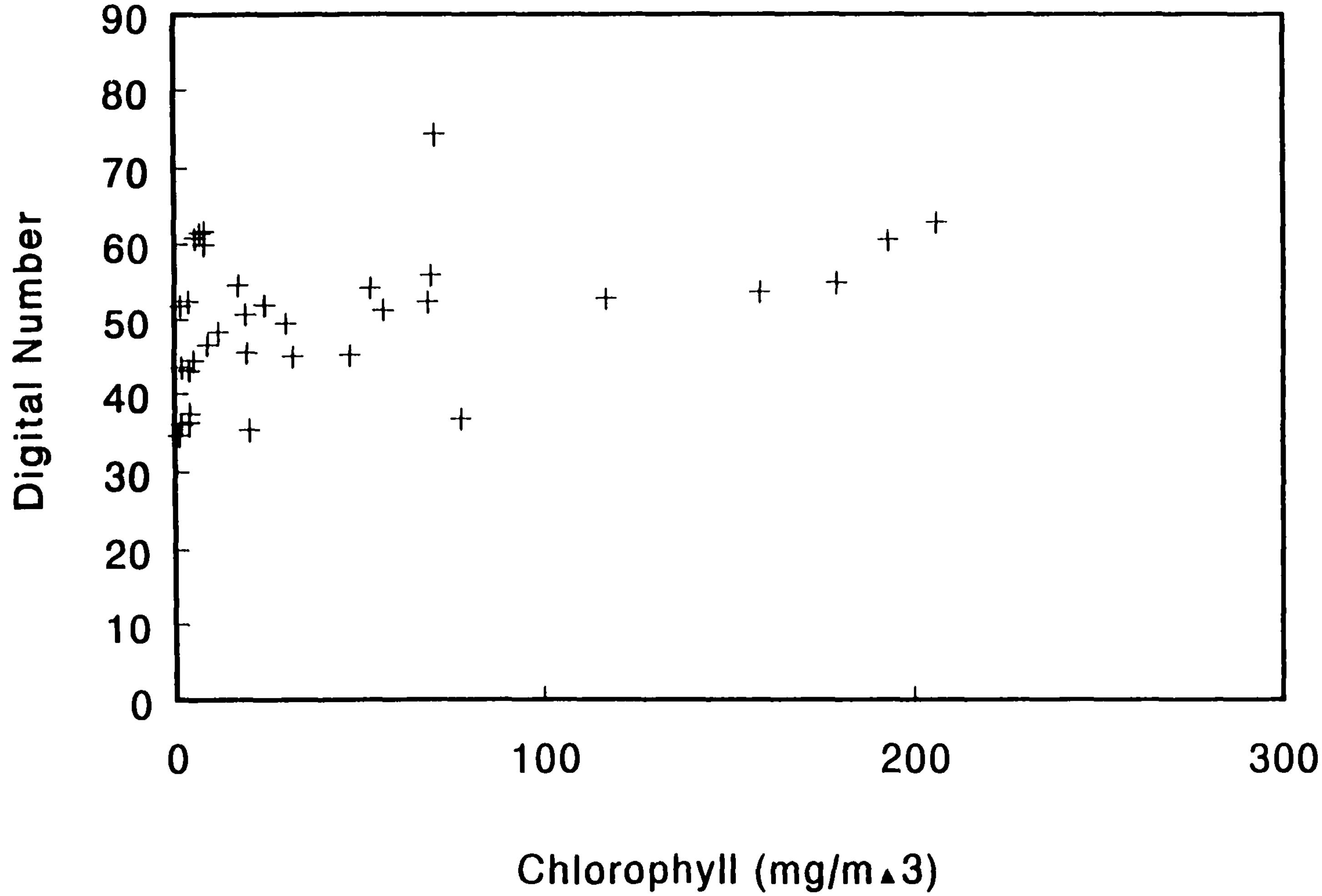

Figure 4.8. Chlorophyll concentration vs radiance.

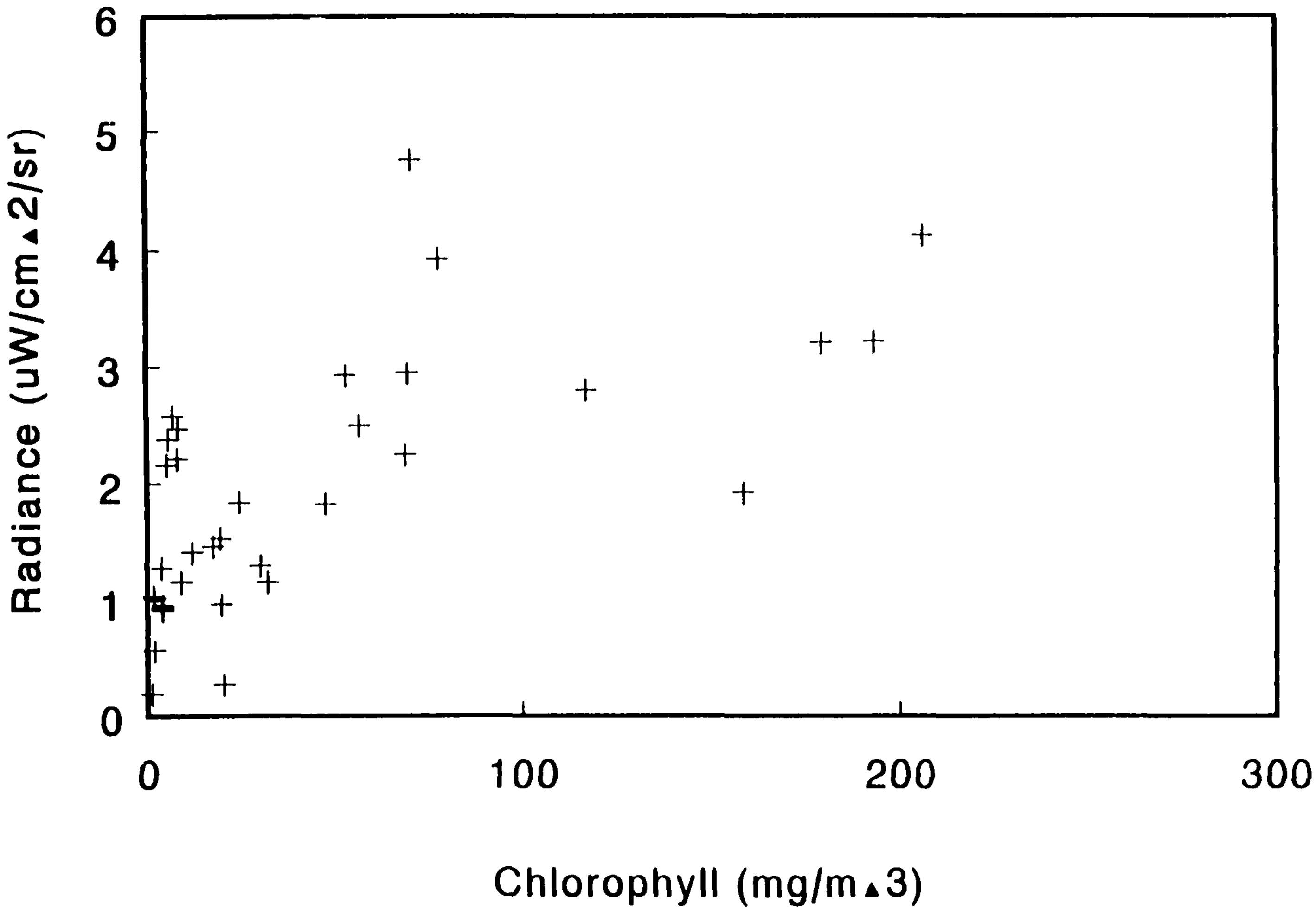

Figure 4.9. Chlorophyll concentration vs reflectance.

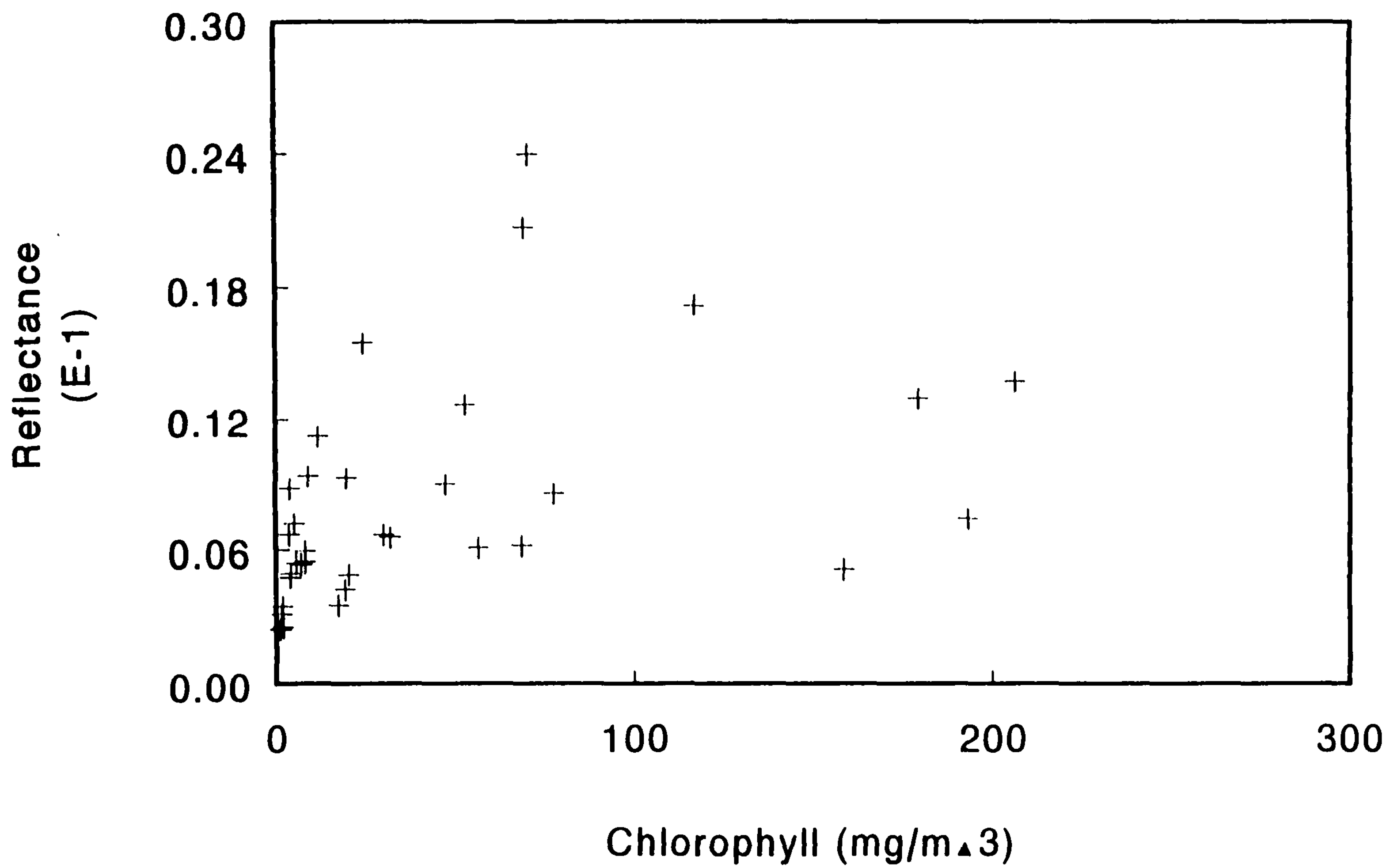

Step 3. The area chosen for analysis was near the dam in the same vicinity that the water sample was collected. The upper-left-hand-corner coordinates in IDRISI for the 10x10 pixel array analyzed were 93 (column), 288 (row) for the 670 nm image and 465, 222 for the 700 nm image. The average DN values from these 10x10 pixel arrays were calculated by IDRISI to be 35.33 at 670 nm and 79.75 at 700 nm.

Step 4. The DN values were converted into radiance values using the radiance equations for 670 nm and 700 nm. Radiance was calculated to be 6.75 uW/cm^2/sr for 670 nm and 8.91 uW/cm^2/sr for 700 nm.

Step 5. The UTM coordinates for the central portion of reservoir #2 were determined to be 601890.0 (x) and 3868102.5 (y). This location was determined in IDRISI using a satellite image of the Little Washita River watershed.

The nearest Micronet stations to reservoir #2 were stations #121 and 137. Since data is collected every 5 minutes at the Micronet stations, solar irradiance at 2:30 pm and 2:35 pm was used in order to bracket the flight time of approximately 2:33 pm. In Table 4.3, it can be seen that at 2:30 pm the irradiance at station #121 was 891.98 W/m^2 and at #137 was 681.93 W/m^2. At 2:35 pm irradiance was 467.59 W/m^2 at #121 and 717.27 W/m^2 at #137. Performing an interpolation in time for 2:33 pm, the irradiance at station #121 was determined to be approximately 577 W/m^2 and at station #137 approximately 706 W/m^2.

Using IDRISI, the coordinates of both Micronet stations (#121, #137) and their respective irradiance values (577 W/m^2, 706 W/m^2) at 2:33 pm were inserted. IDRISI then generated a surface "contour" map of irradiance values. Using the UTM coordinates of the reservoir, an irradiance value for the reservoir at 2:33 pm was approximated from the IDRISI map. This approximation for reservoir #2 was 611.40 W/m^2. This was the total amount of radiation reaching the sensor, however, so it must be corrected using Harrington's data (1996, personal communication) to represent only that amount of radiation in the relevant wavebands.

Radiance values (L) were converted into reflectance (R) using the equation $R=L\pi/Ib$ where b is the portion of the spectrum located in the relevant waveband. Reflectance was found to be 0.0116 for the 670 nm waveband and 0.0188 for the 700 nm waveband.

Result. As a result of the methods previously described, the data set for reservoir #2 used for subsequent analysis included a value of surface chlorophyll concentration (5.24 mg/m^3) and values for DN, radiance, and reflectance at 670 nm and 700 nm:

	670 nm	700 nm
DN	35.33	79.75
radiance	6.75	8.91
reflectance	0.0116	0.0188

Differences were then calculated for DN, radiance, and reflectance (44.42, 2.16 $uW/cm^2/sr$, 0.00719, respectively) and compared to chlorophyll concentration.

CHAPTER 5. MODEL DEVELOPMENT

INTRODUCTION

This chapter describes the various models used in attempting to predict chlorophyll concentration from airborne video data. From these models, a "best" model was chosen and described in detail. A discussion of the best model includes the sources of error present during the research and a chlorophyll sensitivity study.

Previously reported results indicate that the difference between emergent radiance in the 670 nm and 700 nm wavebands is related to chlorophyll-a concentration. This simple difference method between images taken in each of these wavebands is related to the first derivative method described by Han, et al. (1994) and Rundquist, et al. (1996). This study hypothesizes that the relationship between remotely sensed data and chlorophyll-a concentration (chl-a) should improve as the raw video data is processed into physically-meaningful radiance values and improve even further with normalization by solar irradiance data. In order to illustrate this improvement, several mathematical models were applied to the data and analyzed to determine which model most reasonably and accurately described the relationship between emergent radiance and chlorophyll-a concentration.

Some of the models were evaluated for linear trends, while others were nonlinear models. In all models, x represents the independent variable of chlorophyll-a concentration, while y is representative of the dependent variables digital number (DN), radiance (L), or reflectance (R). Simple linear and logarithmic (log) models were examined as well as other linear models including a simple transformation equation ($1/y = a_0 + a_1/x$) and a variation of the Normalized Difference Vegetation Index (NDVI). The nonlinear $y = a_0(1-e^{-x/c})$ of Schiebe et al. (1987) was also evaluated. SlideWrite was the program used for statistical analysis. It applies linear least squares regression analysis for linear curve fits and the Levenberg-Marquardt algorithm to estimate coefficients for nonlinear curve fitting. This algorithm is an iterative process beginning with estimates of the unknown coefficients and continues until the best fit coefficients are found. Like linear least squares analysis, the best coefficients are those that minimize the sum of squared deviations, or Chi-squared. The equation used to calculate r^2 is

$$r^2 = 1 - [(\Sigma(y_i - Y_i)^2)/(\Sigma(y_i - M)^2)] \qquad (1)$$

where y_i = the actual value

Y_i = the value predicted by the equation

M = the mean of the data.

EVALUATION AND CALIBRATION OF VARIOUS MODELS

Linear and Logarithmic Models

Linear regression of the digital number data yielded a coefficient of determination (r^2) of 0.157, while r^2 = 0.424 for the radiance data and 0.171 for the reflectance data (Figures 5.1 - 5.3). Linear regression performed on the log of y yields r^2 values of 0.197, 0.429, and 0.361 for digital number (DN), radiance, and reflectance, respectively (Figures 5.4 - 5.6). In both cases, there is significant improvement in predicting chl-a concentration after processing the raw video data (DN) into radiance values. This would be expected since the raw data was not calibrated and converting to radiance served to do so. Further improvement was expected after incorporation of irradiance data but only occurred for the log model.

Figure 5.1. Linear plot of digital number data.

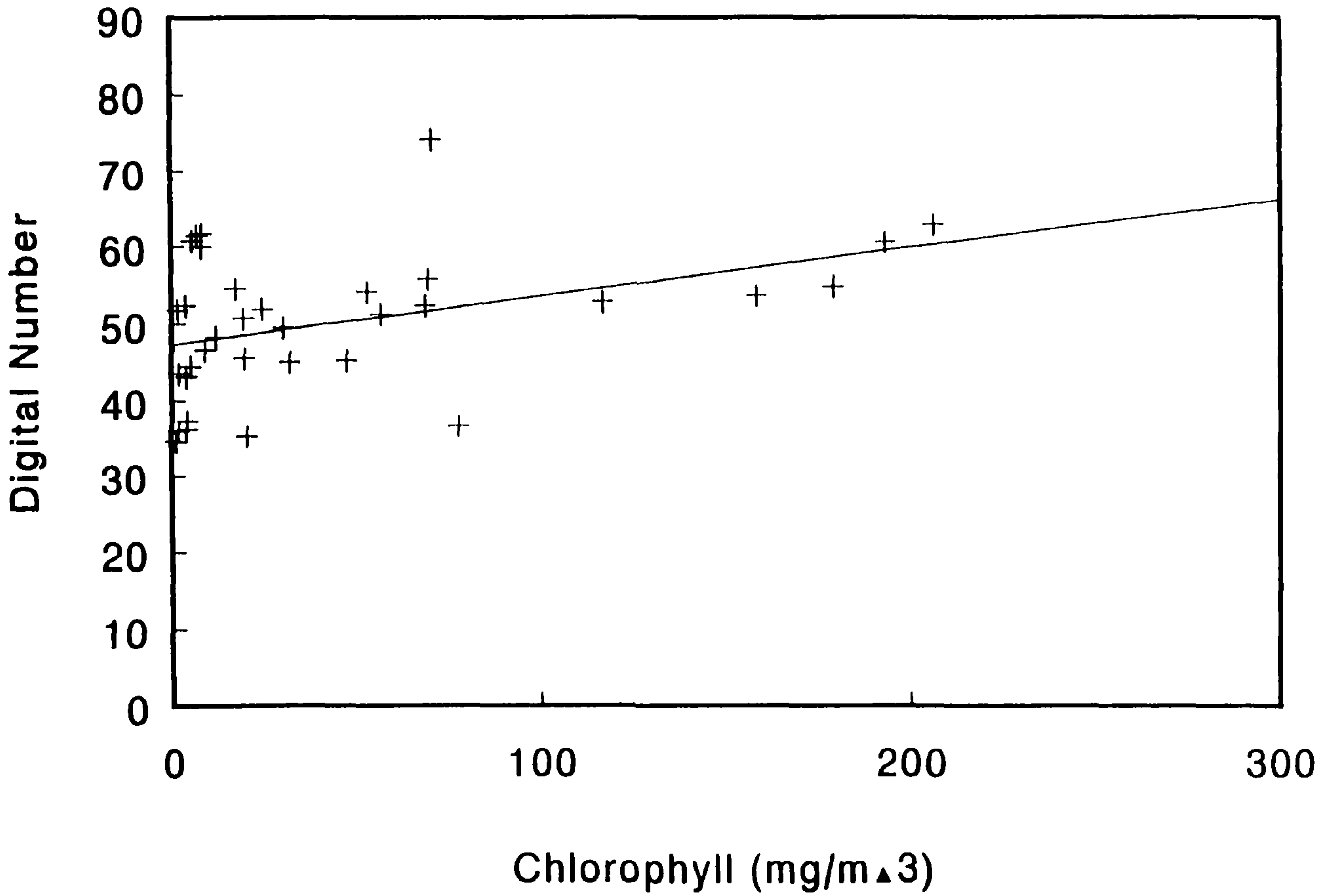

Figure 5.2. Linear plot of radiance data.

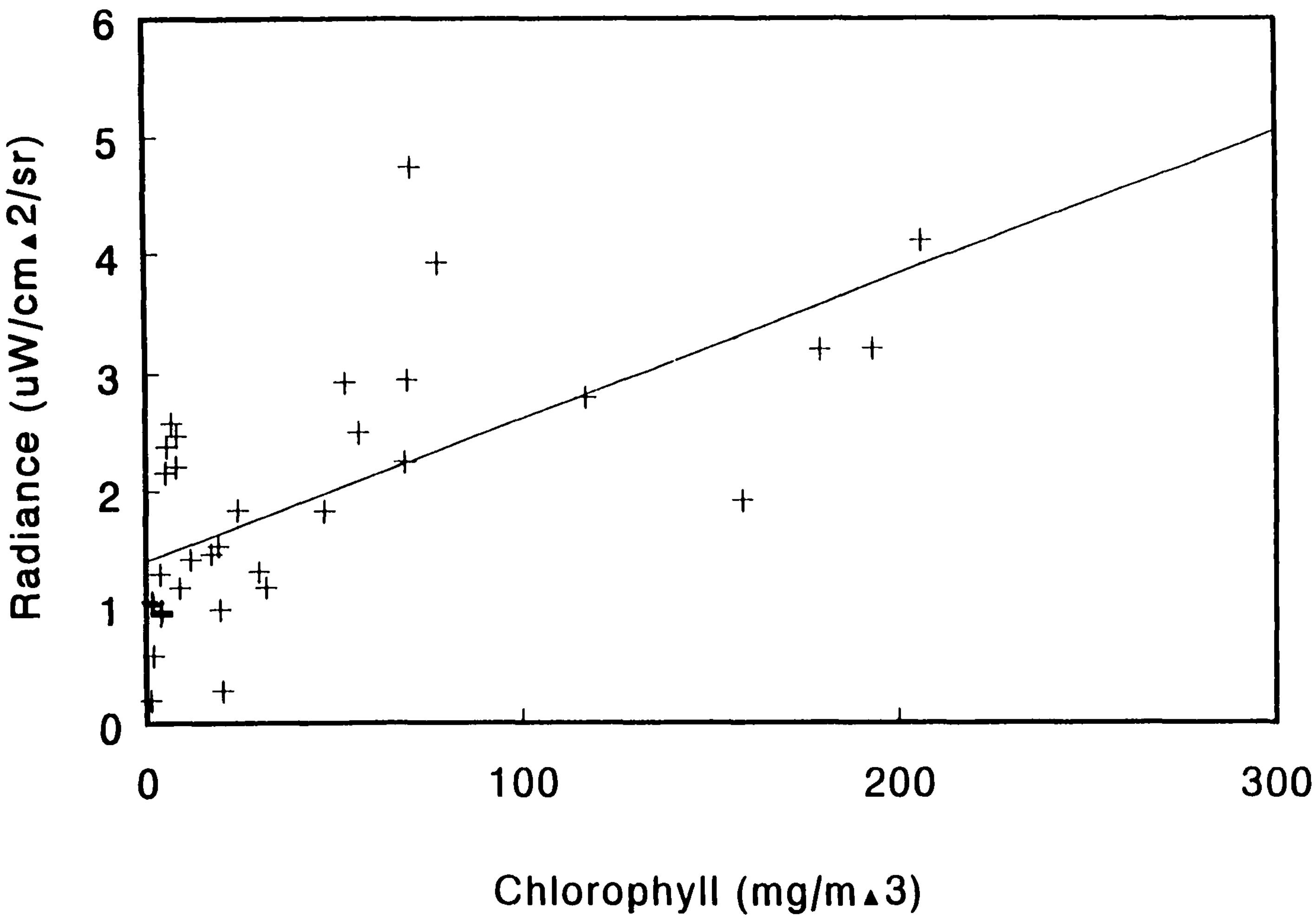

Figure 5.3. Linear plot of reflectance data.

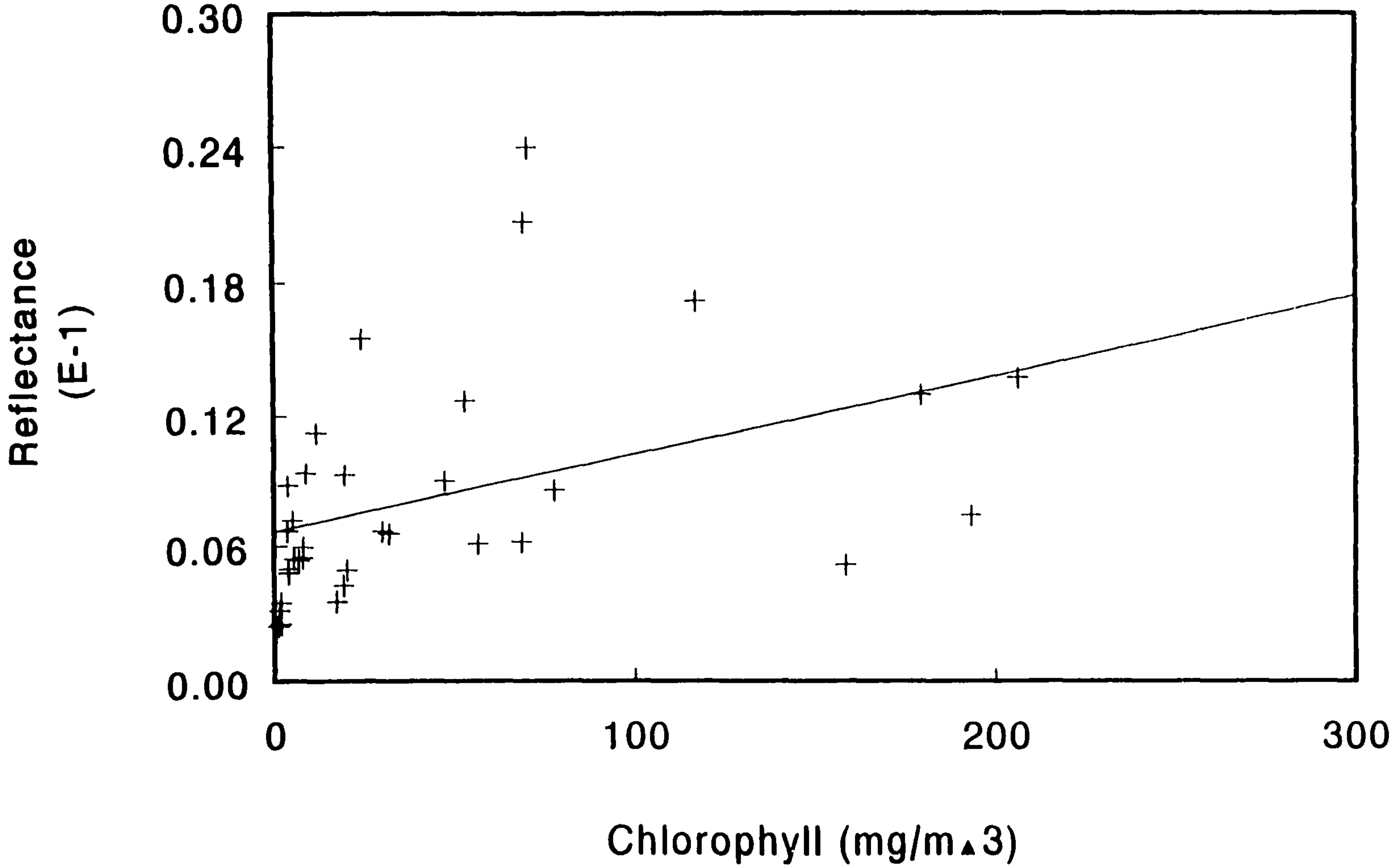

Figure 5.4. Logarithmic plot of digital number data.

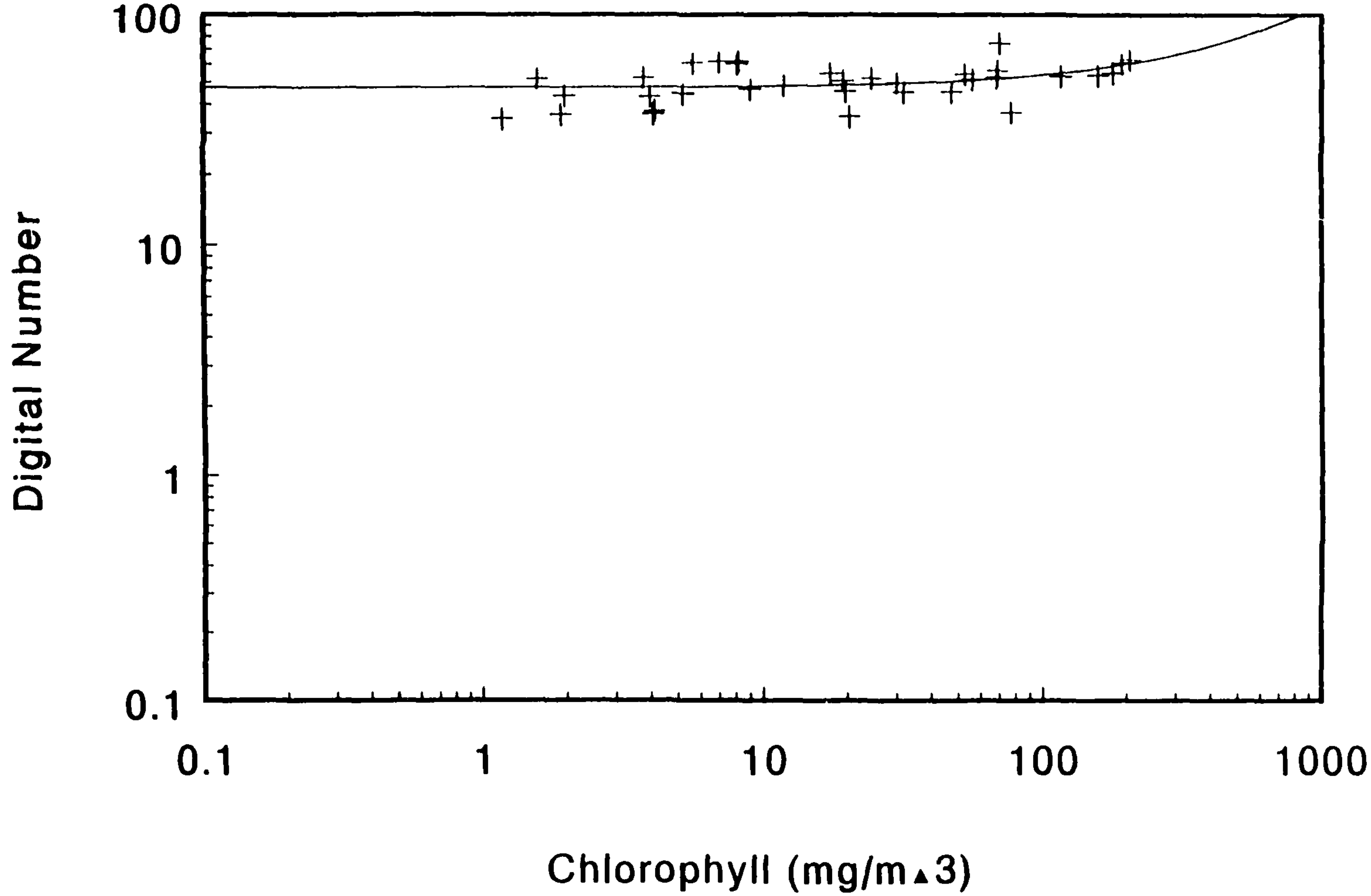

Figure 5.5. Logarithmic plot of radiance data.

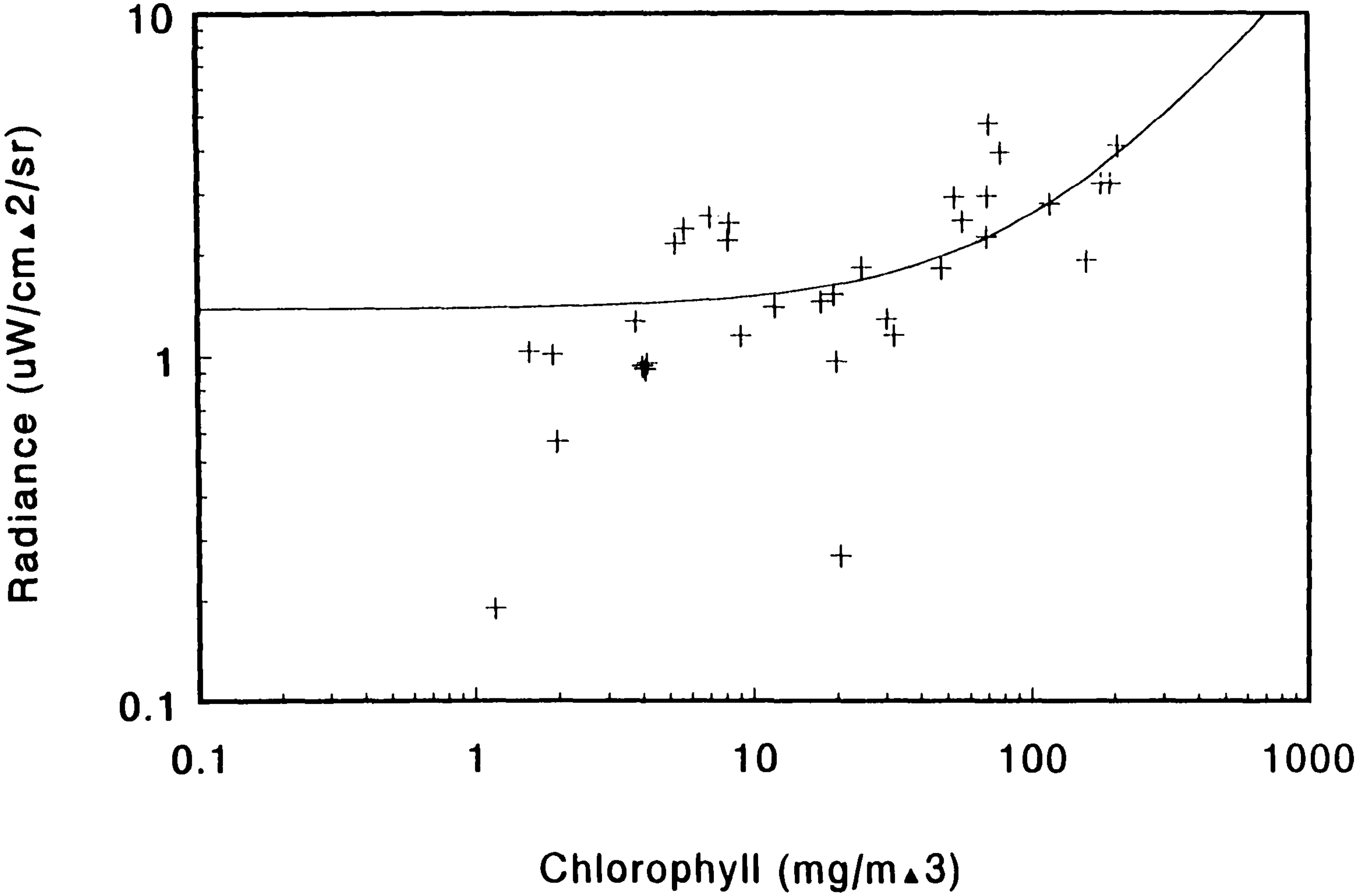

Figure 5.6. Logarithmic plot of reflectance data.

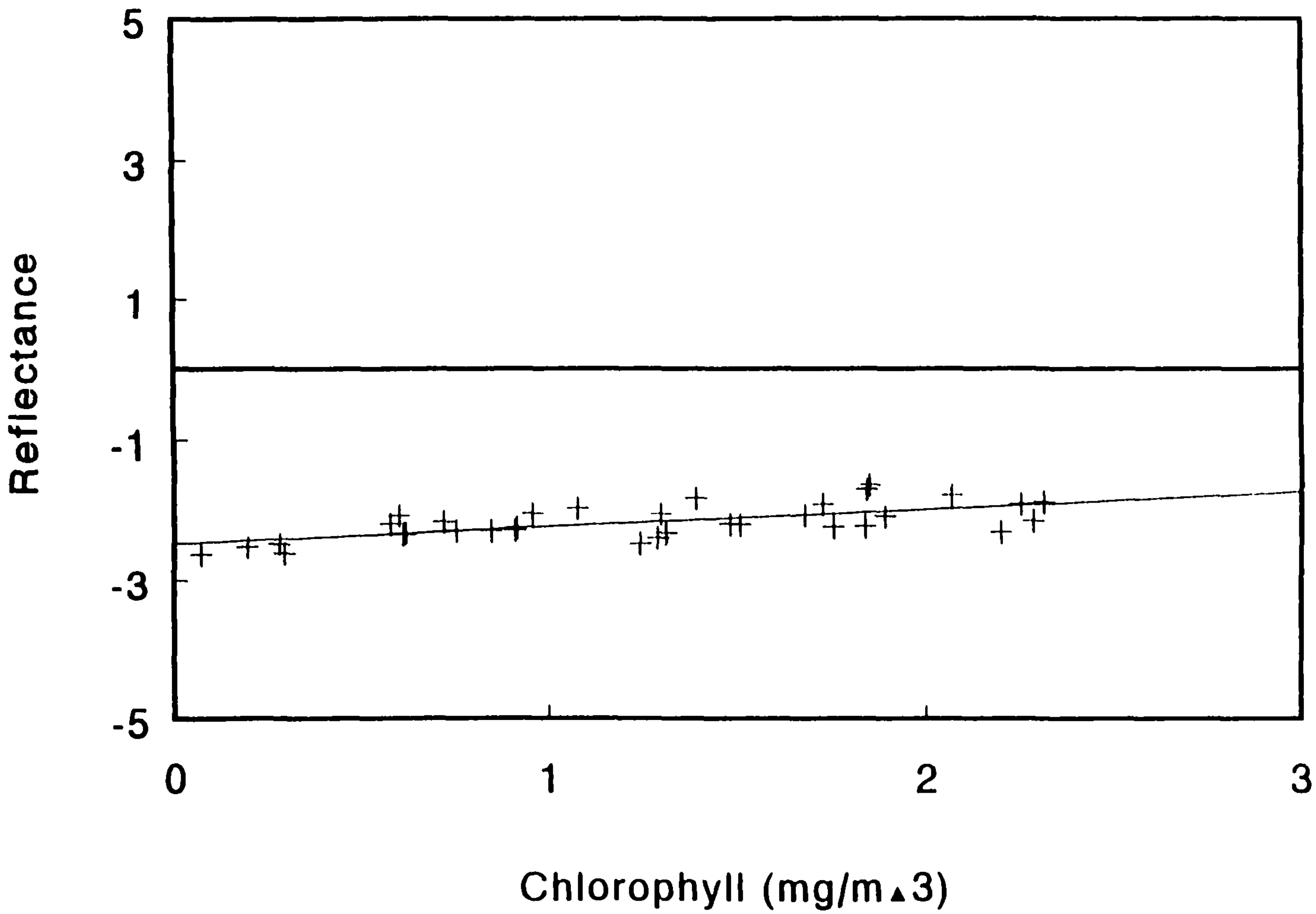

Reflectance for the linear model did not predict chlorophyll-a concentration more accurately than the unprocessed video data. The log of the data did, however, show a slight improvement in the ability to predict chlorophyll-a concentration from reflectance data.

Best Statistical-Fit Model

A simple transformation of the data in the form

$$1/y = a_0 - a_1/x \qquad (2)$$

yielded the best fit between reflectance and chlorophyll concentration ($r^2 = 0.618$). Similar transformations applied to the digital number and radiance data yielded r^2 values of 0.219 and 0.391, respectively. This relationship best described the expected improvements as processing proceeded: reflectance predicted chlorophyll concentration better than radiance and digital number. Prediction potential was greater both after initial processing into units of radiance and after incorporation of the irradiance data in determining reflectance values. This method, however, is purely statistical in nature, and it is difficult to determine the physical meaning of a_0 and a_1.

Other Models.

In order to describe the data, several other models were analyzed including the Michaelis-Menton equation ($y=x/(c+x)$), a variation of the NDVI (700nm-670nm/700nm+670nm), and a model developed by Schiebe, et al. (1987) which predicts reflectance as related to the scattering of light in water:

$$y = a_0(1-e^{-x/c}) \qquad (3)$$

The Michaelis-Menton equation did not yield good results. It indicated that the chlorophyll constant (c) was negative for both digital number and radiance data. This is not physically possible. As a result, this equation will not be discussed further.

The NDVI is commonly used in remote sensing applications because it compensates for differences in illumination and surface slope. NDVI is normally calculated using the wavelengths of 850 nm and 630 nm (850nm-630nm/850nm+630nm) rather than the 700 nm and 670 nm bands used in this study. It is proposed that a similar equation utilizing the 700 nm and 670 nm wavebands be used and referred to as the Normalized Red-Edge Index (NREI). NREI would, therefore, be calculated

$$\text{NREI} = 700\text{nm}-670\text{nm}/700\text{nm}+670\text{nm} \qquad (4).$$

The results of the NREI calculation for the reservoirs in this study were 0.31 to 0.80 for DN, 0 to 0.31 for radiance, and 0.11 to 0.40 for reflectance. Comparing NREI to chlorophyll concentration, r^2 was 0.0007 for DN, 0.3262 for radiance, and 0.3263 for reflectance (Figures 5.7 - 5.9). NREI predicted an improvement in processing DN data into physically-based radiance values but no improvement as a result of incorporating solar irradiance data.

The model developed by Schiebe, et al. (1987) ($y=a_0(1-e^{-x/c})$) is based on the physics of light scattering from particles suspended in water. It describes a saturating exponential relationship with a_0 being the asymptotic value, reflectance, and c representing a chlorophyll constant. To ensure that reasonable results were obtained when evaluating this equation, visual estimates of a_0 and c were determined by inspection of scatterplots of the data:

Figure 5.7. NRET plot of
digital number data.

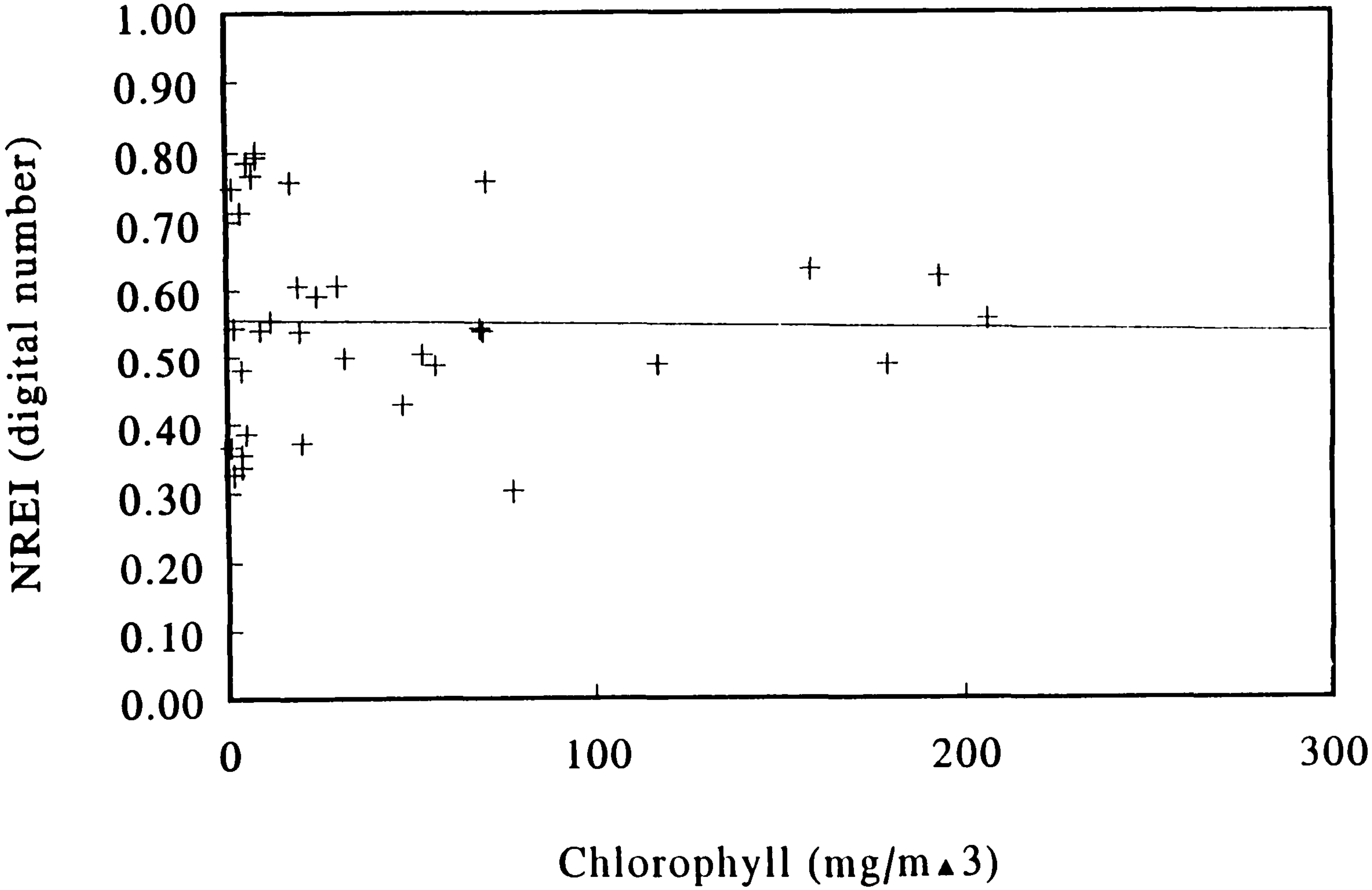

Figure 5.8. NREI plot of
radiance data.

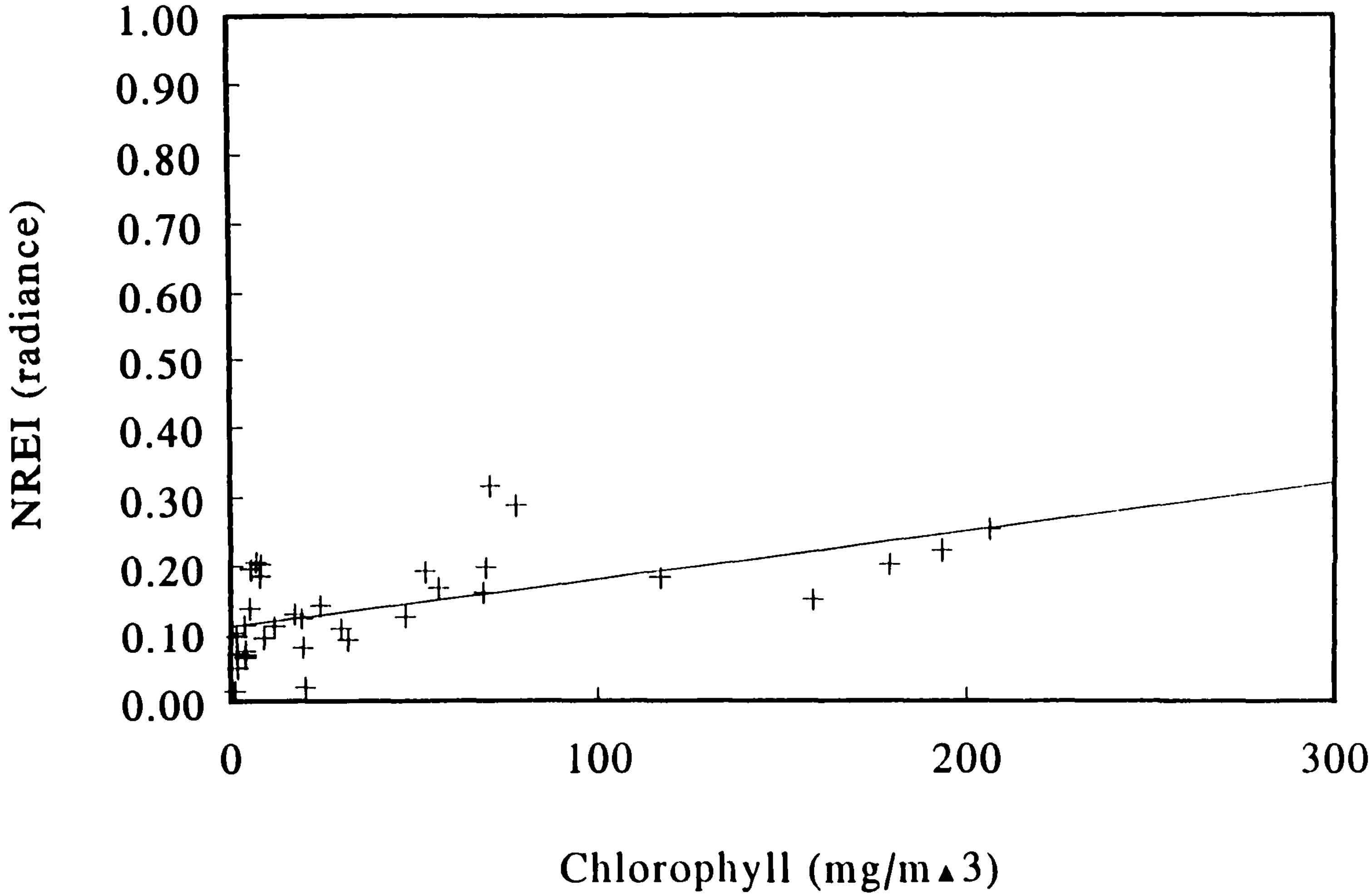

Figure 5.9. NREI plot of reflectance data.

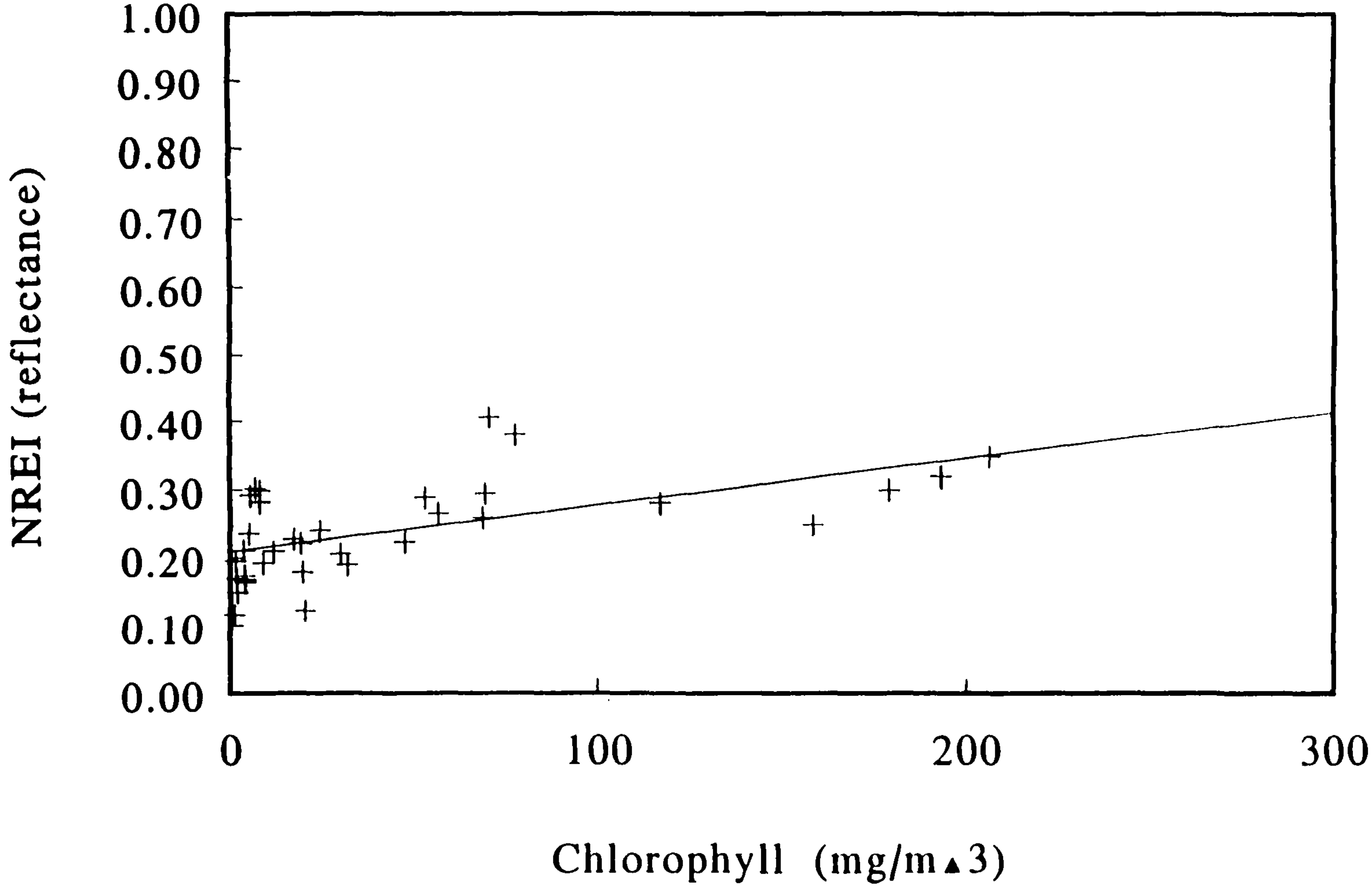

$$y_{DN} = 55(1-e^{-x}) \qquad (5) \qquad \text{(Figure 5.10)}$$

$$y_{Rad} = 3.25(1-e^{-x/25}) \qquad (6) \qquad \text{(Figure 5.11)}$$

$$y_{Refl} = .014(1-e^{-x/7}) \qquad (7) \qquad \text{(Figure 5.12)}$$

The equation was then evaluated in two ways: (1) use of a computer method - allowing the computer to choose the best values of a_0 and c using an iterative, least-squares algorithm, and (2) use of a manual method - manually inserting various values for c and having the computer minimize error to find a_0. The computer-generated values are shown in Table 5.1.

Table 5.1. Computer-generated fit of physical model.

y	r^2	equation
DN	0.184	y=51.7(1-exp(-x/1.1))
Radiance	0.364	y=2.5(1-exp(-x/6.6))
Reflectance	0.349	=.0108(1-exp(-x/7.6)

Other than the chlorophyll constant, c, for radiance, the computer analysis provided results similar to those derived from the visual estimates. The term c should, however, theoretically be a constant since the physical characteristics of chlorophyll are consistent, so the second method mentioned above was performed.

Using the equation $y = a_0(1-e^{-x/c})$, various values of c were input and a_0 minimized (Table 5.2). From the table it can be seen that the best value of c would be between 40 and 50 since both radiance and reflectance have relatively high r^2 values in that range. For a value of $c = 40$, there is a slight improvement when processing DN ($r^2 = 0.528$) into radiance ($r^2 = 0.634$) and no real improvement with the incorporation of solar irradiance data in determining reflectance ($r^2 = 0.533$).

Figure 5.10. Visual estimate of data fit for digital number.

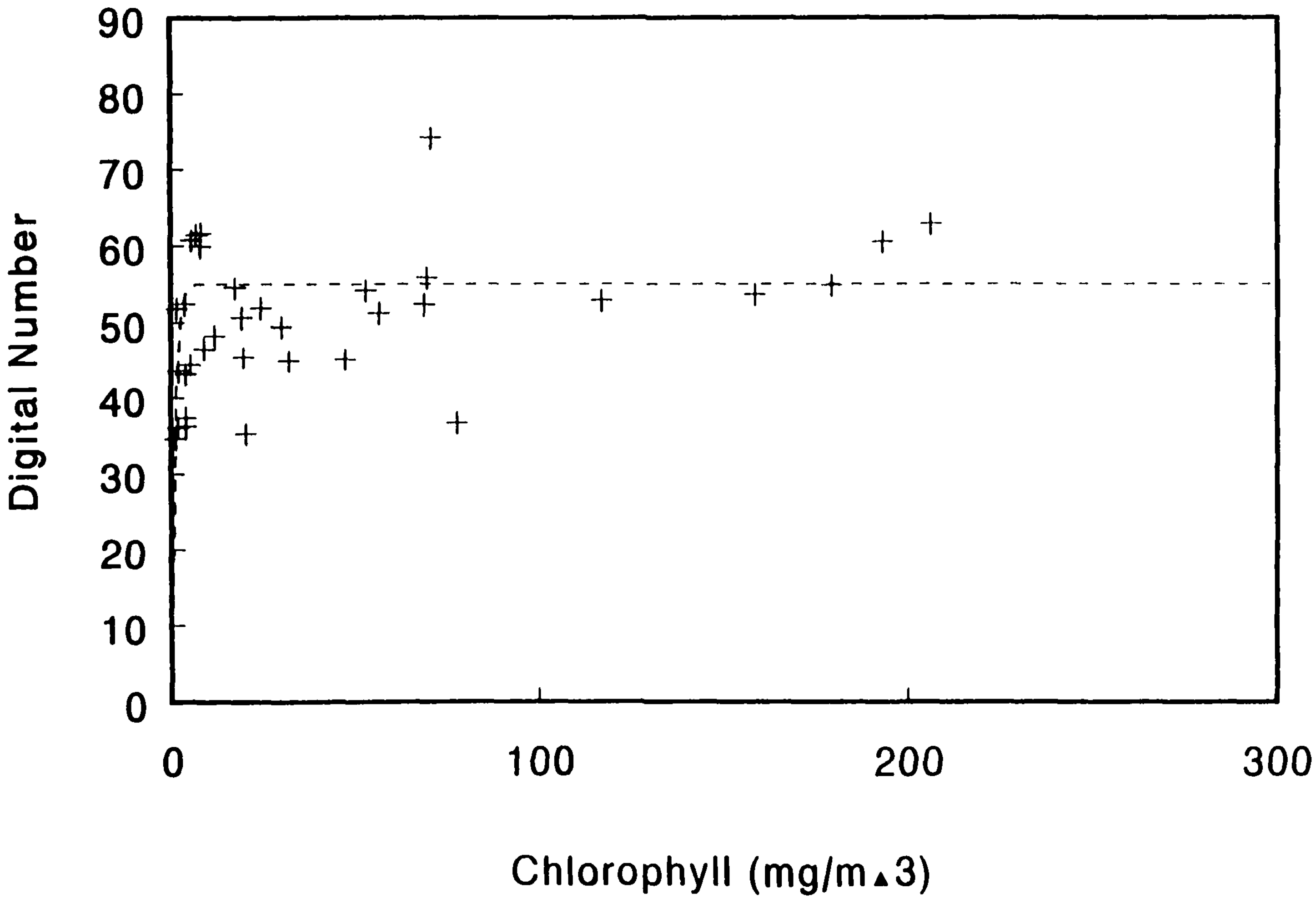

Figure 5.11. Visual estimate of data fit for radiance.

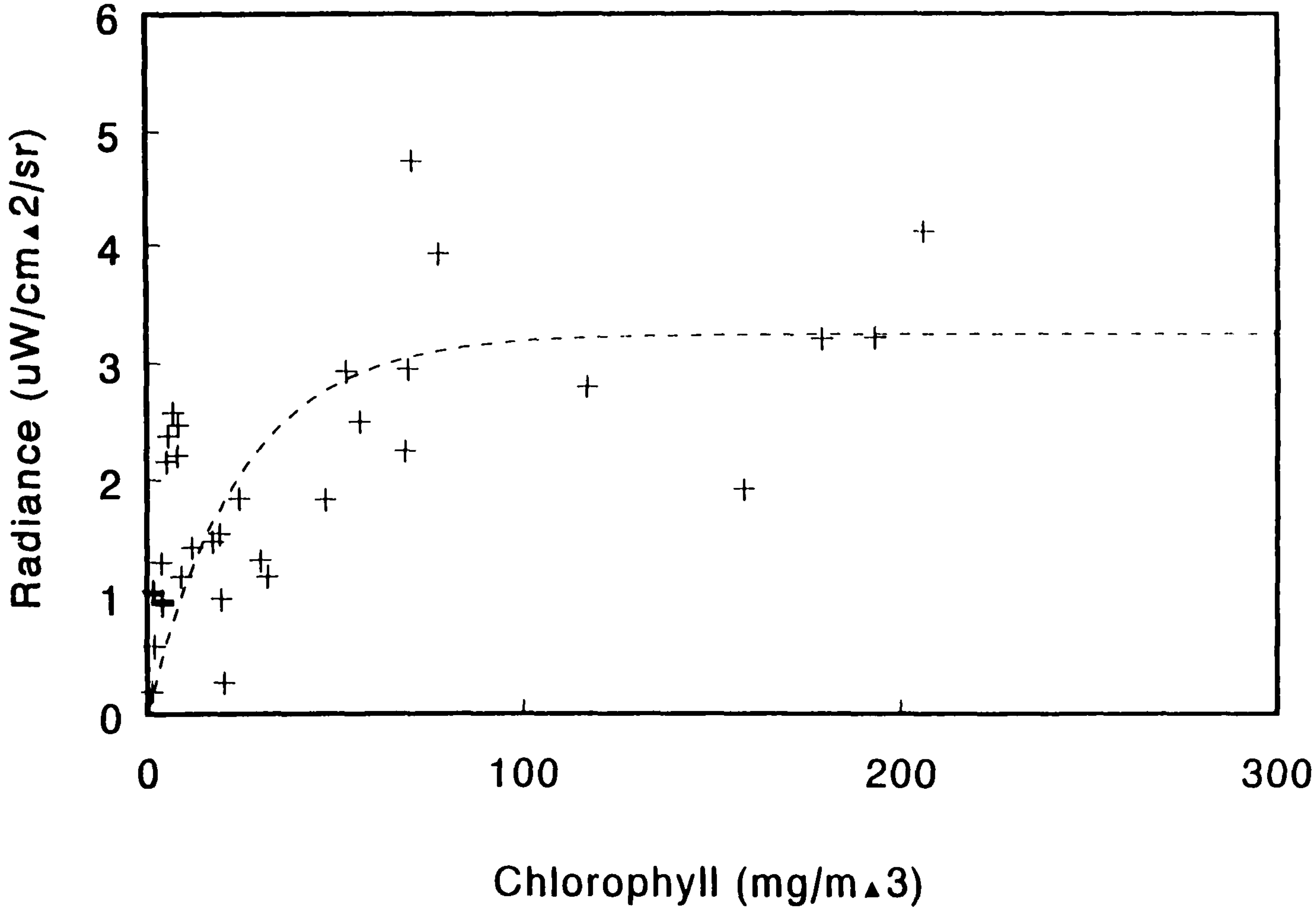

Figure 5.12. Visual estimate of data fit for reflectance.

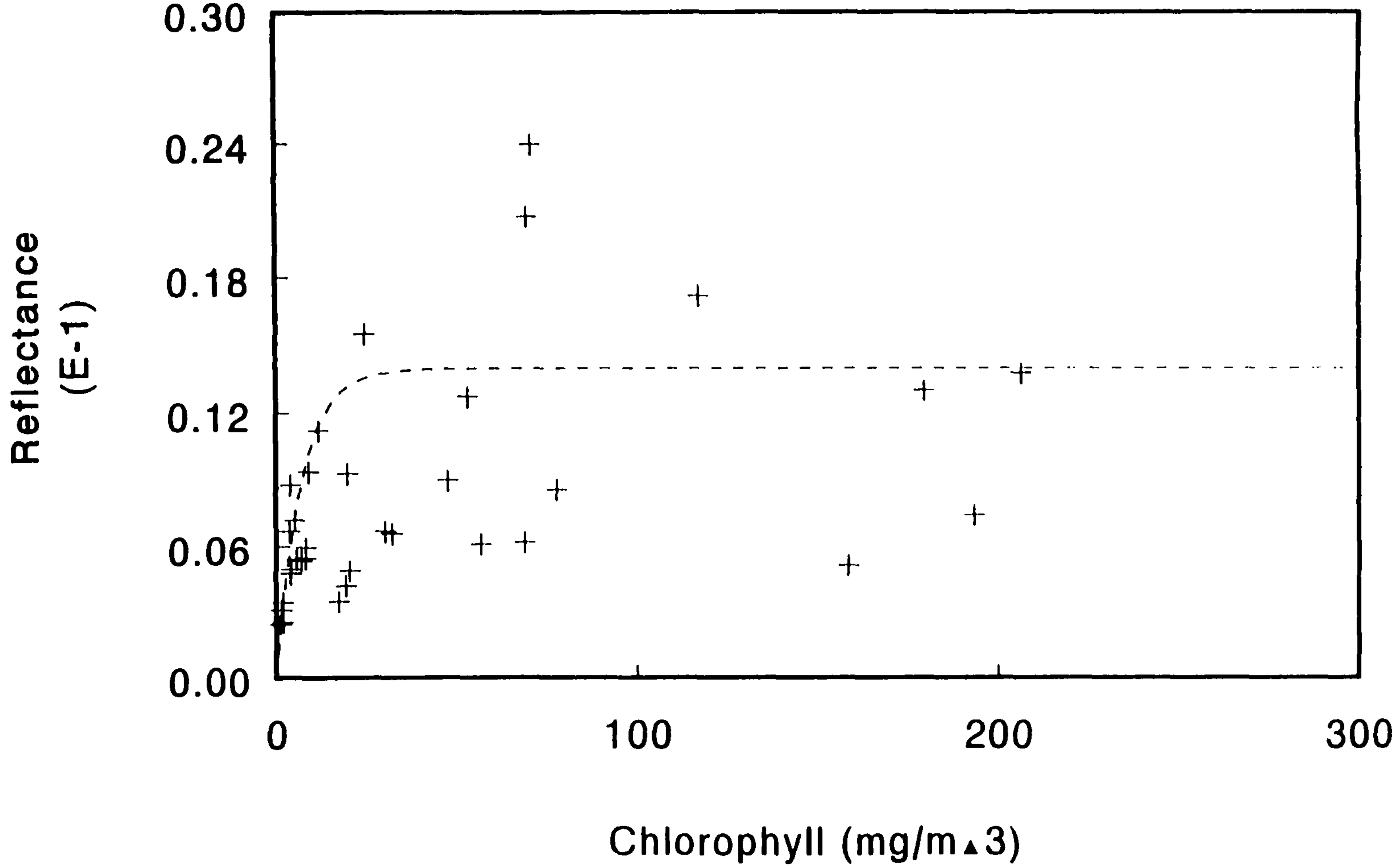

Evaluation of the physical model using $c = 40$ will subsequently be referred to as the manual model.

Table 5.2. r^2 for various values of c.

	5	10	15	20	25	30	35	40	45	50	55
DN	0.528	**0.53**	**0.53**	0.529	0.529	0.528	0.528	0.528	0.528	0.527	0.527
Rad	0.299	0.434	0.456	0.576	0.603	0.619	0.629	0.634	**0.638**	**0.639**	**0.639**
Refl	0.255	0.384	0.404	0.502	0.519	0.527	**0.532**	**0.533**	**0.533**	**0.532**	0.531

Comparisons of the various models are illustrated in Figures 5.13 - 5.15. In summarizing r^2 statistics, regardless of the mathematical model chosen, an improvement was noticed when processing raw video data into physically-meaningful radiance values (Table 5.3).

Table 5.3. r^2 Summary Table

model	DN	Radiance	Reflectance
linear	0.157	0.424	0.171
log-log	0.197	0.429	0.361
NREI	0.001	0.326	0.326
Physical			
computer	0.184	0.364	0.354
manual	0.527	0.638	0.533
Statistical	0.219	0.391	0.618

Incorporating solar irradiance data did not significantly improve results for any method except the best statistical-fit model. It is apparent that the noise, or scatter, introduced by the diffuse light of the overcast sky inhibited improvement by the normalization process. Under clear sky conditions, a much cleaner data set would have been expected.

Figure 5.13. Comparison of models for digital number.

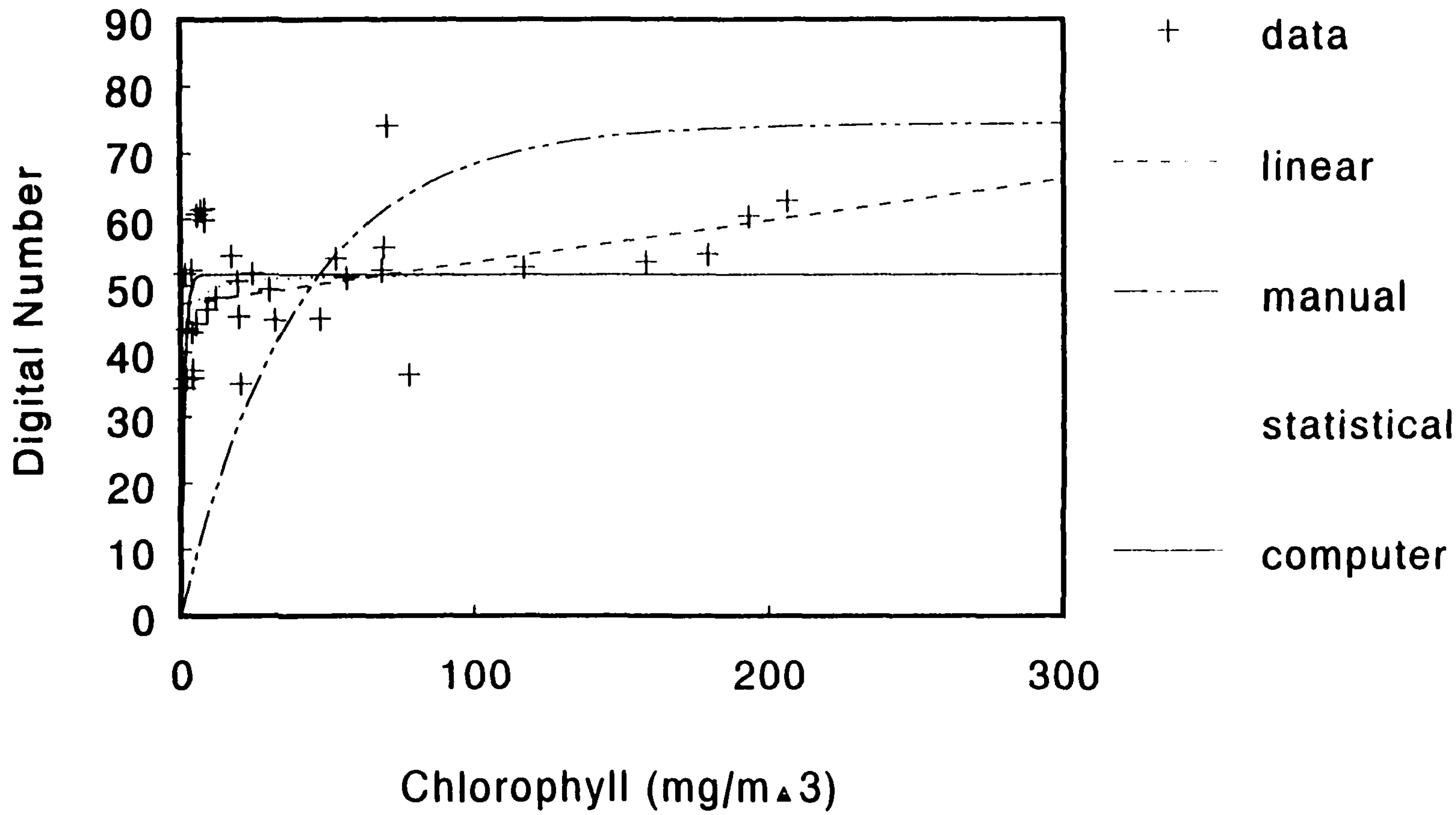

Figure 5.14. Comparison of models for radiance.

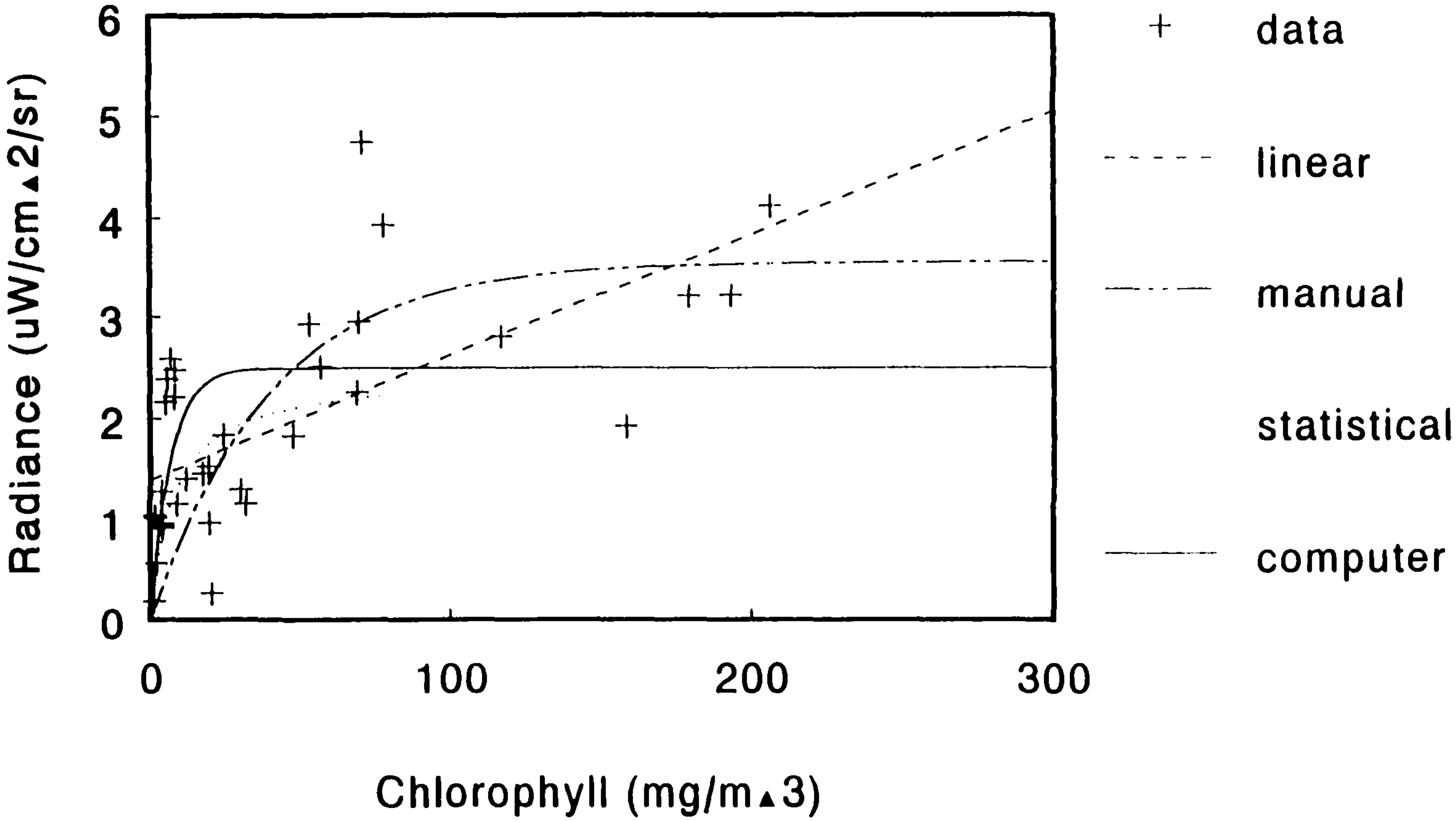

Figure 5.15. Comparison of models for reflectance.

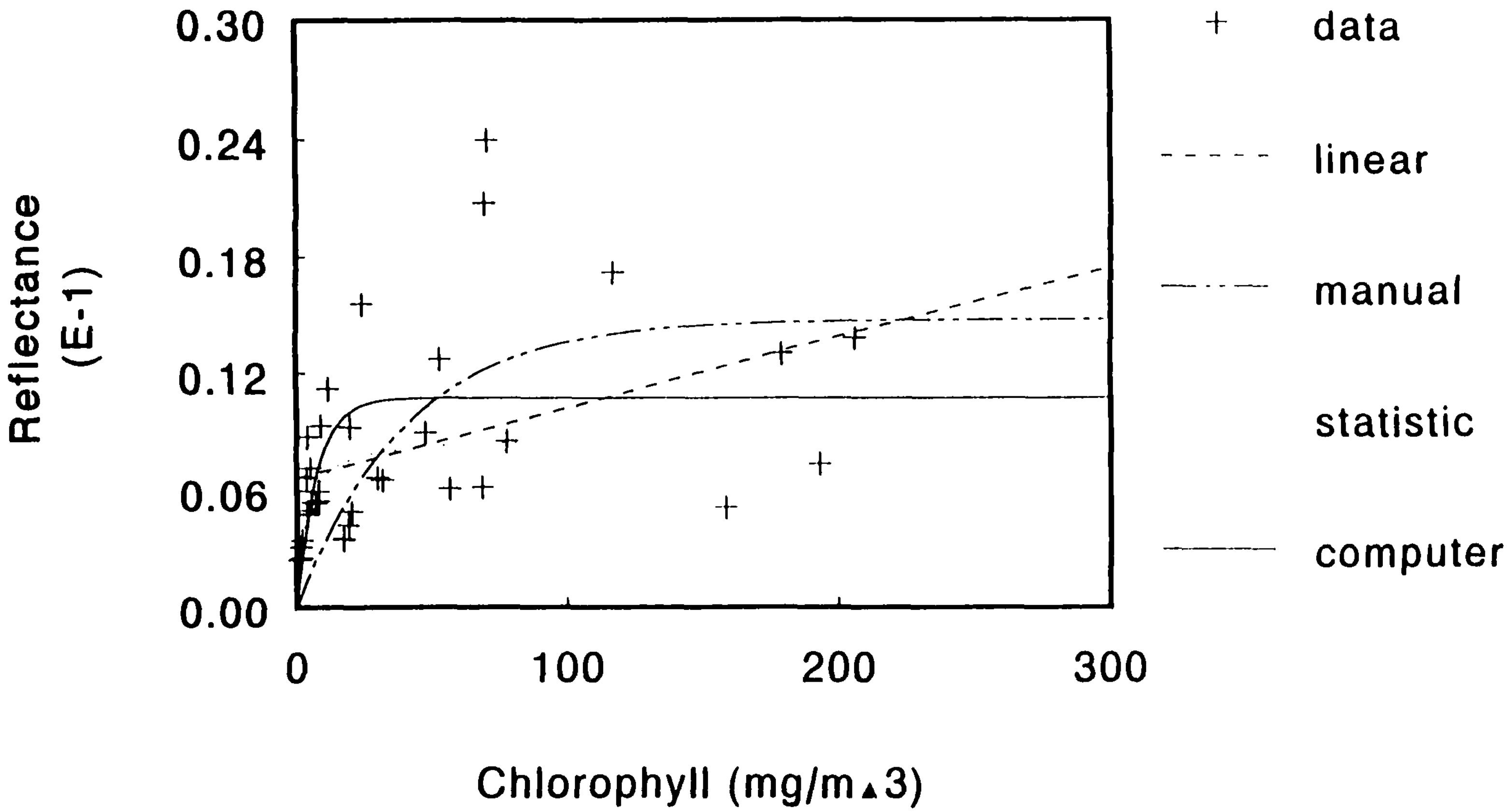

Therefore, the model which best describes the data was the manual version of the physical model:

$$y = a_0(1 - e^{-x/40}) \qquad (8).$$

Complementary Statistics

There is some question about whether r^2 is a reliable measure of model evaluation since the value of r^2 is not consistently related to the accuracy of prediction (Willmott, 1982). For example, large differences between model-predicted and observed values may produce r^2 values near 1, while small variations may result in high r^2 values. This would indicate that the relationship between r^2 and model performance is not well-defined or consistent. Therefore, when using statistical methods to analyze a data set, it is beneficial to examine several goodness-of-fit measures for additional validation. In addition to r^2, the d-statistic (Willmott, 1982) and the root mean square error (RMSE) were evaluated for the models.

D-Statistic. The d-statistic (d-stat) was proposed as an alternative method of evaluating goodness-of-fit by Willmott (1982):

$$d = 1 - [\Sigma(Yi - y_i)^2 / \Sigma(\|Y_i - M\| + |y_i - M|)^2] \qquad (9)$$

where y_i = the actual value

Y_i = the value predicted by the equation

M = the mean of the data.

It is interpreted in the same manner as r^2. A d-stat of 0 indicates no correlation between the model and the data, while 1 is indicative of a perfect fit.

Table 5.4. D-Statistic Summary Table

model	*DN*	*Radiance*	*Reflectance*
linear	0.500	0.758	0.501
log-log	0.227	0.502	0.004
NREI	0.014	0.440	0.222
Physical			
computer	0.490	0.709	0.686
manual	0.426	0.815	0.731
Statistical	0.516	0.706	0.517

Table 5.4 illustrates that the d-stat exhibited the same trend as r^2 for all the models evaluated: radiance predicted chlorophyll-a concentration better than DN, but there was no improvement, and in some cases was worse, with the incorporation of solar irradiance data. Unlike r^2, however, the d-stat showed significant improvement when converting into radiance units. The r^2 had only indicated a very slight improvement with calibration.

Root Mean Square Error (RMSE). In addition to r^2, the root mean square error is commonly used to evaluate goodness-of-fit:

$$RMSE = \sqrt{\Sigma(y_i - Y_i)^2 / n} \qquad (10)$$

where y_i = the actual value

Y_i = the value predicted by the equation

n = the number of data points.

The closer the RMSE is to zero, the better the model fits the data. The results are summarized in Table 5.5.

Table 5.5. RMSE Summary Table

model	DN	Radiance	Reflectance
linear	8.680	0.849	0.005
log-log	0.077	0.262	0.222
NREI	0.150	0.060	0.058
Physical			
computer	8.760	0.936	0.004
manual	29.240	0.976	0.005
Statistical	0.004	0.790	56.760

For all of the models except the log-log and statistical models, the RMSE indicates that the prediction of chlorophyll concentration improves with processing. These results are misleading, however, because the RMSE does not account for scale. The improvement in RMSE actually represents the change in scale between the three parameters. Since the scales of DN, radiance, and reflectance differ by a factor of at least 10, the RMSE is detecting this change rather than a true change in the ability to predict chlorophyll concentration.

Since the scale of the three data sets varies, the data was normalized in order to attempt to effectively evaluate RMSE. This was accomplished by dividing each data set by the maximum value in that set (Figures 5.16 - 5. 18).

Table 5.6. RMSE (corrected) Summary Table

model	DN	Radiance	Reflectance
linear	0.117	0.179	0.197
log-log	0.077	0.262	0.222
NREI	0.150	0.060	0.058
Physical			
computer	0.118	0.197	0.185
manual	0.394	0.205	0.210
Statistical	0.268	3.750	1.360

Figure 5.16. Plot of digital number data normalized by the maximum value.

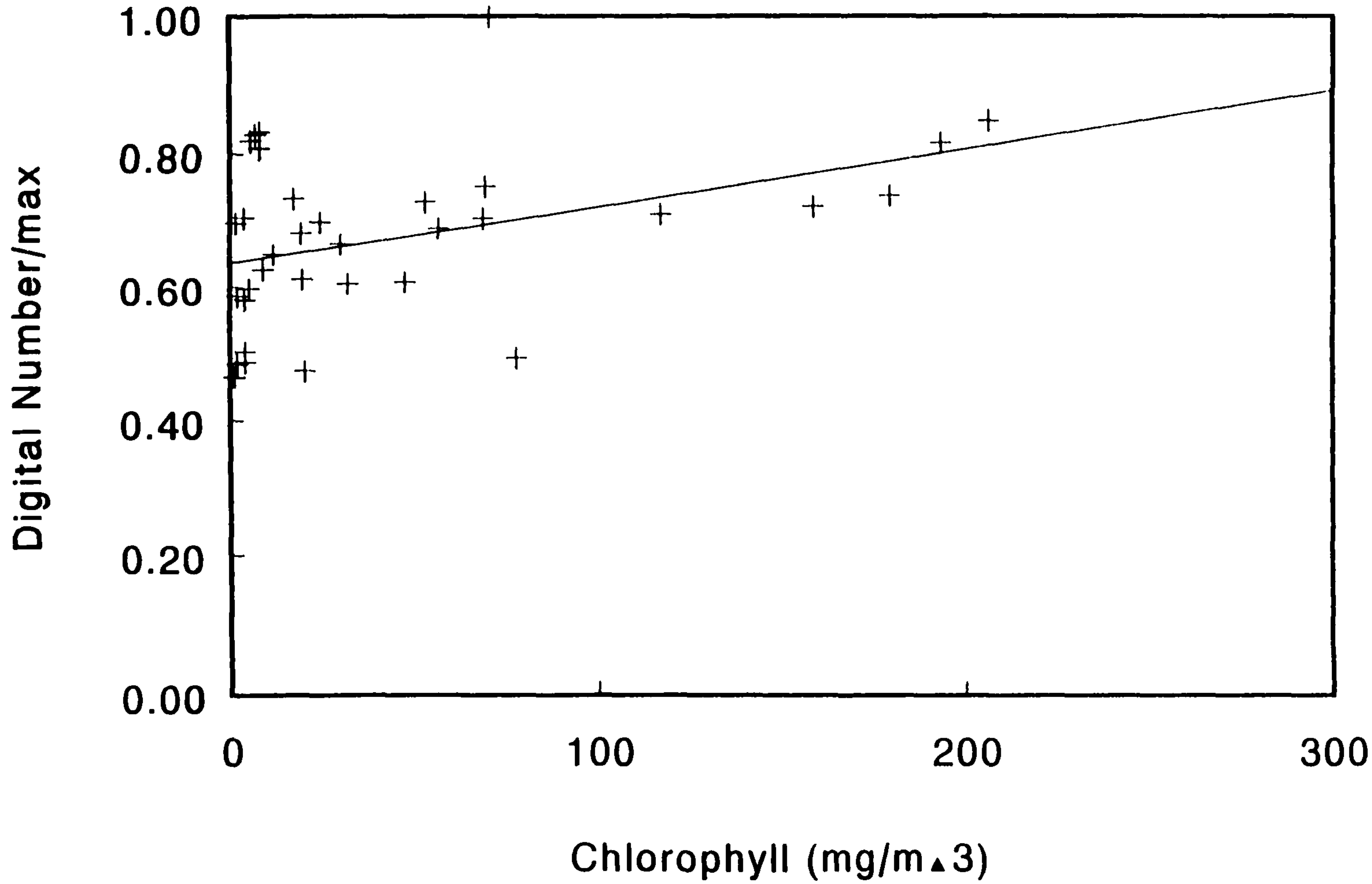

Figure 5.17. Plot of radiance data normalized by the maximum value.

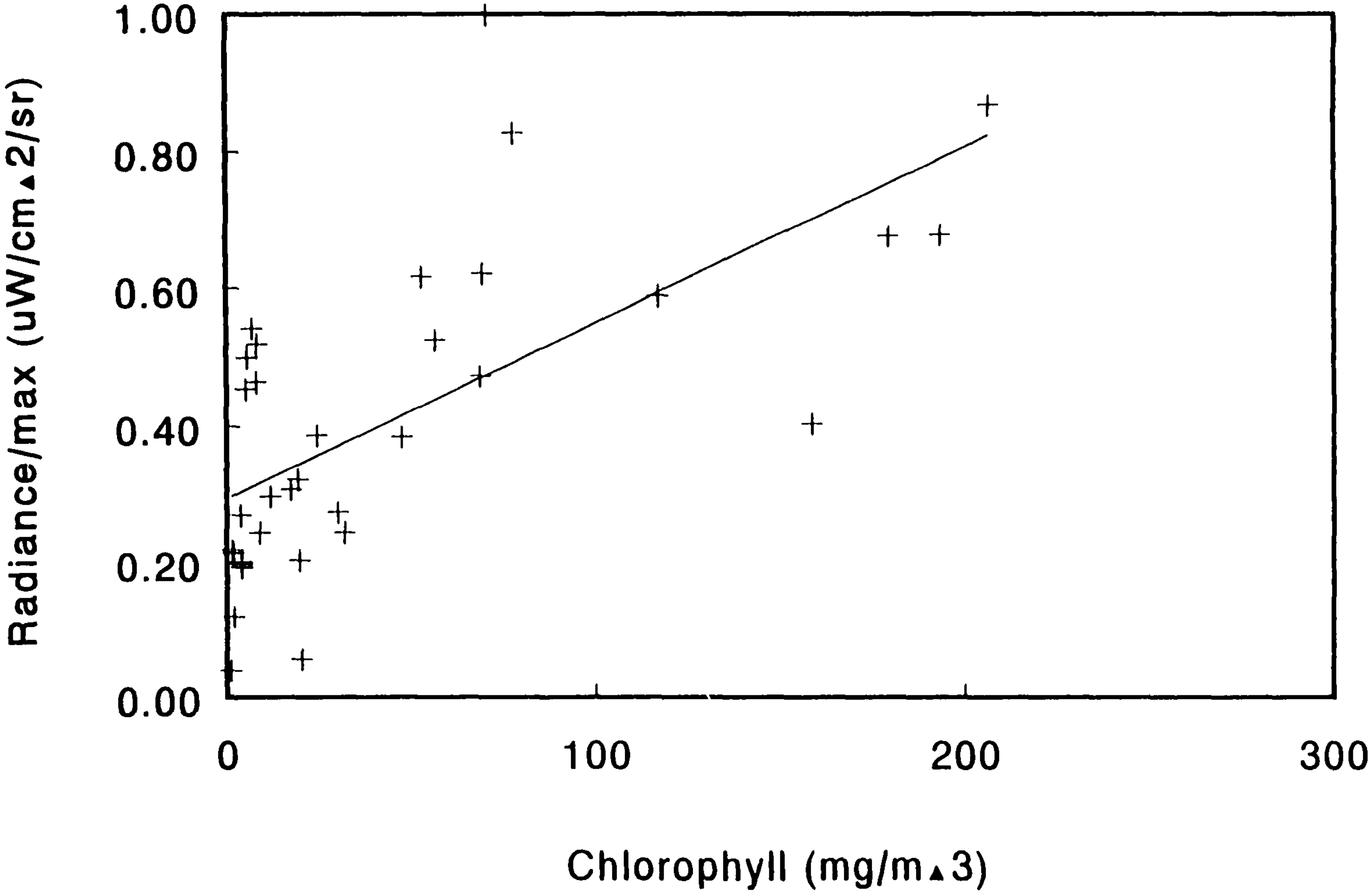

Figure 5.18. Plot of reflectance data normalized by the maximum value.

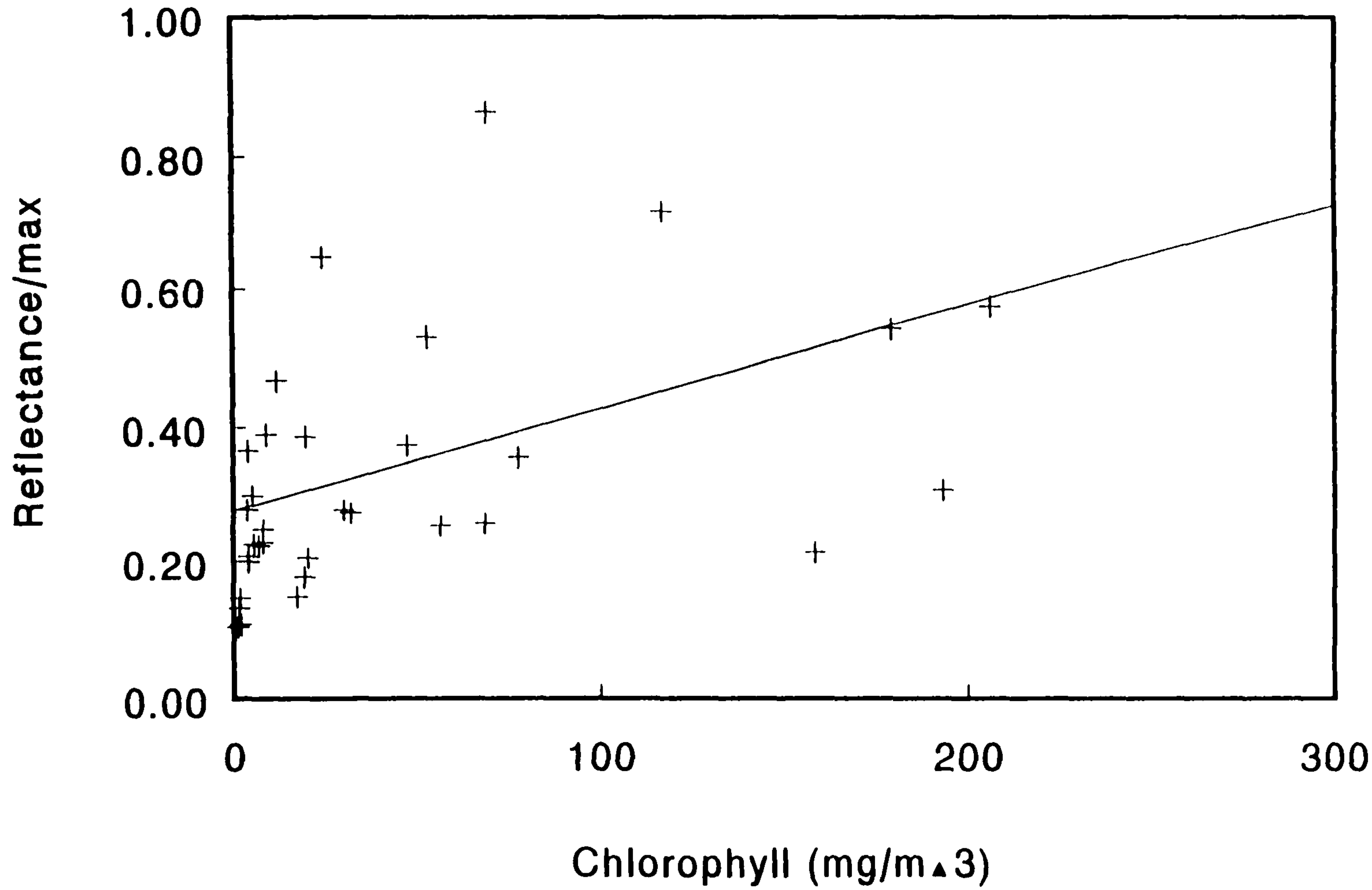

Table 5.6 illustrates that the normalized RMSE results are inconsistent and show trends similar to those of r^2 and the d-statistic for only the manual model and NREI. It would appear that this method of normalizing the data is not effective. Therefore, since the parameters being compared vary significantly in scale, the RMSE is not an appropriate means of evaluating goodness-of-fit for this study.

DISCUSSION OF MODEL

Results

Evaluating the r^2 and d statistics, the physical model of $y = a_0(1-e^{-x/c})$ describes the data most accurately. Further improvement is evidenced when manually setting c equal to 40. The resultant relationship $y = a_0(1-e^{-x/40})$ seems to best fit the data set. Thus, the relationship between chlorophyll-a concentration and remotely sensed data in this study is best described by a saturating exponential model with a chlorophyll constant of 40. The resulting equations from this model were

$$y_{DN} = 74.51(1-e^{-x/40}) \qquad (11) \qquad \text{(Figure 5.19)}$$

$$y_{Rad} = 3.56(1-e^{-x/40}) \qquad (12) \qquad \text{(Figure 5.20)}$$

$$y_{Refl} = .0148(1-e^{-x/40}) \qquad (13) \qquad \text{(Figure 5.21).}$$

A summary of the statistics for this model is given in Table 5.7.

Table 5.7. Manual Method Summary

	data mean	std. dev.	r^2	d	RMSE (c)
DN	50.15	9.31	0.527	0.426	0.394
Radiance	1.95	1.10	0.638	0.815	0.205
Reflectance	0.008	0.005	0.533	0.731	0.210

Figure 5.19. Manual model fit for digital number data.

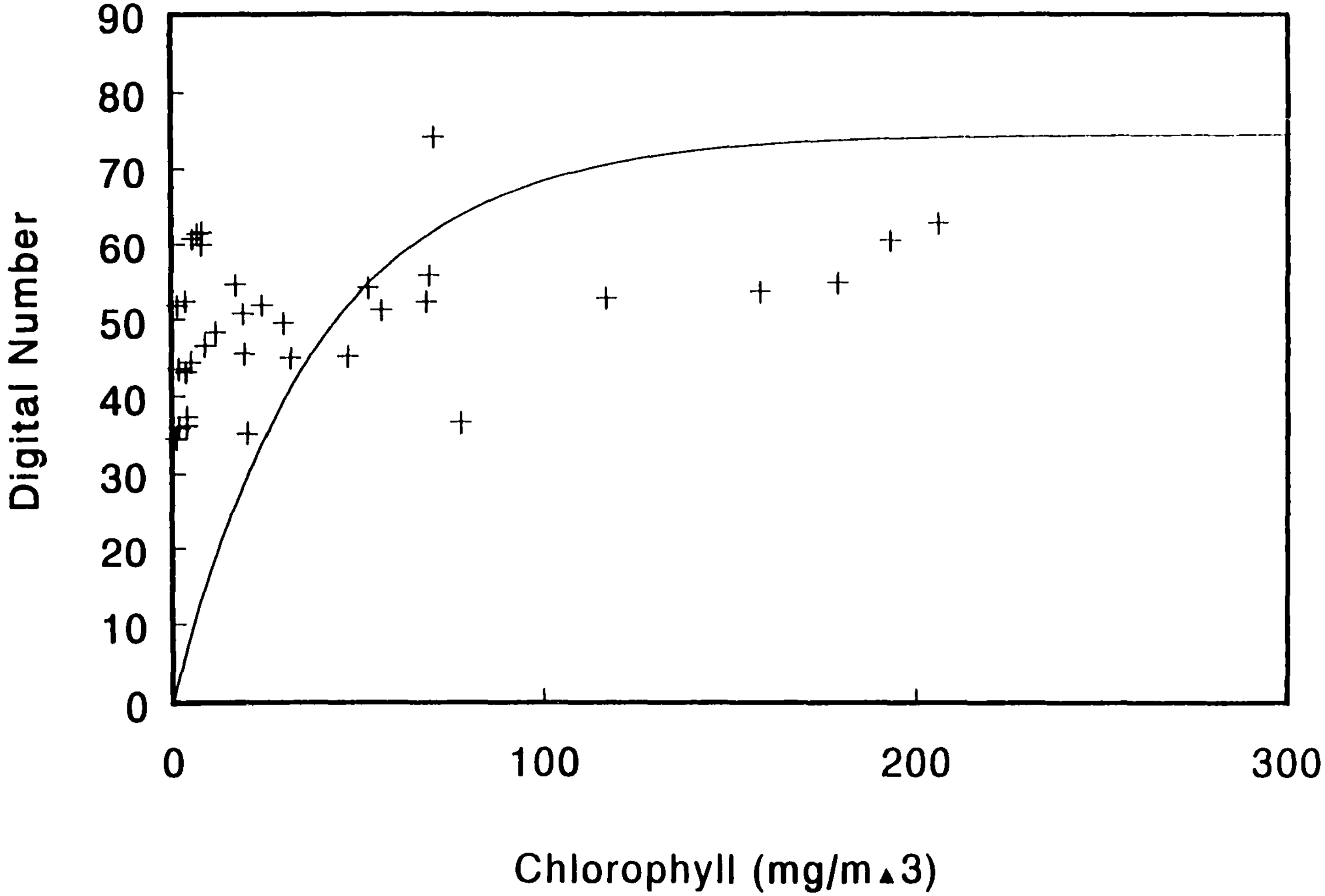

Figure 5.20. Manual model fit of radiance data.

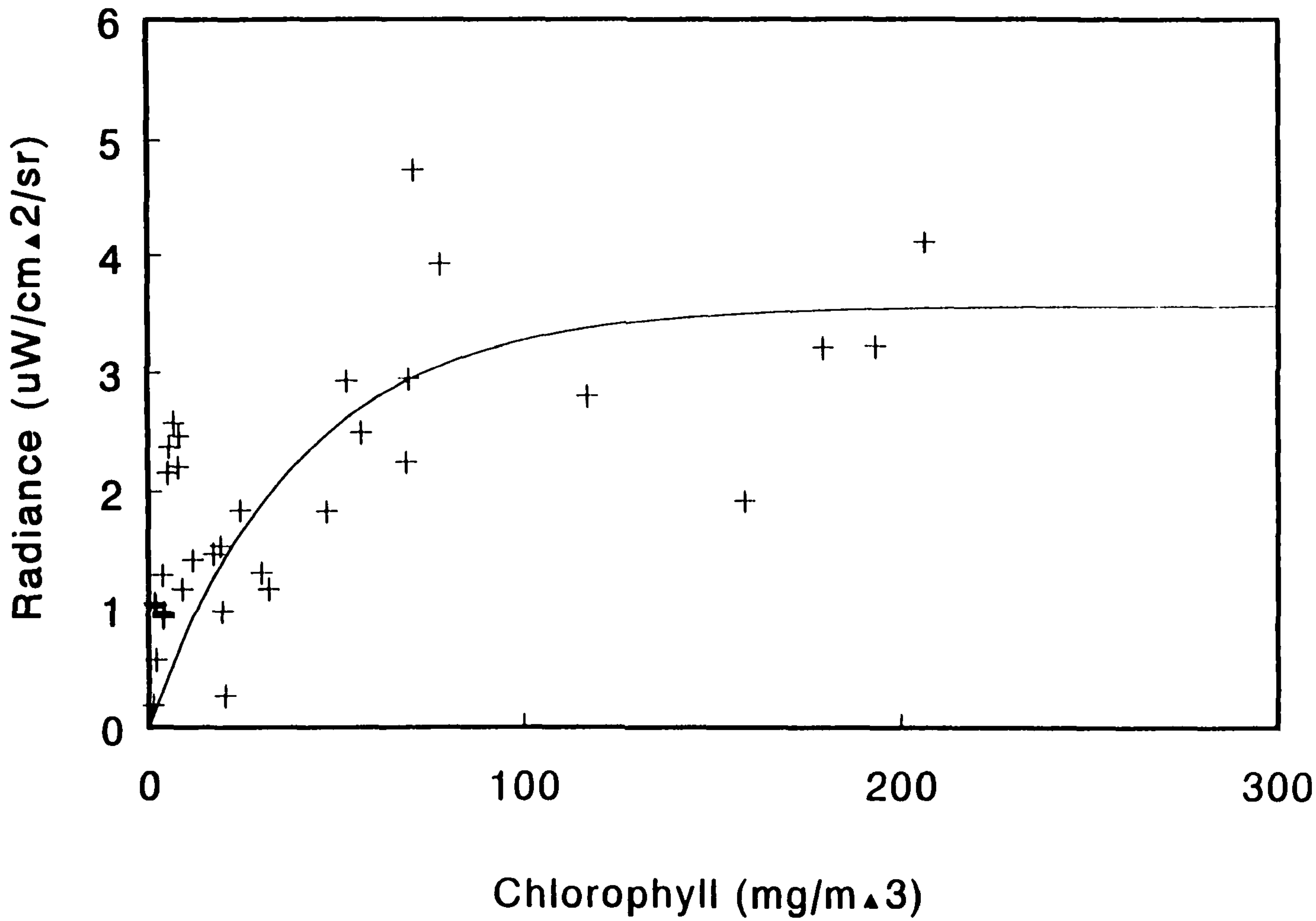

Figure 5.21. Manual model fit for reflectance data.

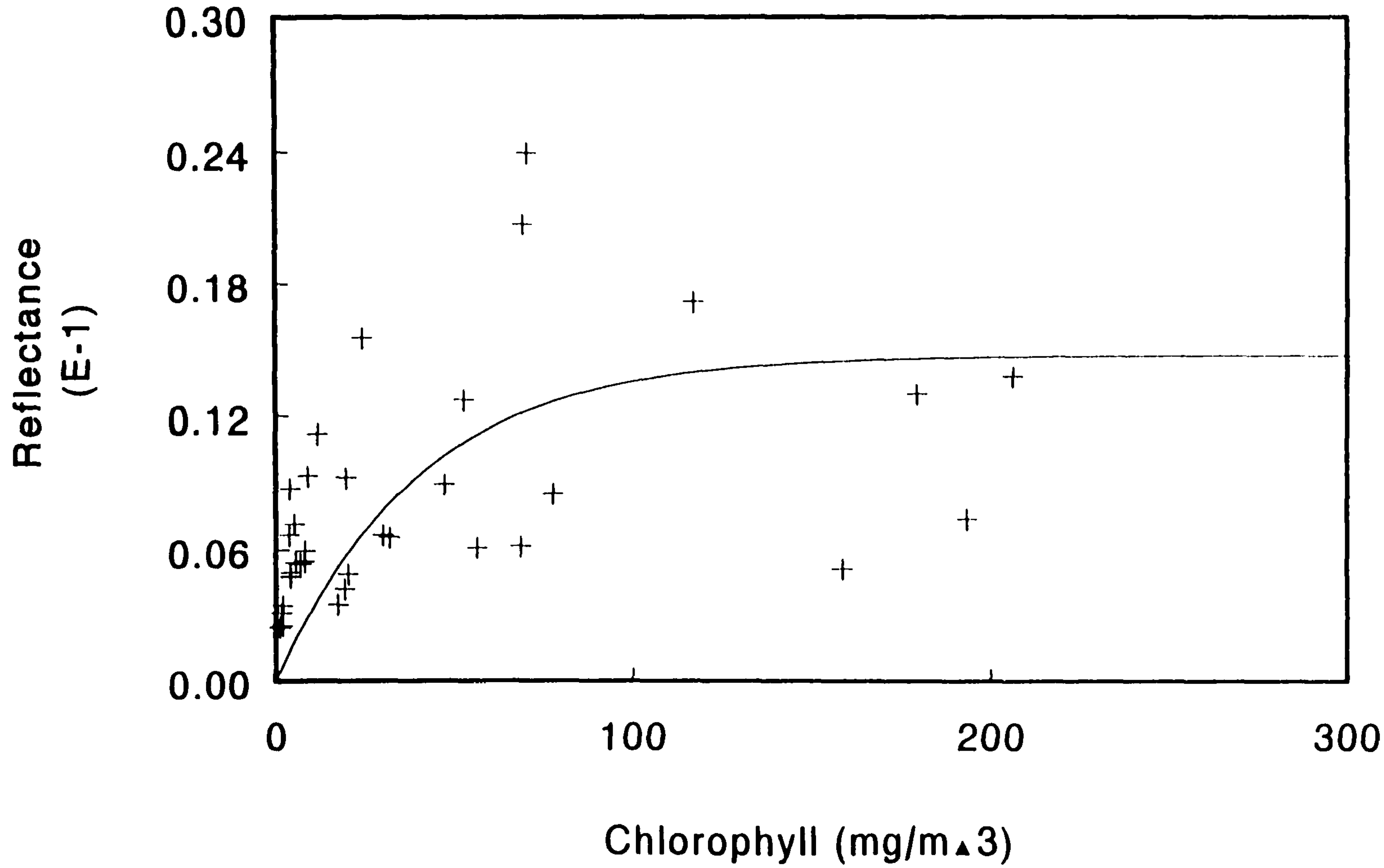

In this study, chlorophyll concentration (x) was established as the dependent variable in order to describe the response of water reflectance (y). For future studies, however, it is the reflectance that will be the dependent variable, and from reflectance chlorophyll concentration will be estimated. The general form that the above equations would take is

$$x = -c \ln(1 - y/a_0) \tag{14}$$

That the model predicts chlorophyll-a concentration better for radiance than for reflectance was not the anticipated result, but may easily be explained. The amount of reflectance from a water body depends, in part, upon the amount of radiation striking the surface (irradiance). The irradiance data was gathered from the Micronet stations nearest each reservoir which required interpolation in both time and space. Further, it required an approximation of the irradiance available in the bands of interest. In performing the space interpolations, irradiance data collected at Micronet stations varied significantly for several of the reservoirs. Omitting these reservoirs from the study, however, did not appreciably change the results. The flights occurred on overcast days so these irradiance interpolations probably lack the accuracy required for the analysis and may serve more appropriately as gross irradiance approximations. It is expected that under clear sky conditions, the incoming solar irradiance would be sufficiently well-behaved and the method could be applied.

Sources of Error

Since this research represents the first attempt at use of a new technology (use of narrow band filter video imaging), many potential sources of error were present.

These may have had origins in a variety of sources including the data collection, camera system and the processing procedure.

Flight. The largest source of error was potentially the timing of the flight itself. Scheduling required that the flight occur at a very specific place and time. Unfortunately, the cloudy atmospheric conditions at this time were not optimal for this type of study. It would be desirable to repeat this study under clear sky conditions.

Data Collection. Other sources of error existed during collection of the data. Trial-and-error is often required to determine which f-stop may provide the best images when using aerial photography. Since this was the first time this technology had been attempted, the camera apertures selected may or may not have been the most desirable f-stops. The images used in this study were, however, reliable.

Error may also have occurred when correlating water sample locations with airborne video images. The water samples may not have been collected at exactly the same locations that the video analysis occurred. Areas near the dams, in the centers of the reservoirs, were chosen for laboratory and video analysis, but may not have corresponded exactly. For future studies, global positioning systems may be used to verify that the sampling locations on the reservoirs are within the areas analyzed on the airborne video images.

Data Processing. During data processing, errors may have occurred in several ways. When the still frames were "grabbed" from the video tapes, it was virtually impossible to retrieve the exact same image from each of the three cameras (670 nm, 700 nm, 800 nm). Therefore, when manipulating the images in IDRISI, the 10x10 pixel arrays varied slightly for the 670 nm, 700 nm, and 800 nm images. An additional result of processing was that some of the reservoir images may not have been truly nadir in nature, but they were all very close.

When evaluating the reflectance data, irradiance data was retrieved from the Micronet. The problems associated with this process arise from the interpolations in time and space and have been discussed previously.

At the present time, a new system is being developed that would correct many of these sources of error. This system would consist of three small video cameras and an irradiance sensor connected to a laptop computer. The three images of the reservoirs would be taken simultaneously and fed immediately into the computer. An irradiance value would also be determined for a specific location thus avoiding interpolation problems.

The possibility also exists that, as technology improves, narrow band sensors may be added to available satellite platforms. This is not feasible at the present time and would probably not be accessible in the near future.

Sensitivity Study

It has been suggested that the amount of chlorophyll in water may have an effect on spectral reflectance. Gitelson (1992) noticed a shift in the chlorophyll maximum as chlorophyll concentration approached 100 mg/m^3. Below 100 mg/m^3, the chlorophyll maximum was generally located between 695 nm and 705 nm but shifted to approximately 715 nm at chlorophyll concentrations of 100 mg/m^3 or greater. This response may indicate that there is some fundamental mechanism in place which causes an increase in chlorophyll concentration to affect spectral response. In order to test this hypothesis, the data from this study was analyzed to determine whether a change in reflectance is noticed near a chlorophyll concentration of 100 mg/m^3. The data is divided into two groups: chl-a > 100 mg/m^3 and chl-a <

100 mg/m^3. The majority of the data was located in the chl-a < 100 mg/m^3 group. Only 5 points fell into the chl-a > 100 mg/m^3 category.

For the first group (chl-a > 100 mg/m^3), the data for both DN and radiance was most accurately described by an exponential fit ($y = a_0 + a_1 e^{-x/a_2}$) (Figures 5.22 and 5.23). This yielded r^2 values of 0.943 and 0.728, respectively. It was difficult to describe the fit of the reflectance data. The best fit was determined to be linear ($y = a_0 + a_1 x$) which resulted in an r^2 of only 0.1076 (Figure 5.24).

The second group (chl-a < 100 mg/m^3) was evaluated using the same procedure as described in the results section. The manual physical model once again described the data sets most accurately. The results for chl-a < 100 mg/m^3 were similar to the results for the entire range of chl-a data: the best model was $y = a_0(1-e^{-x/40})$, and r^2 was 0.5092, 0.5898, and 0.5434 for DN, radiance, and reflectance, respectively (Figures 5.25 - 5.27). The resulting model equations were:

$$y_{DN} = 87.58(1-e^{-x/40}) \quad (15)$$

$$y_{Rad} = 3.92(1-e^{-x/40}) \quad (16)$$

$$y_{Refl} = 0.017(1-e^{-x/40}) \quad (17).$$

The coefficients determined for chl-a < 100 mg/m^3 vary only slightly from the results obtained from analysis of the entire data set described earlier:

$$y_{DN} = 74.51(1-e^{-x/40}) \quad (11)$$

$$y_{Rad} = 3.56(1-e^{-x/40}) \quad (12)$$

$$y_{Refl} = 0.0148(1-e^{-x/40}) \quad (13).$$

Figure 5.22. Chlorophyll concentration
vs DN (chl >100 mg/m▲3).

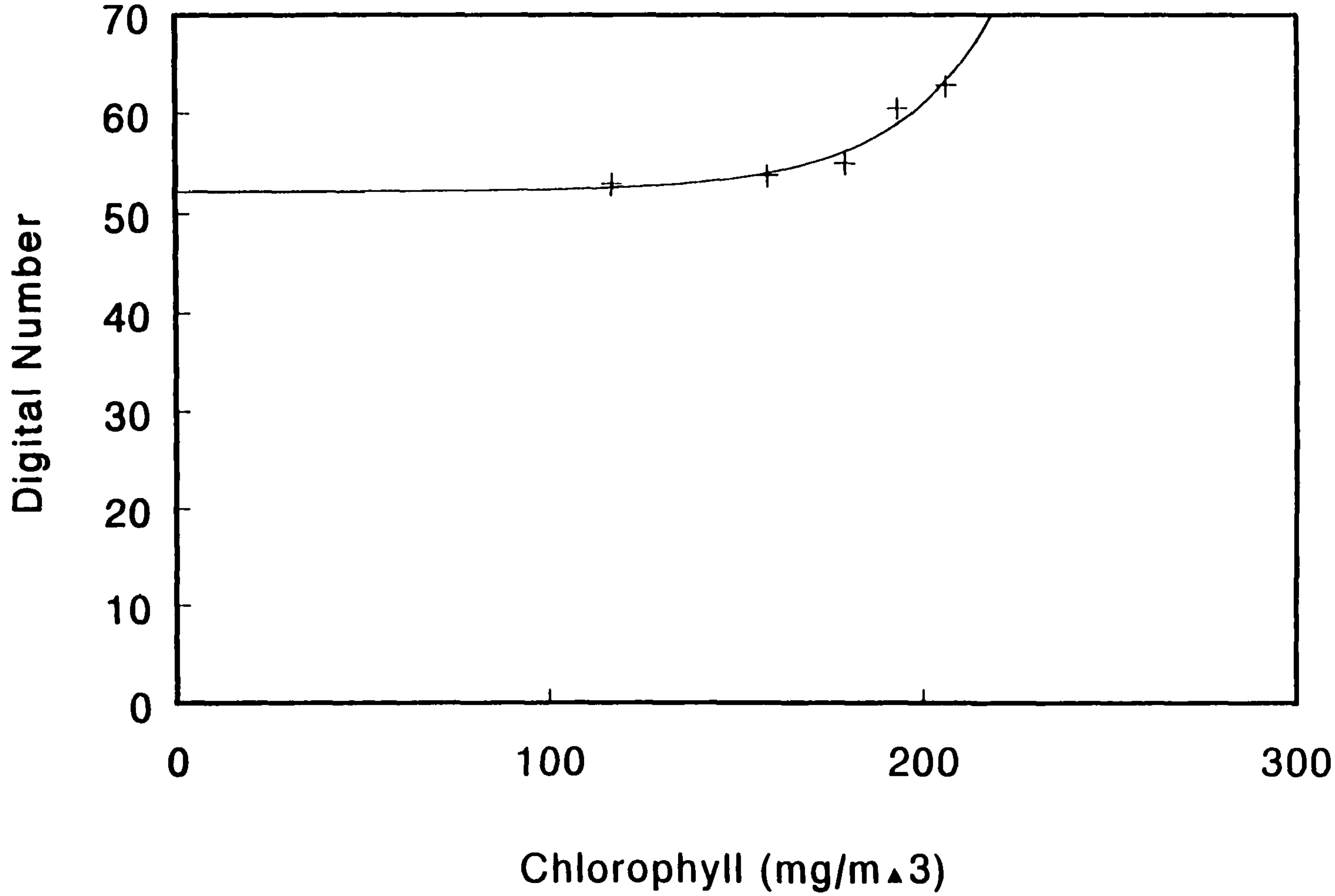

Figure 5.23. Chlorophyll concentration vs radiance (chl>100 mg/m▲3).

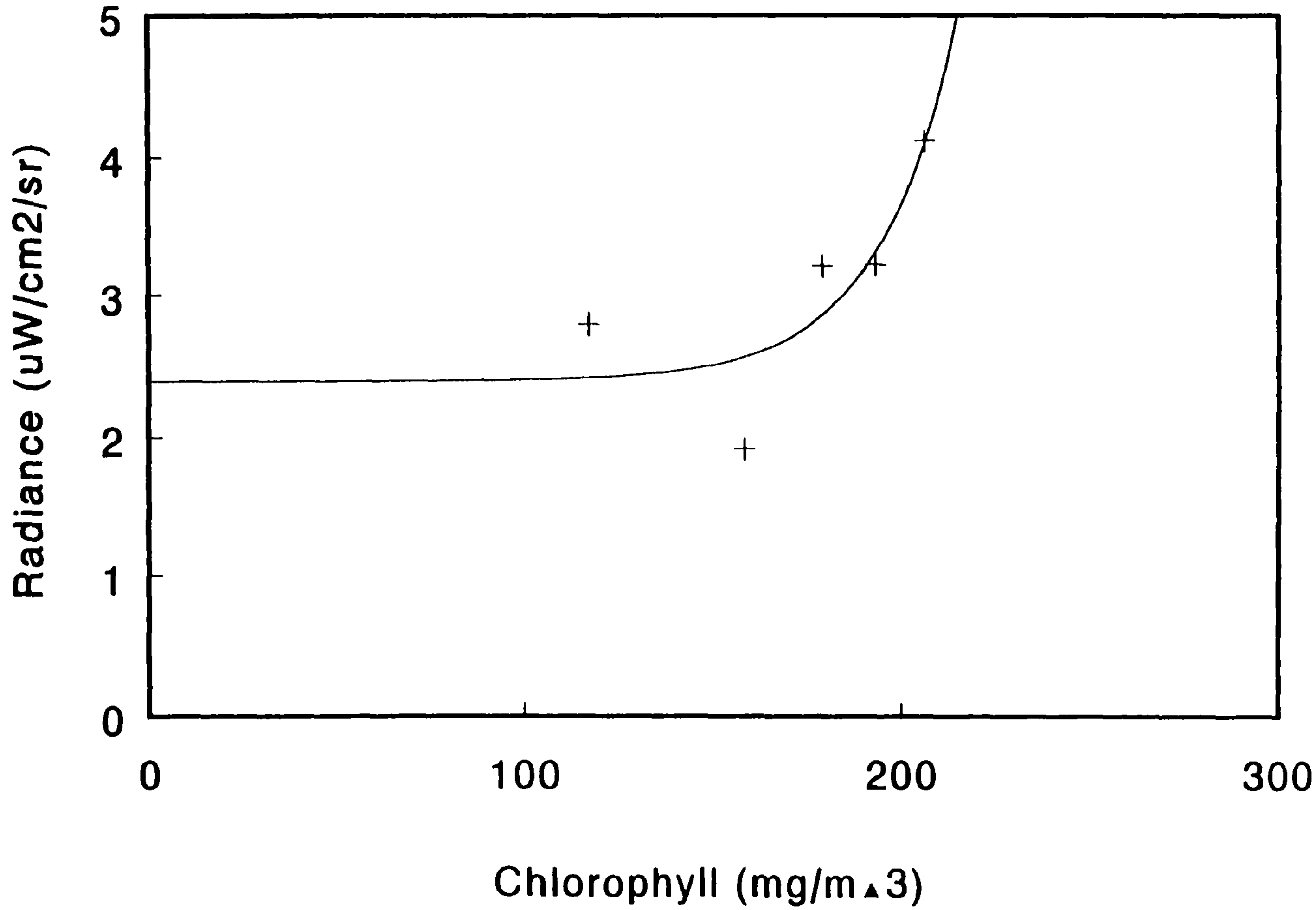

Figure 5.24. Chlorophyll concentration vs reflectance (chl>100 mg/m▲3).

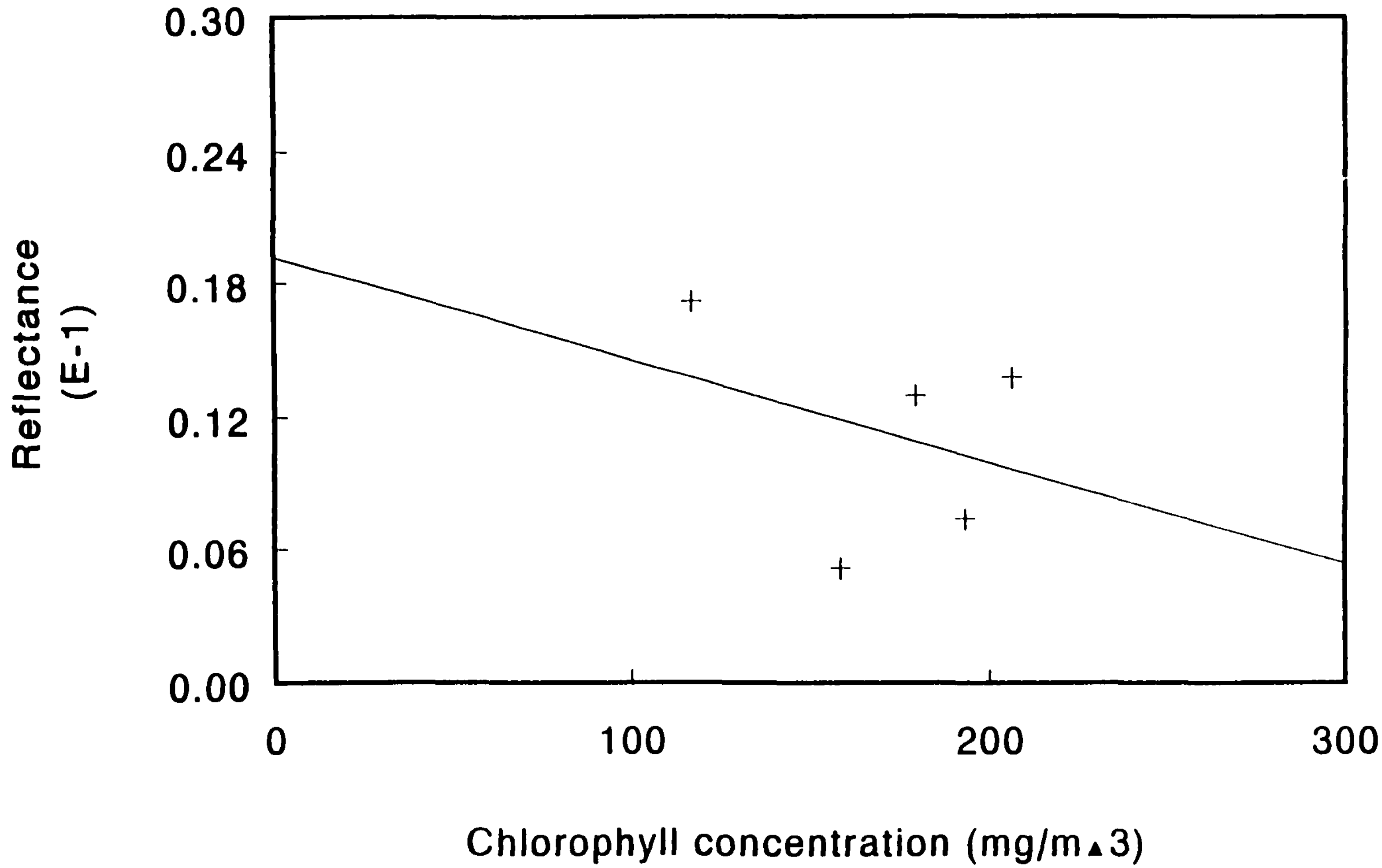

Figure 5.25. Chlorophyll concentration
vs DN (chl<100 mg/m▲3).

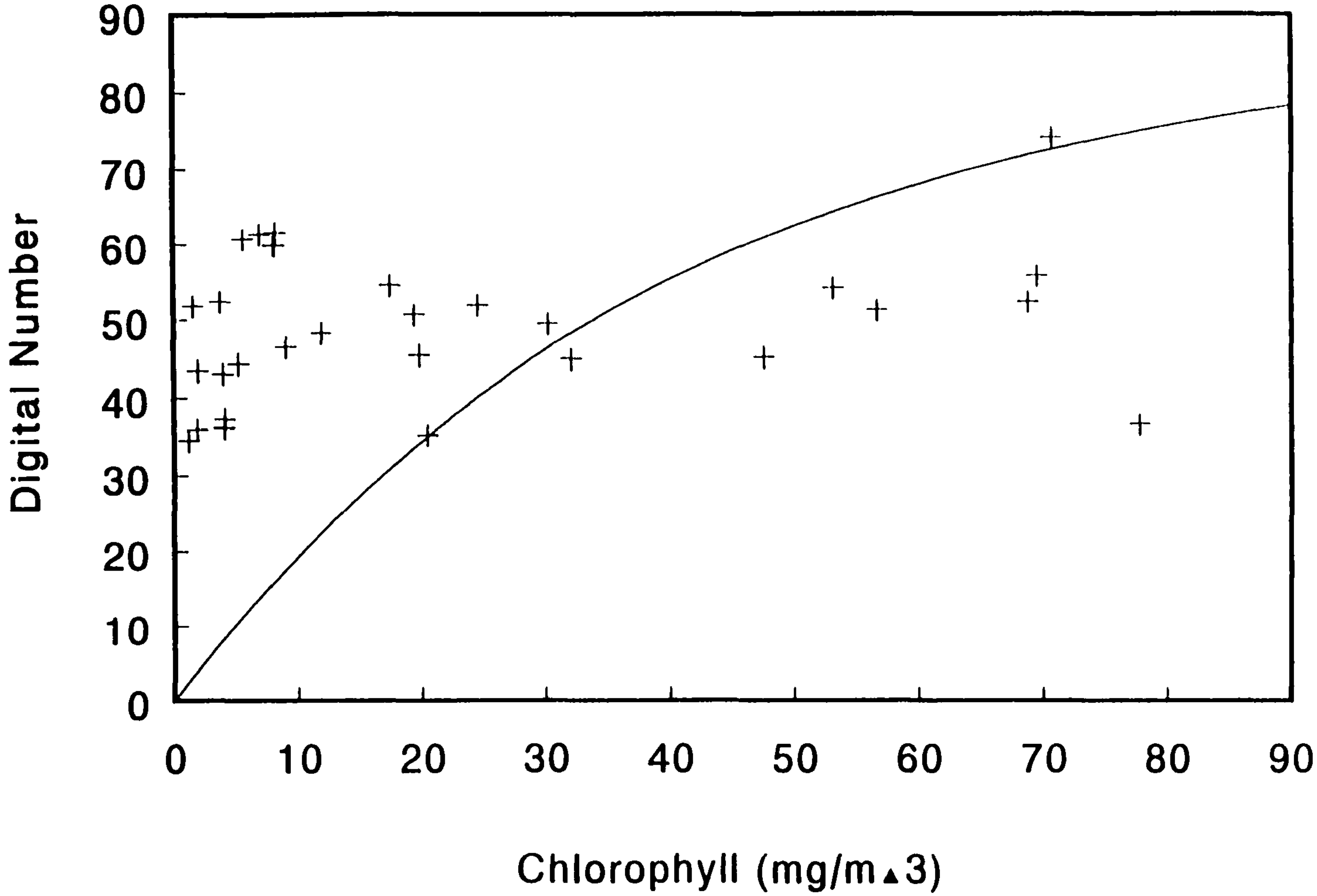

Figure 5.26. Chlorophyll concentration vs radiance (chl<100 mg▲3).

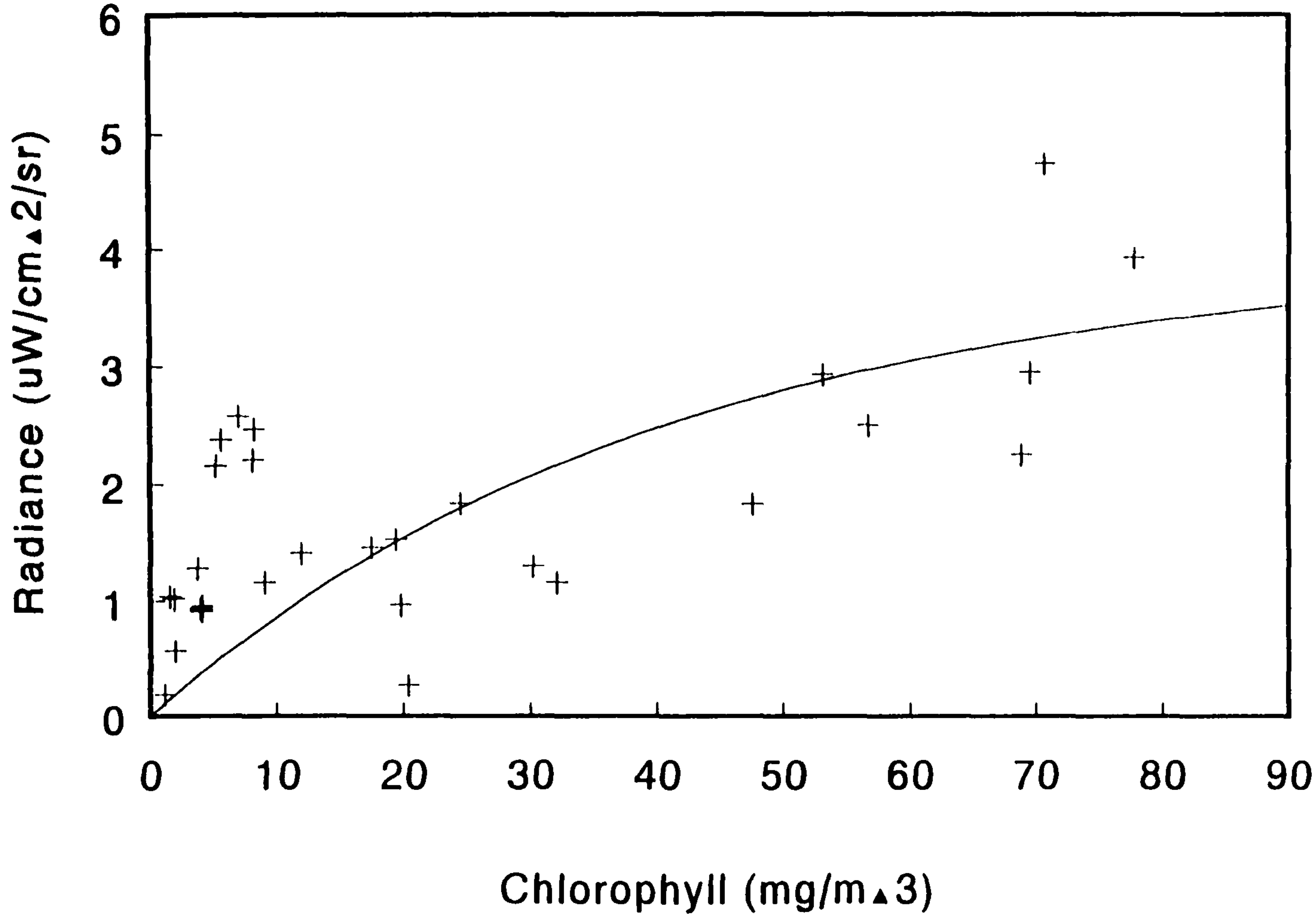

Figure 5.27. Chlorophyll concentration vs reflectance (chl<100 mg/m▲3).

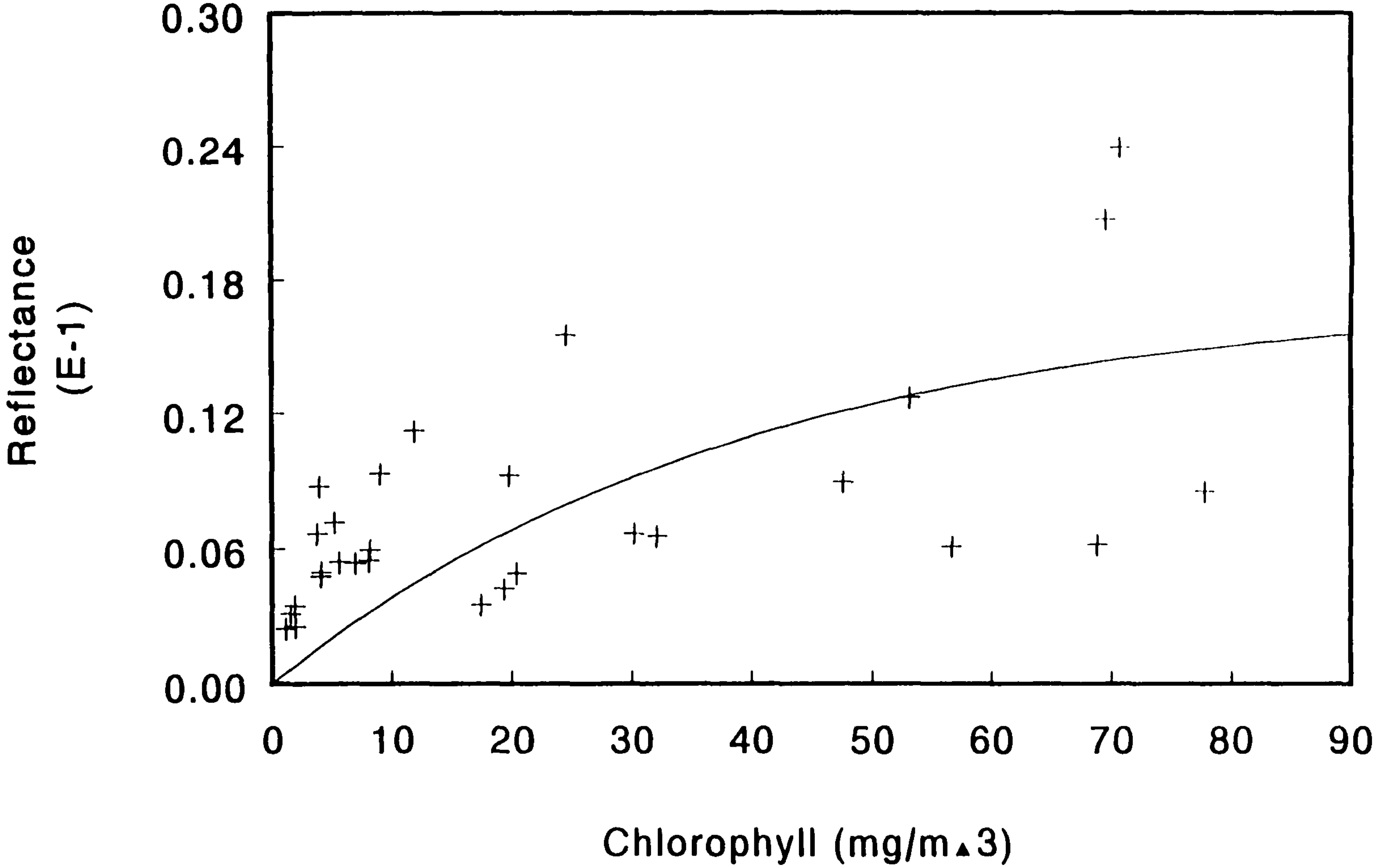

These results indicate that the model yields consistent results for chlorophyll concentrations < 100 mg/m^3, but careful consideration must be given when analyzing water having chlorophyll concentrations > 100 mg/m^3. So few data points existed for high chlorophyll concentrations, however, that these results are not conclusive. For DN and radiance, the model works well until chlorophyll concentrations of approximately 175 mg/m^3 are reached. At this point, the spectral response, which had seemingly reached a saturation value, began to increase exponentially. Results for reflectance were inconclusive.

CHAPTER 6. APPLICATIONS

INTRODUCTION

The narrow band filter airborne videography technology would potentially have many applications that could benefit many fields including environmental impact assessment, post-Environmental Impact Statement (EIS) monitoring, project management, water resources management, and agricultural assessment. In order to illustrate how the technology may be used in practical applications, a hypothetical case study will be considered.

CASE STUDY

Scenario

It is assumed that three new, small reservoirs are proposed for location in the upper part of the Little Washita River Watershed. Further, it is assumed that five years of baseline water quality data may be collected in the watershed prior to construction of the new reservoirs. It is also assumed that a follow-on study will be conducted for 10 years in order to examine the water quality effects of the new reservoirs and the cumulative effects on all reservoirs. This section describes what studies would need to be performed and how narrow band filter airborne videography may be applied.

Baseline Water Quality Data

A comprehensive study of the existing watershed can be performed in a five year period. Several different aspects must be considered: the condition of the river system itself would need to be defined, and the water quality of the existing reservoirs would need to be evaluated.

Little Washita River System. The existing reservoirs, for the most part, are located on tributaries of the Little Washita River (LWR). It is therefore desirable to obtain information about the dynamics of the river system.

The Micronet measures various meteorological parameters numerous times during the day, so could be used to identify climatological changes in the watershed. Flow data, both in the LRW and its tributaries, may be obtained from a series of hydrographs allowing the relationship between climatological change and river flow to be approximated. Estimates of runoff into the watershed may also be approximated.

It would also be beneficial to examine the temperature, suspended and dissolved sediment loads, dissolved oxygen, and nitrogen and phosphorous concentration in the streams. These parameters would represent a solid baseline for subsequent studies in the LWR Watershed.

Reservoirs of the Little Washita River Watershed. The water quality of the existing reservoirs would also need to be examined. The new technology may be applied in this analysis, since it is useful for both short-term and long-term monitoring of reservoirs.

Daily variations in surface algal activity, as well as seasonal variations in chlorophyll concentration, may be estimated. The video technology was originally performed on single sampling sites on fairly small reservoirs but may be applicable to numerous sites on a single reservoir. This would make detailed reservoir analysis of surface algal activity possible since numerous locations on a reservoir of any size may be evaluated to determine variations in surface productivity. This, in turn, could help to identify problem areas on the reservoirs.

In some cases, areas of point and/or non-point source contributions may be identified. By identifying regions of high chlorophyll-a concentration, it may be possible to locate problem areas and to determine if point or non-point pollution is contributing to eutrophication. If so, mitigation measures may be undertaken.

Suspended sediment concentration may also be detected with incorporation of data collected in the 800 nm waveband making it easy to evaluate sedimentary influx into the reservoirs. Relative amounts of suspended sediment can readily be established in order to determine locations of high sedimentary influx into reservoirs. This may aid in determining whether or not sedimentary control measures are needed and, if so, where they should be located to be most effective.

The proposed video system may also act as an early warning system for undesirable algal growth or large sedimentary influxes since studies can be conducted very quickly. Upon detection of these problems, mitigation measures may be undertaken quickly thereby preventing potentially negative impacts.

For future assessment and analyses, it is important to establish baseline water quality conditions for any lake or reservoir. Long-term monitoring is useful for any reservoir, but the data may be especially useful in monitoring water quality changes when proposed projects become operational. For this case study, the impact of the three new reservoirs may be estimated by comparing baseline water quality conditions in the reservoirs to post-installation water quality conditions.

Impact of New Reservoirs

It is assumed that, for this case study, an EIA has been conducted and an EIS prepared. The project was approved, so installation of the reservoirs was initiated five years after beginning the study of baseline water quality conditions. A continuation of the studies described above would be necessary in order to determine the impact of the new reservoirs. This would enable areas to be defined that have undergone significant changes since the addition of the new reservoirs.

Short-Term Environmental Impact Assessment. The most immediate impacts of the installation of the new reservoirs would probably be changes in stream flow rates and sedimentary influx into the existing reservoirs. The changes in flow rate would be detected by stream hydrographs, and the sedimentary impact in the reservoirs could be assessed during flights carrying the video array.

The proposed technique is versatile and may be used to evaluate ground-based parameters as well as water quality parameters. For example, existing environmental conditions may be evaluated by examining areas for overall health of vegetation and habitat. Problem areas that may easily be detected from the air may be more difficult to locate in field-based assessments. Many studies have been performed which indicate that healthy vegetation and vegetation in poor condition result in differing spectral responses. Contaminated areas may, therefore, be located by observing patterns of water and vegetation distress.

Project Management and Long-Term Post-EIS Monitoring. After installation of the new reservoirs, the watershed will be monitored for an additional 10 years in order to determine the impact of the project. The studies mentioned above will be continued for the entire time period. The proposed technology would be useful as a quick-detection system during project management and for long term monitoring.

Potential problems may have been identified during the EIA. As the project progresses, the immediate and surrounding areas will necessarily be affected. Changes occurring within a watershed as development proceeds may be identified and monitored quickly using airborne video imagery. If the effects are worse than anticipated, mitigation measures can be taken immediately. In addition, the effects of these mitigation measures may be observed in the video studies.

Both long and short term monitoring of suspended sediment and chlorophyll concentrations in water will need to be performed to assess the impact of development. Water resources must be protected from sediment-laden runoff of construction sites.

Cost Analysis

A cost analysis was performed to estimate the savings provided by the incorporation of the proposed method as applicable to the case study. This analysis applies to the reservoir study only. Data would need to be collected from 45 reservoirs for the first five years and from 48 reservoirs for the next ten years. Two cases were considered: a field study by a governmental agency and the proposed video-camera array. Both were evaluated using the Little Washita River Watershed (LWRW) in a year-long study. It was assumed that data would be collected six times per year.

The field study would require a crew of two personnel for approximately 10 days during each sampling period. Samples would be collected and sent to a laboratory for analysis (Bill Cauthran, 1997, Oklahoma Water Resources Board, personal communication). The cost for a governmental study would be approximately $1100 per day. Table 6.1 summarizes the costs incurred for each of the collection methods. For the first five years of the study, sampling of the 45 reservoirs would take approximately 60 days, while sampling would take approximately 66 days during the ten years of the follow-up study.

A governmental study would cost $1100/day for 10 days ($11,000). Data would be collected 6 times per year, so the total charge for collection would be $66,000. In addition, costs are incurred for overhead (transportation, equipment, supplies). This is generally estimated to be half of the collection costs (Frank Schiebe,

Table 6.1 Yearly Costs

Collection

Cost	Video	Government
Equipment		
Flight/Collection	$3,960	$66,000
Analyst	$25,000	
Overhead/Profit	$12,980	$33,000
Total	$41,940	$99,000

Collection + Equipment purchase

Cost	Video	Government
Equipment	$4,867	
Flight/Collection	$3,960	$66,000
Analyst	$25,000	
Overhead/Profit	$15,413	$33,000
Total	$49,240	$99,000

1997, Agricultural Research Service Water Quality Laboratory, personal communication) which would be $33,000 in this example. Approximate cost for a one year governmental study is therefore $99,000.

The video-camera array would require the use of an airplane, so cost estimates include plane/pilot fees of $80 per hour. The reservoirs could be flown in approximately two hours. Cost for the plane/pilot is $960 for collection six times per year. The video system also requires the services of an analyst, who would be hired for 6 months ($25,000), to assemble and interpret the data. To be certain that the camera systems are correctly calibrated, the cost of sampling one reservoir per flight is included ($500). These spot-checks would cost $3000 for the year. Data collection for the entire year would take 6 days whether sampling 45 or 48 reservoirs.

Since the camera system might require the purchase of equipment, this purchase is incorporated into the cost with payments being amortized over 5 years. The proposed purchase price of the video-camera system is approximately $20,000. An interest rate of 8% is assumed. The yearly cost of the LWRW study, including the equipment purchase, would be $49,240 for the video array system. The cost of use during years subsequent to the purchase of equipment would be $44,037 (that is $41,940 + 5 years' inflation).

If all equipment is owned, the camera system provides substantial savings over traditional ground-based data collection. Even with the purchase of equipment, the video camera system represents significant savings.

For smaller projects as well, the video-camera system is still cost competitive assuming the equipment has already been purchased. If only two reservoirs need to be analyzed, the cost of analysis using the video system would be approximately $1940 versus $1650 for a governmental study. These estimates include plane/pilot fees for two hours ($960), the services of an analyst ($200), one water sample ($300) and overhead ($480) for the video system and collection ($1100) and overhead ($550) for the field-based study.

To summarize, Table 6.2 depicts the yearly costs incurred for each method of data collection for the entire length of the case study (15 years). An inflation rate of 1% is assumed for each year. Data collected from the airborne video-camera system is less expensive than data gathered by traditional field-based studies. The time of data collection also varies significantly. Field studies range from 60 to 66 days while the camera system requires only 6 days. Thus, the proposed video technology would be both less expensive and less time-consuming than traditional field-based data collection.

Table 6.2. Cost Summary

Year	Video	Government
1	$49,241	$99,000
2	$49,733	$99,990
3	$50,231	$100,990
4	$50,733	$102,000
5	$51,240	$103,020
6	$44,037	$104,050
7	$44,477	$105,090
8	$44,922	$106,141
9	$45,371	$107,203
10	$45,825	$108,275
11	$46,283	$109,358
12	$46,746	$110,451
13	$47,214	$111,556
14	$47,686	$112,671
15	$48,163	$113,798
Total	$711,903	$1,593,593

CHAPTER 7. SUMMARY AND CONCLUSIONS

SUMMARY

The primary objective of this study was to develop a convenient method, based on aerial videography, to assess water quality and surface productivity in surface impoundments. The ultimate goal was to provide a rapid, economic method of determining chlorophyll concentration in surface impoundments. This study provided a valuable first step in describing the relationship between remotely sensed data using airborne sensors and chlorophyll-a concentration of surface waters.

Several models were considered when trying to determine a mathematical model to best describe the data. The physics-based equation $y = a_0(1-e^{-x/40})$ was found to best describe the relationship between reflectance and surface chlorophyll concentration in reservoirs of the Little Washita River Watershed.

It was hoped that an improvement in describing chlorophyll concentration would be evident when converting the raw video data (DN) into radiance values and that further improvement would occur with the incorporation of solar irradiance data in determining reflectance. For this study, however, radiance most accurately described chlorophyll concentration in the reservoirs. It is believed that this was largely due to the fact that the study was conducted under cloudy conditions. In the future, a similar study will be performed under clear sky conditions. The technique seems to be sound but needs to undergo some fine-tuning in order to perfect the process. It is hoped that reflectance will best describe chlorophyll concentration as the process undergoes refinement. At the present time, airborne video imaging of reservoirs might perhaps be used most appropriately as a first approximation in determination of chlorophyll concentration of surface waters of inland water bodies.

The proposed technology is especially attractive because studies can be conducted rapidly, few personnel are needed, and the method is very cost effective. This technique has a great deal of potential, and studies should continue in order to further refine the process and obtain more accurate results. Subsequent studies might focus on video imaging under cloudless conditions, incorporating irradiance sensors capable of determining incoming solar radiation spatially and contemporaneously with the video imaging process, and adapting the technology so it may effectively be utilized under variable sky conditions. A new camera system is currently being developed that will make the entire process easier and more user-friendly.

CONCLUSIONS

More work remains to be done in order to perfect this technology, but a sound foundation now exists from which to conduct further studies. Several conclusions can be reached as a result of this study:

- A physics-based empirical model $y = a_0(1-e^{-x/40})$ best described the relationship between chlorophyll concentration and reflectance.
- The use of aerial videography in assessing chlorophyll concentration in surface impoundments is rapid and cost effective. In a hypothetical case study, traditional field-based collection for a study of 45 reservoirs for one year required 60 days and would cost $99,000. The same study using aerial videography would take only 6 days and cost $41,940.
- Remotely sensed data must be correlated with field-based data in order to obtain physically-meaningful results from airborne platforms. This is

evidenced by the improvement in describing chlorophyll concentration when converting digital numbers into the physically-based radiance units.

- Care must be used when interpreting reflectance results. Several sources of error may be present including variable sky conditions and questionable solar irradiance interpolations.
- The GIS IDRISI was used to analyze data and generate surface contour maps of solar irradiation. It is evident that GIS technology has become an integral part of analysis of remotely sensed data.

This study provides a solid foundation for airborne video imaging of water reservoirs and should be encouraging to those interested in using airborne videography as a management tool. There are applications in several fields that may benefit from further development of this tool.

References

Allen, P. B., and Naney, J. W. 1991. Hydrology of the Little Washita River Watershed, Oklahoma. U. S. Department of Agriculture, Agricultural Research Service, ARS-90.

Agricultural Research Service (ARS). 1994. Personal communication.

Boland, D. H. P. 1976, April. Trophic classification of lakes using Landsat-1 (ERTS-1) multispectral scanner data. EPA-600/3-76-037. Ecological Research Series. Corvallis, Oregon: U.S. Environmental Protection Agency.

Burrough, P. A. 1988. Principles of Geographic Information Systems for Land Resource Assessments. Oxford, England: Oxford University Press.

Cauthran, B. 1997. Personal communication. Oklahoma Water Resources Board.

Chen, Z., Hanson, J. D., and Curran, P. J. 1991. The form of the relationship between suspended sediment concentration and spectral reflectance: its implications for the use of Daedalus 1268 data. Int. J. Remote Sens., v. 12, no. 1, p. 215-222.

Chen, Z., Curran, P. J., and Hansom, J. D. 1992. Derivative reflectance spectroscopy to estimate suspended sediment concentration. Remote Sens. Environ., v. 40, p. 67- 77.

Crippen, R. E. 1989, March. Simple spatial filtering routine for the cosmetic removal of scan-line noise from Landsat TM P-tape imagery. Photogramm. Eng. Remote Sens., v. 55, no. 3, p. 327 - 331.

Curran, P. J., and Novo, E. M. M. 1988. The relationship between suspended sediment concentration and remotely-sensed spectral radiance: a review. J. of Coastal Research, v. 4, p. 351-368.

DeCoursey, D. G., and Snyder, W. M. 1969. Computer-oriented method of optimizing hydrologic model parameters. J. Hydrol., v. 9, p. 34-56.

Dekker, A. G., Malthus, T.J., and Seyhan, E. 1991, Jan. Quantitative modeling of inland water quality for high-resolution MSS systems. IEEE Transactions on Geoscience and Remote Sensing, v. 29, no. 1, p. 89 - 95.

Duggin, M. J. 1980, May. Field measurement of reflectance factors. Photogramm. Eng. Remote Sens., v. 46, no. 5, p. 643 - 647.

Filella, I., and Penuelas, J. 1994. The red edge position and shape as indicators of plant chlorophyll content, biomass, and hydric status. Int. J. Remote Sens., v.15, no. 7, p. 1459 - 1470.

Gitelson, A. 1992. The peak near 700 nm on reflectance spectra of algae and water: relationships of its magnitude and position with chlorophyll concentration. Int. J. Remote Sens., v. 13, p. 3367 - 3373.

Gitelson, A. A., and Kondratyev, K. Y. 1991. Optical models of mesotrophic and eutrophic water bodies. Int. J. Remote Sens., v. 12, no. 3, p. 373 - 385.

Gitelson, A., Garbuzov, G., Szilagyi, F., Mittenzwey, K. H., Karniela, A., and Kaiser, A. 1993. Quantitative remote sensing methods for real-time monitoring inland water quality. Int. J. Remote Sens., v. 14, p. 1269 - 1295.

Han, L., Rundquist, D. C., Liu, L. L., Fraser, R. N., and Schalles, J. F. 1994. The spectral responses of algal chlorophyll in water with varying levels of suspended sediment. Int. J. Remote Sens., v. 15, no. 18, p. 3707 - 3718.

Harrington, J. A. 1996. Personal communication.

Harrington, J. A., and Schiebe, F. R. 1989. Landsat MSS images of the clean-up of Lake Chicot. Geocarto Int., v. 4, p. 59-62.

Harrington, J. A., Schiebe, F. R., and Nix, J. F. 1992. Remote sensing of Lake Chicot, Arkansas: monitoring suspended sediments, turbidity, and Secchi depth with Landsat MSS data. Remote Sens. Environ., v. 39, p. 15 - 27.

Hilton, J. 1984. Airborne remote sensing for freshwater and estuarine monitoring. Water Res., v. 18, no. 10, p. 1195-1223.

Hinton, J. C. 1991. Application of eigenvector analysis to remote sensing of coastal water quality. Int. J. Remote Sens., v. 12, no. 7, p. 1441-1460.

Holyer, R. J. 1978. Toward universal multispectral suspended sediment algorithms. Remote Sens. of Env., v. 7, p. 323-338.

Iqbal, M. 1983. An Introduction to Solar Radiation. New York: Academic Press.

Kirk, J. T. O. 1981. Monte Carlo study of the nature of the underwater light field in and the relationship between optical properties of turbid yellow waters. Australian J. Freshwater Research, v. 32, p. 517-532.

Kirk, J. T. O. 1983. Light and Photosynthesis in Aquatic Ecosystems. Cambridge, England: Cambridge University Press.

Lathrop, R. G. 1992, April. Landsat thematic mapper monitoring of turbid inland water quality. Photogram. Eng. Remote Sens., v. 58, no. 4, p. 465-470.

Lathrop, R. G., Lillesand, T. M., and Yandell, B. S. 1991. Testing the utility of simple multi-date Thematic Mapper calibration algorithms for monitoring turbid inland waters. Int. J. Remote Sens., v. 12, no. 10, p. 2045 - 2063.

LeCroy, S. R. 1982. Determination of turbidity patterns in Lake Chicot from Landsat MSS imagery. NASA Contractor Report 165870. Hampton, VA: Langley Research Center.

Lillesand, T. M., and Kiefer, R. W. 1987. Remote Sensing and Image Interpretation. New York: Wiley.

Lin, S., Borstad, G. A., and Gower, F. R. 1984. Remote sensing of chlorophyll in the red spectral region. Remote Sens. of Shelf Sea Hydrodynamics. Amsterdam: Elsevier, p. 317 - 336.

Lind, O. T. 1979. Handbook of Common Methods in Limnology. St. Louis: Mosby Co.

Markham, B. L., and Barker, J. L. 1986. Landsat MSS and TM post-calibration dynamic ranges, exoatmospheric reflectances and at-satellite temperatures. EOSAT Technical Notes, v. 1, p. 3-8.

McHenry, J. R., Ritchie, J. C., and Schiebe, F. R. 1977. Estimating suspended sediment loads in reservoirs. Water Resources Bulletin, v. 13, p. 81-93.

Meinert, D. L., Malone, A. W., Voss, A. W., and Scarpace, F. L. 1978. Trophic classification of Tennessee area reservoirs derived from LANDSAT multispectral scanner data. Chattanooga, TN: Tennessee Valley Authority.

Menzel, R. G., Troeger, W. W., and Schiebe, F. R. 1989. Properties of selected Oklahoma lakes in relation to remote sensing of suspended sediment. Lake and Reservoir Manag., v. 5, no. 2, p. 31-37.

Novo, E. M., and Shimabukuro, Y. E. 1994. Spectral mixture analysis of inland tropical waters. Int. J. Remote Sens., v. 15, no. 6, p. 1351 - 1356.

Palmer, J. M. 1984. Effective band-widths for Landsat-4 and Landsat-D MSS and TM subsystems. Inst. Electrical and Electronics Eng.: Geoscience and Remote Sens., GE-22, p. 336-338.

Palmer, K. F. and Williams, D. 1974. Optical properties of water in the near-infrared. J. Opt. Soc. Amer., v. 64, pp. 1107-10.

Pickard, G. L. and Emery, W. J. 1982. Descriptive Physical Oceanography. Oxford, England: Pergamon Press.

Price, J. C. 1987. Calibration of satellite radiometers and the comparison of vegetation indicies. Remote Sens. Env., v. 21, p.15-27.

Quibell, G. 1991. The effect of suspended sediment on reflectance from freshwater algae. Int. J. Remote Sens., v. 12, no. 1, p. 177 - 182.

Quibell, G. 1992. Estimating chlorophyll concentrations using upwelling radiance from different freshwater algal genera. Int. J. Remote Sens., v. 13, p. 2611 - 2621.

Repic, R. L., Harrington, J. A., Schiebe, F. R., Everitt, J. H., Escobar, D. E., and Davis, M. R. 1995. Integrating airborne videography and close range remote sensing for surface water quality investigation. 15th Biennial Workshop on Videography and Color Photography in Resource Assessment. Terre Haute, Indiana. p. 172 - 181.

Ritchie, J. C., and Cooper, C. M. 1991, June. An algorithm for estimating surface suspended sediment concentrations with Landsat MSS digital data. Water Resources Bulletin, v. 27, no. 3, p. 373-379.

Ritchie, J. C., and Cooper, C. M. 1987. Comparison of Landsat MSS pixel array size for estimating water quality. Photogramm. Eng. Remote Sens., v. 53, p. 1549 - 1553.

Ritchie, J. C., McHenry, J. R., and Schiebe, F. R. 1978. The relationship between suspended sediments in surface water and vertical distribution of suspended sediments. J. Water Pollution Control Federation, v. 50, p. 734-738.

Ritchie, J. C., Schiebe, F. R., Cooper, C. M., and Harrington, J. A. 1994, September. Chlorophyll measurements in the presence of suspended sediment using broad band spectral sensors aboard satellites. J. Freshwater Ecology, v. 9, p. 197 - 206.

Ritchie, J. C., and Schiebe, F. R. 1986. Monitoring suspended sediments with remote sensing techniques. *In* Hydrologic Applications of Space Technology, International Association of Hydrological Sciences, v. 160, p. 233-243.

Ritchie, J. C., Schiebe, F. R., and McHenry, J. R. 1976. Remote sensing of suspended sediments in surface waters. Photogramm. Eng. Remote Sens., v. 42, p. 1539-1545.

Ritchie, J. C., Schiebe, F. R., and Cooper, C. M. 1983. Spectral measurements of surface suspended matter in an oxbow lake in the lower Mississippi Valley. J. of Freshwater Ecology, v. 2, p. 175-181.

Robinove, C. J. 1982, May. Computation with physical values from Landsat digital data. Photogramm. Eng. Remote Sens., v. 48, no. 5, p. 781-784.

Ross, J. D., Schiebe, F. R., Harrington, J. A., and Grimshaw, H. J. 1991. Satellite mapping of suspended sediment and its application to reservoir assessment. Lake and Reserv. Manage., v. 7, no. 1, p. 89-95.

Rundquist, D. C., Han, L., Schalles, J. F., and Peake, J. S. 1996. Remote measurement of algal chlorophyll in surface waters: the case for the first derivative of reflectance near 690 nm. Photogramm. Eng. Remote Sens. v. 62, no. 2, p.195-200.

Scarpace, F. L., Holmquist, K. W., and Fisher, L. T. 1979. Landsat analysis of lake quality. Photogramm. Eng. Remote Sens., v. 45, p. 423-433.

Schalles, J. F., Schiebe, F. R., Starks, P. J. and Troeger, W. W. 1997. Estimation of algal and suspended sediment loads (singly and combined) using hyperspectral sensors and integrated mesocosm experiments. Fourth International Conference on Remote Sensing for Marine and Coastal Environments, Orlando, FL.

Schiebe, F. R. 1997. Personal communication. SST Development Group.

Schiebe, F. R., Harrington, J. A., and Ritchie, J. C. 1987. Remote sensing of suspended sediments of Lake Chicot, Arkansas. Proceedings of the 6th Corps of Eng. Remote Sens. Symposium:Galveston, TX, p. 7-85.

Schiebe, F. R., Harrington, J. A., and Ritchie, J. C. 1992. Remote sensing of suspended sediments: the Lake Chicot, Arkansas project. Int. J. Remote Sens., v. 13, no.8, p. 1487-1509.

Schiebe, F. R., and Ritchie, J. C. 1986. Suspended sediment monitored by satellite. Proceedings of the 4th Federal Interagency Sedimentation Conference: Las Vegas, v. 1, p. 70-78 .

Schiebe, F. R., Ritchie, J. C., and Boatwright, G. O. 1985. A first evaluation of Landsat TM to monitor suspended sediment in lakes. Landsat-4 Science Characterization Early Results. NASA Conference Publication 2355, v. 4, p. 337-347.

Smith, R. C. and Baker, K. S. 1981. Optical properties of the clearest natural waters (200 - 800 nm), Appl. Opt., v. 20. p 177-84.

Stefan, H. G., Dhamotharan, S., Fu, A. Y., and Cardoni, J. J. 1984. Mathematical model simulation of Lake Chicot, Arkansas. Limnological Studies of Lake Chicot, Arkansas. Arkadelphia, Arkansas: Ouachita Baptist University, p. 72 - 134.

Stumpf, R. P., and Pennock, J. R. 1991. Remote estimation of the diffuse attenuation coefficient in a moderately turbid estuary. Remote Sens. Environ., v. 38, p. 183-191.

Thekaekara, M. P. 1970. The solar constant and the solar spectrum measured from a research aircraft. NASA Technical Report R-351. Greenbelt, MD: Goddard Space Flight Center.

Topliss, B. J., Almos, C. L., and Hill, P. R. 1990. Algorithms for remote sensing of high concentration, inorganic suspended sediment. Int. J. Remote Sens., v. 11, no. 6, p. 947-966.

Turner, R. and Spencer, M. 1972. Atmospheric model for the correction of spacecraft data. Proceedings of the 8th International Symposium of Remote Sensing of Environment 1972. Ann Arbor, Michigan: Environmental Research Institute of Michigan, p. 895 - 934.

Verdin, J. P. 1983. Corrected vs. uncorrected Landsat-4 MSS data. Landsat Data

Users Notes, v. 27, p. 4-8.

Verdin, J. P. 1985. Monitoring water quality in a large western reservoir with Landsat imagery. Photogramm. Eng. Remote Sens., v. 51, p. 343-353.

Vos, W. L., Donze, M., and Buiteveld, H. 1986. On the reflectance spectrum of algae in water: The nature of the peak at 700 nm and its shift with varying concentration. Communication San. Eng. and Water Manage. Netherlands, p. 86-22.

Whitlock, C. H., Witte, W. G., Talany, T. A., Morris, W. D., Usry, J. W., and Poole, L. R.1981. Research for a reliable quantification of water sediment concentrations from multispectral scanner remote sensing data. *in* Applied Modeling in Catchment Hydrology. V. P. Singh editor. Littleton, Colorado: Water Resources Publication, p. 495-510.

Wiesnet, D. R. 1976. Remote Sensing and Its Application to Hydrology. J. C. Rodda editor. New York: Wiley and Sons, p. 37-59.

Willmott, C. J., 1982. Some comments on the evaluation of model performance. Bull. Am. Meteor. Soc., v. 63, no. 11, p. 1309-1313.

Witte, W. G., Whitlock, C. H., Usry, J. W., Morris, W. D., and Gurganus, E. A. 1981. Laboratory measurements of physical, chemical, and optical characteristics of Lake Chicot sediment waters. NASA Technical Paper 1941. Hampton, VA: Langley Research Center.

Yacobi, Y. Z., Gitelson, A., and Mayo, M. 1995. Remote sensing of chlorophyll in Lake Kinneret using high-spectral-resolution radiometer and Landsat TM: spectral features of reflectance and algorithm development. J. Plankton Research, v. 17, no. 11, p. 2155 - 2173.

Glossary of Abbreviations

AGC	Automatic Gain Control
ARS	Agricultural Research Service
AVHRR	Advanced Very High Resolution Radiometer
CCD	Charge Coupled Detector
CCT	Computer Compatible Tape
DN	Digital Number
D-STAT	D-statistic of Willmott (1982)
EIA	Environmental Impact Assessment
EIS	Environmental Impact Statement
EREF	Exoatmospheric Reflectance
ERTS	Earth Resources Technology Satellites
GIS	Geographic Information System
I	Irradiance
L	Radiance
MSS	Multispectral Scanner System
LWRW	Little Washita River Watershed
NDVI	Normalized Difference Vegetation Index
NREI	Normalized Difference Red Edge Index
NOAA	National Oceanic and Atmospheric Administration
PMI	Programmable Multispectral Imager
R	Reflectance
RIPS	Remote Image Processing System
RMSE	Root Mean Square Error

SSC	Suspended Sediment Concentration
TM	Thematic Mapper
TSS	Total Suspended Solids
UTM	Universal Transverse Mercator
VCR	Video Cassette Recorder

APPENDIX A

Original Digital Number Pixel Values

Explanation of Symbols and Data

A brief explanation of the following diagrams is needed to understand their meanings. Each reservoir has two diagrams: one at 670 nm and the other at 700 nm. There are three parts to each image: a diagram of symbols, the name of the image, and a legend of symbols.

Each diagram is representative of the 10x10 digital number (DN) pixel array taken from the airborne videos which was analyzed for each reservoir. There are, therefore, 100 symbols in each diagram. Each symbol represents a single digital number value. The symbols are written in triplicate on the legend, but appear as a single symbol in the diagrams.

The "IDRISI image" lists the wavelength at which the image was taken, the number of the reservoir, and that the image is a DN window (dnw). For example, on the following page, the DN window of reservoir #1 was taken at 670 nm.

Also listed are the number of cells in the array having a particular value and the corresponding percentage of the total array. For example, the data from the 10x10 DN window at 670 nm of reservoir #1 is shown. **n** has a DN value of 33, **o** of 34, **p** of 35, etc. Two pixels have a value of 33 which represents 2% of the total array, 16 pixels have a value of 34 which is 16% of the array, etc.

The diagrams on the following pages represent the original DN windows taken from the video tapes. Each shade of gray is assigned a separate value and range from 0 to 41 for the 670 nm waveband and from 0 to 91 for the 700 nm waveband. Black is assigned the low DN values, while white is assigned the high values.

There are two small reservoirs located in close proximity to one another that are both referred to as reservoir 1. They are distinguished from one another in the text as 1S and 1L but are referred to as dnw and dn2 in this appendix.

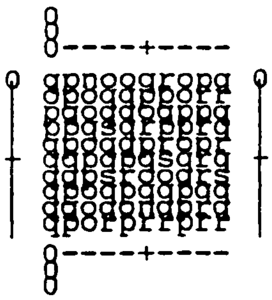

IDRISI image : 67001dnw

nnn	33	2	cells	=	2.00	%
ooo	34	16	cells	=	16.00	%
ppp	35	25	cells	=	25.00	%
qqq	36	37	cells	=	37.00	%
rrr	37	16	cells	=	16.00	%
sss	38	4	cells	=	4.00	%

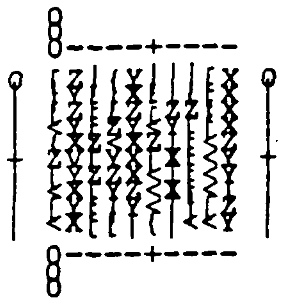

IDRISI image : 70001dnw

VVV	67	1	cells	=	1.00 %
XXX	69	13	cells	=	13.00 %
YYY	70	13	cells	=	13.00 %
ZZZ	71	14	cells	=	14.00 %
|||	72	15	cells	=	15.00 %
[[[	73	25	cells	=	25.00 %
<<<	74	14	cells	=	14.00 %
(((	75	5	cells	=	5.00 %

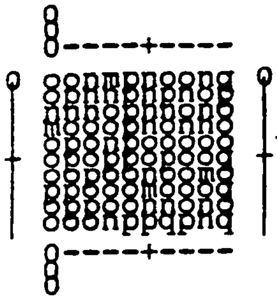

IDRISI image : 67001dn2

mmm	32	4	cells	=	4.00	%
nnn	33	23	cells	=	23.00	%
ooo	34	47	cells	=	47.00	%
ppp	35	21	cells	=	21.00	%
qqq	36	5	cells	=	5.00	%

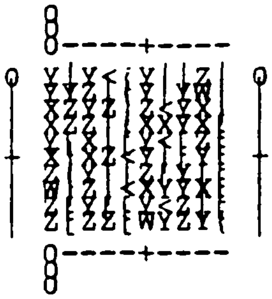

IDRISI image : 70001dn2

WWW	68	3	cells	=	3.00 %
XXX	69	11	cells	=	11.00 %
YYY	70	22	cells	=	22.00 %
ZZZ	71	18	cells	=	18.00 %
|||	72	19	cells	=	19.00 %
[[[	73	16	cells	=	16.00 %
<<<	74	6	cells	=	6.00 %
(((	75	5	cells	=	5.00 %

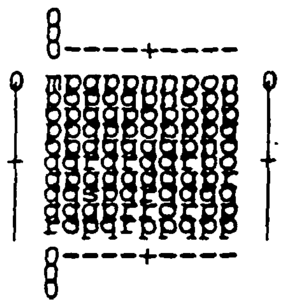

IDRISI image : 67002dnw

mmm	32	1	cells	=	1.00	%
nnn	33	5	cells	=	5.00	%
ooo	34	12	cells	=	12.00	%
ppp	35	36	cells	=	36.00	%
qqq	36	35	cells	=	35.00	%
rrr	37	10	cells	=	10.00	%
sss	38	1	cells	=	1.00	%

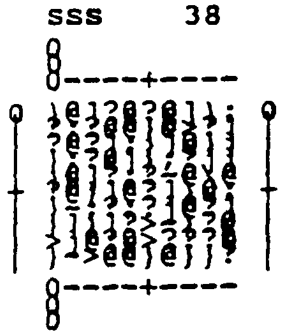

IDRISI image : 70002dnw

\\\	76	1	cells	=	1.00	%
>>>	77	5	cells	=	5.00	%
)))	78	18	cells	=	18.00	%
???	79	23	cells	=	23.00	%
]]]	80	17	cells	=	17.00	%
@@@	81	23	cells	=	23.00	%
;;;	82	9	cells	=	9.00	%
~~	83	4	cells	=	4.00	%

```
0
0
0----+----
 deddecbede
 dedbfecddf
 eeedeeeece
 fdddecbecd
 eeeceeeeee
 ddeceecdde
 dcddbcdede
 cbddeddfde
 efeccccede
 ceeceeeece
0----+----
0
0
```

IDRISI image : 67004dnw

bbb	21	5	cells	=	5.00	%
ccc	22	18	cells	=	18.00	%
ddd	23	27	cells	=	27.00	%
eee	24	44	cells	=	44.00	%
fff	25	6	cells	=	6.00	%

```
0
0
0----+----
 TUUTXUTVTV
 TYVVVRXWTW
 UUUUVTUXTU
 SXSTWTXWTW
 STUSVSTWUU
 UYTUURUVUW
 STWTUUUXUV
 UYUUUSXUUX
 UVYUXYUUTX
 TXTVVTWVUX
0----+----
0
0
```

IDRISI image : 70004dnw

RRR	63	2	cells	=	2.00	%
SSS	64	7	cells	=	7.00	%
TTT	65	20	cells	=	20.00	%
UUU	66	32	cells	=	32.00	%
VVV	67	15	cells	=	15.00	%
WWW	68	9	cells	=	9.00	%
XXX	69	12	cells	=	12.00	%
YYY	70	3	cells	=	3.00	%

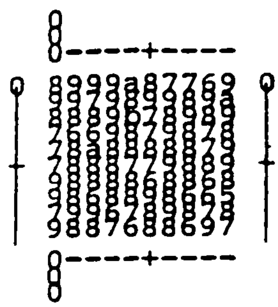

IDRISI image : 67006dnw

555	15	1	cells	=	1.00 %
666	16	11	cells	=	11.00 %
777	17	17	cells	=	17.00 %
888	18	41	cells	=	41.00 %
999	19	26	cells	=	26.00 %
aaa	20	3	cells	=	3.00 %
bbb	21	1	cells	=	1.00 %

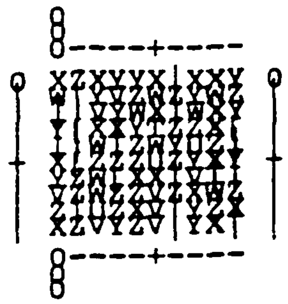

IDRISI image : 70006dnw

TTT	65	1	cells	=	1.00	%
UUU	66	3	cells	=	3.00	%
VVV	67	8	cells	=	8.00	%
WWW	68	10	cells	=	10.00	%
XXX	69	19	cells	=	19.00	%
YYY	70	16	cells	=	16.00	%
ZZZ	71	23	cells	=	23.00	%
|||	72	16	cells	=	16.00	%
[[[	73	4	cells	=	4.00	%

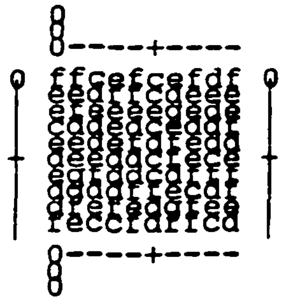

IDRISI image : 67007dnw

ccc	22	12	cells	=	12.00 %
ddd	23	27	cells	=	27.00 %
eee	24	31	cells	=	31.00 %
fff	25	26	cells	=	26.00 %
ggg	26	4	cells	=	4.00 %

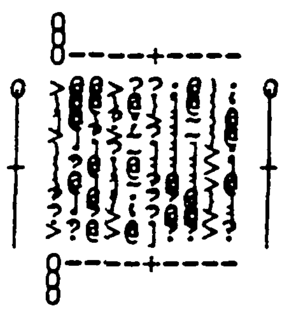

IDRISI image : 70007dnw

>>>	77	13	cells	=	13.00 %
})}	78	14	cells	=	14.00 %
???	79	18	cells	=	18.00 %
]]]	80	20	cells	=	20.00 %
@@@	81	21	cells	=	21.00 %
;;;	82	9	cells	=	9.00 %
~~	83	5	cells	=	5.00 %

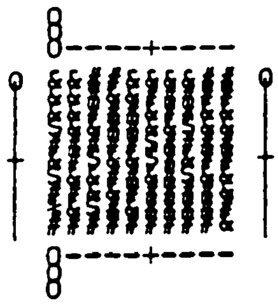

IDRISI image : 67008dnw

%%%	6	1	cells	=	1.00 %
&&&	7	36	cells	=	36.00 %
###	8	55	cells	=	55.00 %
$$$	9	8	cells	=	8.00 %

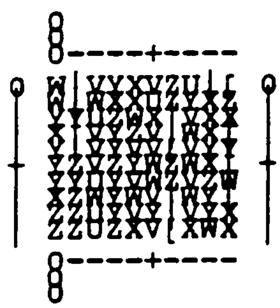

IDRISI image : 70008dnw

UUU	66	6	cells	=	6.00 %
VVV	67	16	cells	=	16.00 %
WWW	68	13	cells	=	13.00 %
XXX	69	15	cells	=	15.00 %
YYY	70	19	cells	=	19.00 %
ZZZ	71	16	cells	=	16.00 %
|||	72	12	cells	=	12.00 %
[[[	73	3	cells	=	3.00 %

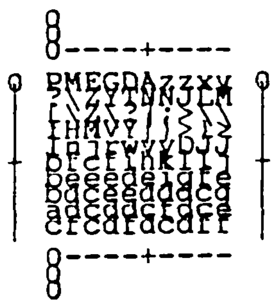

IDRISI image : 67009dnw

aaa	20	1	cells	=	1.00	%
bbb	21	3	cells	=	3.00	%
ccc	22	9	cells	=	9.00	%
ddd	23	12	cells	=	12.00	%
eee	24	8	cells	=	8.00	%
fff	25	8	cells	=	8.00	%
ggg	26	2	cells	=	2.00	%
hhh	27	1	cells	=	1.00	%
iii	28	2	cells	=	2.00	%
jjj	29	2	cells	=	2.00	%
kkk	30	1	cells	=	1.00	%
lll	31	3	cells	=	3.00	%
nnn	33	1	cells	=	1.00	%
rrr	37	1	cells	=	1.00	%
vvv	41	1	cells	=	1.00	%
www	42	1	cells	=	1.00	%
xxx	43	1	cells	=	1.00	%
yyy	44	2	cells	=	2.00	%
zzz	45	2	cells	=	2.00	%
AAA	46	1	cells	=	1.00	%
DDD	49	2	cells	=	2.00	%
EEE	50	1	cells	=	1.00	%
GGG	52	1	cells	=	1.00	%
HHH	53	1	cells	=	1.00	%
III	54	1	cells	=	1.00	%
JJJ	55	3	cells	=	3.00	%
LLL	57	1	cells	=	1.00	%
MMM	58	3	cells	=	3.00	%
NNN	59	2	cells	=	2.00	%
PPP	61	1	cells	=	1.00	%
TTT	65	1	cells	=	1.00	%
VVV	67	1	cells	=	1.00	%

IDRISI image : 67009dnw continued.

YYY	70	2	cells	=	2.00 %
ZZZ	71	2	cells	=	2.00 %
|||	72	1	cells	=	1.00 %
[[[	73	1	cells	=	1.00 %
\\\	76	5	cells	=	5.00 %
>>>	77	3	cells	=	3.00 %
)))	78	2	cells	=	2.00 %
???	79	2	cells	=	2.00 %
]]]	80	1	cells	=	1.00 %
;;;	82	1	cells	=	1.00 %

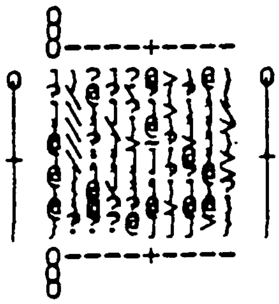

IDRISI image : 70009dnw

(((	75	3	cells	=	3.00 %
\\\	76	9	cells	=	9.00 %
>>>	77	9	cells	=	9.00 %
)))	78	23	cells	=	23.00 %
???	79	17	cells	=	17.00 %
]]]	80	21	cells	=	21.00 %
@@@	81	15	cells	=	15.00 %
;;;	82	2	cells	=	2.00 %
~~	83	1	cells	=	1.00 %

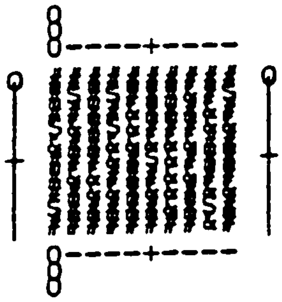

IDRISI image : 67011dnw

&&&	7	27	cells	=	27.00 %
###	8	65	cells	=	65.00 %
$$$	9	8	cells	=	8.00 %

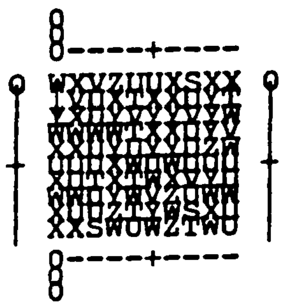

IDRISI image : 70011dnw

SSS	64	3	cells	=	3.00 %
TTT	65	7	cells	=	7.00 %
UUU	66	25	cells	=	25.00 %
VVV	67	7	cells	=	7.00 %
WWW	68	19	cells	=	19.00 %
XXX	69	20	cells	=	20.00 %
YYY	70	13	cells	=	13.00 %
ZZZ	71	5	cells	=	5.00 %
|||	72	1	cells	=	1.00 %

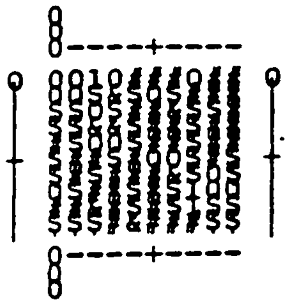

IDRISI image : 67013dnw

&&&	7	7	cells	=	7.00 %
###	8	39	cells	=	39.00 %
$$$	9	35	cells	=	35.00 %
000	10	16	cells	=	16.00 %
111	11	3	cells	=	3.00 %

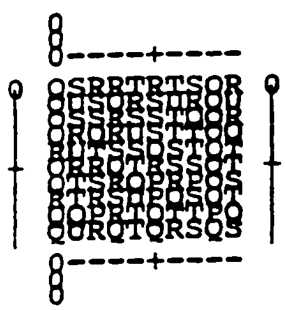

IDRISI image : 70013dnw

OOO	60	5	cells	=	5.00 %
PPP	61	5	cells	=	5.00 %
QQQ	62	25	cells	=	25.00 %
RRR	63	21	cells	=	21.00 %
SSS	64	20	cells	=	20.00 %
TTT	65	17	cells	=	17.00 %
UUU	66	7	cells	=	7.00 %

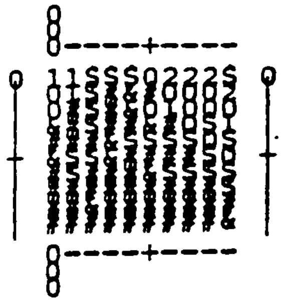

IDRISI image : 67016dnw

&&&	7	10	cells	=	10.00 %
###	8	46	cells	=	46.00 %
$$$	9	22	cells	=	22.00 %
000	10	13	cells	=	13.00 %
111	11	5	cells	=	5.00 %
222	12	4	cells	=	4.00 %

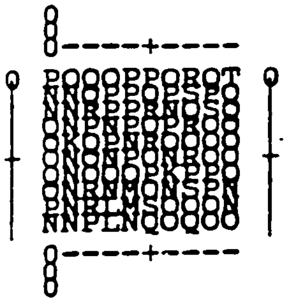

IDRISI image : 70016dnw

KKK	56	2	cells	=	2.00 %
LLL	57	2	cells	=	2.00 %
MMM	58	2	cells	=	2.00 %
NNN	59	21	cells	=	21.00 %
OOO	60	27	cells	=	27.00 %
PPP	61	20	cells	=	20.00 %
QQQ	62	13	cells	=	13.00 %
RRR	63	8	cells	=	8.00 %
SSS	64	4	cells	=	4.00 %
TTT	65	1	cells	=	1.00 %

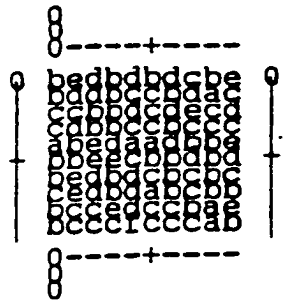

IDRISI image : 67018dnw

aaa	20	7	cells	=	7.00 %
bbb	21	32	cells	=	32.00 %
ccc	22	30	cells	=	30.00 %
ddd	23	19	cells	=	19.00 %
eee	24	11	cells	=	11.00 %
fff	25	1	cells	=	1.00 %

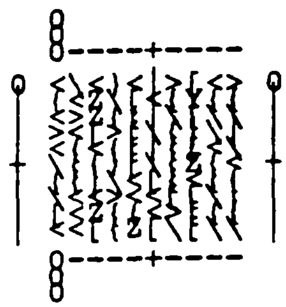

IDRISI image : 70018dnw

YYY	70	1	cells	=	1.00 %
ZZZ	71	5	cells	=	5.00 %
|||	72	7	cells	=	7.00 %
[[[	73	16	cells	=	16.00 %
<<<	74	22	cells	=	22.00 %
(((	75	24	cells	=	24.00 %
\\\	76	16	cells	=	16.00 %
>>>	77	7	cells	=	7.00 %
)))	78	2	cells	=	2.00 %

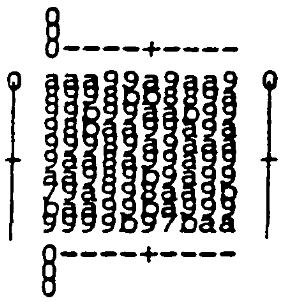

IDRISI image : 67019dnw

777	17	2	cells	=	2.00	%
888	18	9	cells	=	9.00	%
999	19	46	cells	=	46.00	%
aaa	20	32	cells	=	32.00	%
bbb	21	11	cells	=	11.00	%

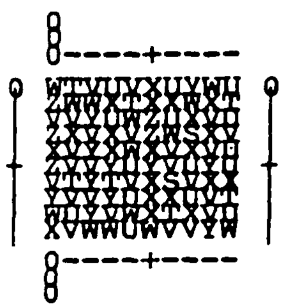

IDRISI image : 70019dnw

SSS	64	2	cells	=	2.00	%
TTT	65	7	cells	=	7.00	%
UUU	66	15	cells	=	15.00	%
VVV	67	25	cells	=	25.00	%
WWW	68	14	cells	=	14.00	%
XXX	69	21	cells	=	21.00	%
YYY	70	11	cells	=	11.00	%
ZZZ	71	5	cells	=	5.00	%

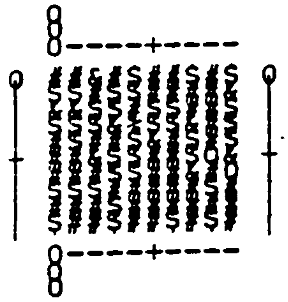

IDRISI image : 67020dnw

%%%	6	1	cells	=	1.00 %
&&&	7	10	cells	=	10.00 %
###	8	51	cells	=	51.00 %
$$$	9	36	cells	=	36.00 %
000	10	2	cells	=	2.00 %

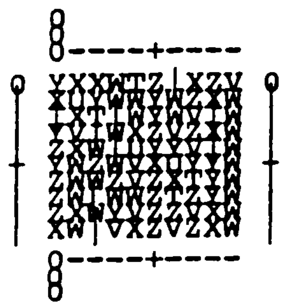

IDRISI image : 70020dnw

TTT	65	4	cells	=	4.00 %
UUU	66	3	cells	=	3.00 %
VVV	67	11	cells	=	11.00 %
WWW	68	26	cells	=	26.00 %
XXX	69	16	cells	=	16.00 %
YYY	70	13	cells	=	13.00 %
ZZZ	71	18	cells	=	18.00 %
|||	72	8	cells	=	8.00 %
[[[	73	1	cells	=	1.00 %

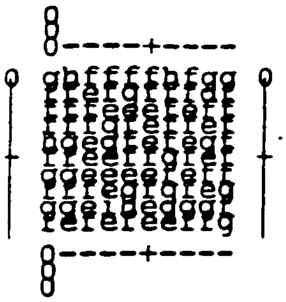

IDRISI image : 67021dnw

ddd	23	1	cells	=	1.00 %
eee	24	26	cells	=	26.00 %
fff	25	48	cells	=	48.00 %
ggg	26	20	cells	=	20.00 %
hhh	27	4	cells	=	4.00 %
iii	28	1	cells	=	1.00 %

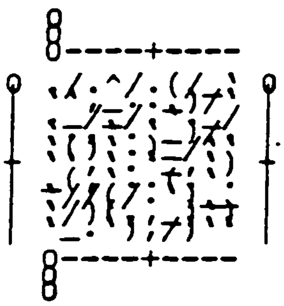

IDRISI image : 70021dnw

^^^	84	1	cells	=	1.00 %
(((	85	6	cells	=	6.00 %
___	86	14	cells	=	14.00 %
\\\	87	27	cells	=	27.00 %
///	88	14	cells	=	14.00 %
...	89	19	cells	=	19.00 %
)))	90	11	cells	=	11.00 %
,,,	91	8	cells	=	8.00 %

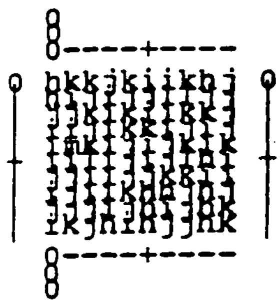

IDRISI image : 67022dnw

hhh	27	12	cells	=	12.00 %
iii	28	32	cells	=	32.00 %
jjj	29	32	cells	=	32.00 %
kkk	30	19	cells	=	19.00 %
lll	31	4	cells	=	4.00 %
mmm	32	1	cells	=	1.00 %

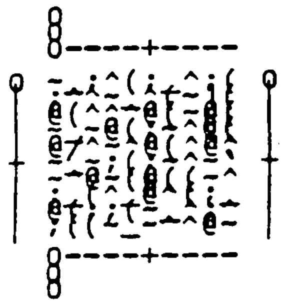

IDRISI image : 70022dnw

]]]	80	1	cells	=	1.00	%
@@@	81	13	cells	=	13.00	%
;;;	82	13	cells	=	13.00	%
~~	83	19	cells	=	19.00	%
^^^	84	22	cells	=	22.00	%
(((	85	20	cells	=	20.00	%
___	86	10	cells	=	10.00	%
\\\	87	1	cells	=	1.00	%
///	88	1	cells	=	1.00	%

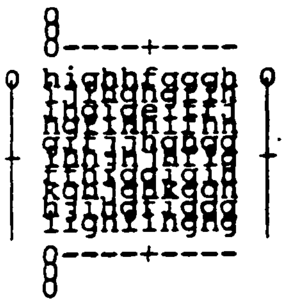

IDRISI image : 67023dnw

eee	24	1	cells	=	1.00 %
fff	25	11	cells	=	11.00 %
ggg	26	28	cells	=	28.00 %
hhh	27	29	cells	=	29.00 %
iii	28	21	cells	=	21.00 %
jjj	29	8	cells	=	8.00 %
kkk	30	2	cells	=	2.00 %

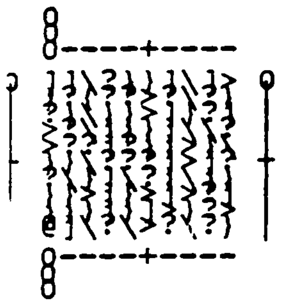

IDRISI image : 70023dnw

(((	75	1	cells	=	1.00 %
\\\	76	15	cells	=	15.00 %
>>>	77	13	cells	=	13.00 %
)))	78	28	cells	=	28.00 %
???	79	24	cells	=	24.00 %
]]]	80	18	cells	=	18.00 %
@@@	81	1	cells	=	1.00 %

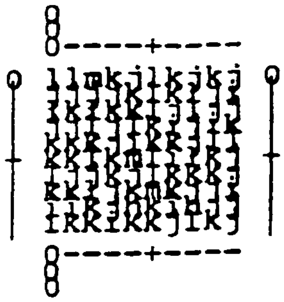

IDRISI image : 67026dnw

hhh	27	2	cells	=	2.00 %
iii	28	11	cells	=	11.00 %
jjj	29	30	cells	=	30.00 %
kkk	30	34	cells	=	34.00 %
lll	31	20	cells	=	20.00 %
mmm	32	3	cells	=	3.00 %

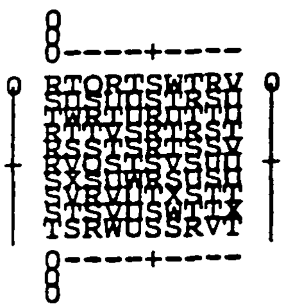

IDRISI image : 70026dnw

QQQ	62	2	cells	=	2.00 %
RRR	63	16	cells	=	16.00 %
SSS	64	27	cells	=	27.00 %
TTT	65	23	cells	=	23.00 %
UUU	66	15	cells	=	15.00 %
VVV	67	9	cells	=	9.00 %
WWW	68	5	cells	=	5.00 %
XXX	69	3	cells	=	3.00 %

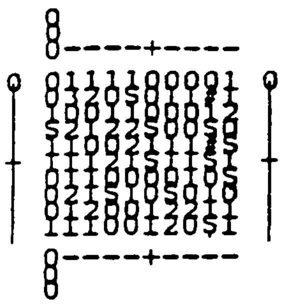

IDRISI image : 67027dnw

###	8	2	cells	=	2.00 %
$$$	9	11	cells	=	11.00 %
000	10	34	cells	=	34.00 %
111	11	40	cells	=	40.00 %
222	12	12	cells	=	12.00 %
333	13	1	cells	=	1.00 %

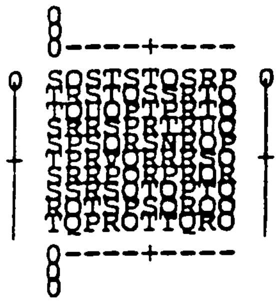

IDRISI image : 70027dnw

NNN	59	1	cells	=	1.00	%
OOO	60	7	cells	=	7.00	%
PPP	61	12	cells	=	12.00	%
QQQ	62	18	cells	=	18.00	%
RRR	63	24	cells	=	24.00	%
SSS	64	19	cells	=	19.00	%
TTT	65	16	cells	=	16.00	%
UUU	66	2	cells	=	2.00	%
VVV	67	1	cells	=	1.00	%

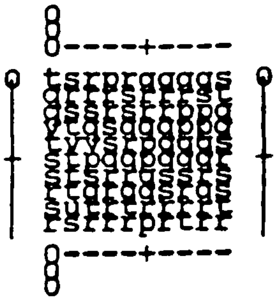

IDRISI image : 67029dnw

ppp	35	9	cells	=	9.00 %
qqq	36	25	cells	=	25.00 %
rrr	37	31	cells	=	31.00 %
sss	38	20	cells	=	20.00 %
ttt	39	11	cells	=	11.00 %
uuu	40	1	cells	=	1.00 %
vvv	41	3	cells	=	3.00 %

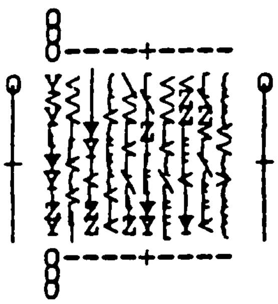

IDRISI image : 70029dnw

YYY	70	10	cells	=	10.00 %
ZZZ	71	8	cells	=	8.00 %
|||	72	15	cells	=	15.00 %
[[[	73	22	cells	=	22.00 %
<<<	74	23	cells	=	23.00 %
{{{	75	15	cells	=	15.00 %
\\\	76	6	cells	=	6.00 %
>>>	77	1	cells	=	1.00 %

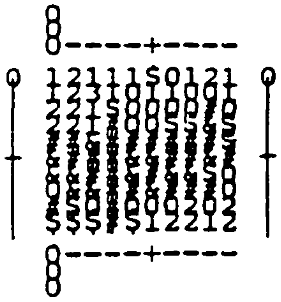

IDRISI image : 67030dnw

&&&	7	14	cells	=	14.00 %
###	8	27	cells	=	27.00 %
$$$	9	12	cells	=	12.00 %
000	10	19	cells	=	19.00 %
111	11	15	cells	=	15.00 %
222	12	12	cells	=	12.00 %
333	13	1	cells	=	1.00 %

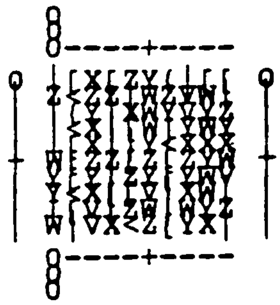

IDRISI image : 70030dnw

VVV	67	6	cells	=	6.00	%
WWW	68	12	cells	=	12.00	%
XXX	69	11	cells	=	11.00	%
YYY	70	15	cells	=	14.00	%
ZZZ	71	14	cells	=	14.00	%
|||	72	20	cells	=	20.00	%
[[[	73	15	cells	=	15.00	%
<<<	74	5	cells	=	5.00	%
{{{	75	2	cells	=	2.00	%

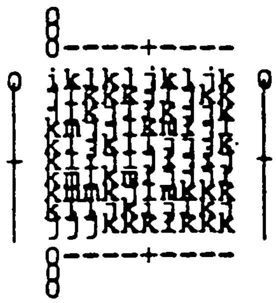

IDRISI image : 67031dnw

iii	28	5	cells	=	5.00 %
jjj	29	30	cells	=	30.00 %
kkk	30	34	cells	=	34.00 %
lll	31	24	cells	=	24.00 %
mmm	32	7	cells	=	7.00 %

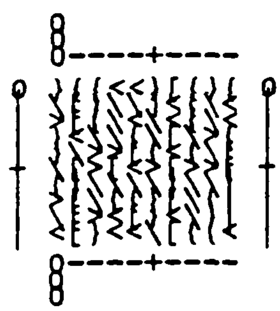

IDRISI image : 70031dnw

|||	72	5	cells	=	5.00 %
[[[	73	16	cells	=	16.00 %
<<<	74	16	cells	=	16.00 %
(((	75	17	cells	=	17.00 %
\\\	76	25	cells	=	25.00 %
>>>	77	10	cells	=	10.00 %
)))	78	10	cells	=	10.00 %
]]]	80	1	cells	=	1.00 %

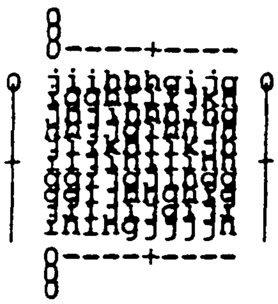

IDRISI image : 67032dnw

fff	25	1	cells	=	1.00	%
ggg	26	17	cells	=	17.00	%
hhh	27	27	cells	=	27.00	%
iii	28	30	cells	=	30.00	%
jjj	29	22	cells	=	22.00	%
kkk	30	3	cells	=	3.00	%

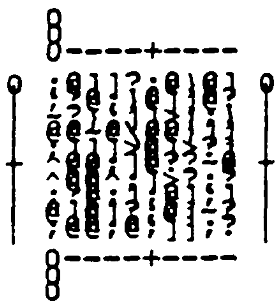

IDRISI image : 70032dnw

\\\	76	1	cells	=	1.00	%
>>>	77	4	cells	=	4.00	%
}}}	78	6	cells	=	6.00	%
???	79	13	cells	=	13.00	%
]]]	80	24	cells	=	24.00	%
@@@	81	26	cells	=	26.00	%
;;;	82	19	cells	=	19.00	%
~~	83	4	cells	=	4.00	%
^^^	84	3	cells	=	3.00	%

```
  0
  0
  0----+----
0 6555777666 0
| 2987677787 |
| 5377677676 |
| 5677698668 |
| 6678877698 |
+ 5665778977 +
| 5776762776 |
| 4767767656 |
| 5555887667 |
| 4767668689 |
  0----+----
  0
  0
```

IDRISI image : 67033dnw

333	13	1	cells	=	1.00 %
444	14	2	cells	=	2.00 %
555	15	13	cells	=	13.00 %
666	16	34	cells	=	34.00 %
777	17	37	cells	=	37.00 %
888	18	11	cells	=	11.00 %
999	19	2	cells	=	2.00 %

```
  0
  0
  0----+----
0 UWVUZTUYSX 0
| [illegible] |
| [illegible] |
| [illegible] |
| [illegible] |
+ [illegible] +
| [illegible] |
| [illegible] |
| [illegible] |
| WWSWWTUTVW |
  0----+----
  0
  0
```

IDRISI image : 70033dnw

SSS	64	4	cells	=	4.00 %
TTT	65	11	cells	=	11.00 %
UUU	66	24	cells	=	24.00 %
VVV	67	18	cells	=	18.00 %
WWW	68	20	cells	=	20.00 %
XXX	69	15	cells	=	15.00 %
YYY	70	7	cells	=	7.00 %
ZZZ	71	1	cells	=	1.00 %

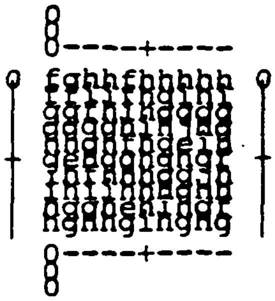

IDRISI image : 67034dnw

eee	24	3	cells	=	3.00 %
fff	25	10	cells	=	10.00 %
ggg	26	30	cells	=	30.00 %
hhh	27	42	cells	=	42.00 %
iii	28	13	cells	=	13.00 %
jjj	29	2	cells	=	2.00 %

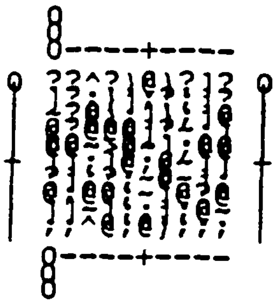

IDRISI image : 70034dnw

>>>	77	1	cells	=	1.00 %
)))	78	6	cells	=	6.00 %
???	79	14	cells	=	14.00 %
]]]	80	21	cells	=	21.00 %
@@@	81	23	cells	=	23.00 %
;;;	82	23	cells	=	23.00 %
~~	83	10	cells	=	10.00 %
^^^	84	2	cells	=	2.00 %

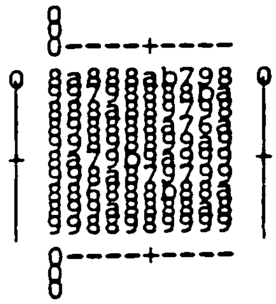

IDRISI image : 67036dnw

666	16	2	cells	=	2.00 %
777	17	7	cells	=	7.00 %
888	18	42	cells	=	42.00 %
999	19	32	cells	=	32.00 %
aaa	20	13	cells	=	13.00 %
bbb	21	4	cells	=	4.00 %

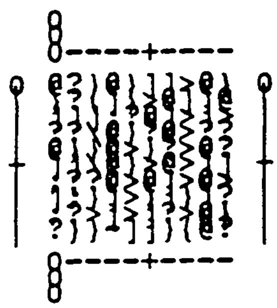

IDRISI image : 70036dnw

{{{	75	2	cells	=	2.00 %
\\\	76	2	cells	=	2.00 %
>>>	77	16	cells	=	16.00 %
}}}	78	17	cells	=	17.00 %
???	79	17	cells	=	17.00 %
]]]	80	23	cells	=	23.00 %
@@@	81	18	cells	=	18.00 %
;;;	82	4	cells	=	4.00 %
~~	83	1	cells	=	1.00 %

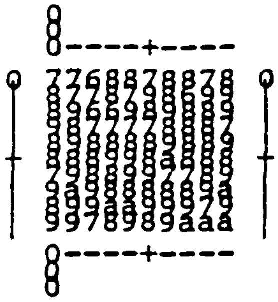

IDRISI image : 67038dnw

666	16	4	cells	=	4.00 %
777	17	17	cells	=	17.00 %
888	18	41	cells	=	41.00 %
999	19	30	cells	=	30.00 %
aaa	20	8	cells	=	8.00 %

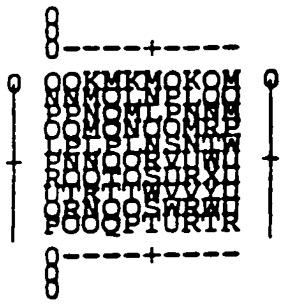

IDRISI image : 70038dnw

KKK	56	3	cells	=	3.00 %
LLL	57	6	cells	=	6.00 %
MMM	58	8	cells	=	8.00 %
NNN	59	12	cells	=	12.00 %
OOO	60	14	cells	=	14.00 %
PPP	61	10	cells	=	10.00 %
QQQ	62	10	cells	=	10.00 %
RRR	63	9	cells	=	9.00 %
SSS	64	3	cells	=	3.00 %
TTT	65	7	cells	=	7.00 %
UUU	66	8	cells	=	8.00 %
VVV	67	3	cells	=	3.00 %
WWW	68	5	cells	=	5.00 %
XXX	69	1	cells	=	1.00 %
YYY	70	1	cells	=	1.00 %

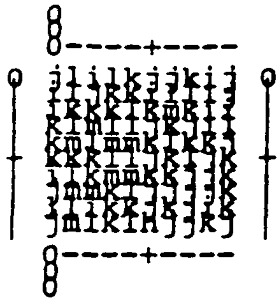

IDRISI image : 67041dnw

hhh	27	1	cells	=	1.00 %
iii	28	12	cells	=	12.00 %
jjj	29	24	cells	=	24.00 %
kkk	30	32	cells	=	32.00 %
lll	31	21	cells	=	21.00 %
mmm	32	10	cells	=	10.00 %

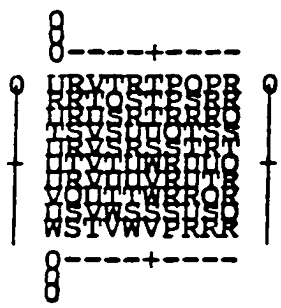

IDRISI image : 70041dnw

PPP	61	4	cells	=	4.00 %
QQQ	62	8	cells	=	8.00 %
RRR	63	25	cells	=	25.00 %
SSS	64	16	cells	=	16.00 %
TTT	65	15	cells	=	15.00 %
UUU	66	17	cells	=	17.00 %
VVV	67	10	cells	=	10.00 %
WWW	68	5	cells	=	5.00 %

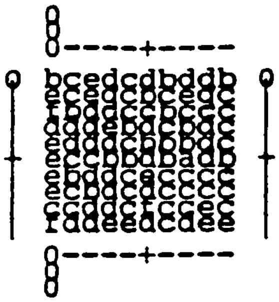

IDRISI image : 67042dnw

aaa	20	1	cells	=	1.00 %
bbb	21	17	cells	=	17.00 %
ccc	22	35	cells	=	35.00 %
ddd	23	27	cells	=	27.00 %
eee	24	15	cells	=	15.00 %
fff	25	3	cells	=	3.00 %
ggg	26	2	cells	=	2.00 %

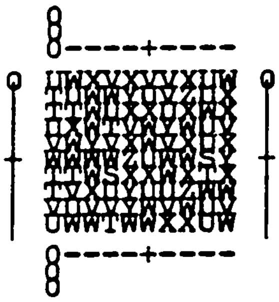

IDRISI image : 70042dnw

SSS	64	2	cells	=	2.00 %
TTT	65	9	cells	=	9.00 %
UUU	66	18	cells	=	18.00 %
VVV	67	15	cells	=	15.00 %
WWW	68	28	cells	=	28.00 %
XXX	69	19	cells	=	19.00 %
YYY	70	6	cells	=	6.00 %
ZZZ	71	3	cells	=	3.00 %

```
  0
  0
  0----+----
0 5455685664 0
| 5556665552 |
| 3526685654 |
| 6654576533 |
| 6666656654 |
+ 6478545653 +
| 8765786772 |
| 6677666676 |
| 9766667826 |
| 6559755555 |
  0----+----
  0
  0
```

IDRISI image : 67043dnw

222	12	1	cells	=	1.00 %
333	13	4	cells	=	4.00 %
444	14	7	cells	=	7.00 %
555	15	28	cells	=	28.00 %
666	16	37	cells	=	37.00 %
777	17	15	cells	=	15.00 %
888	18	6	cells	=	6.00 %
999	19	2	cells	=	2.00 %

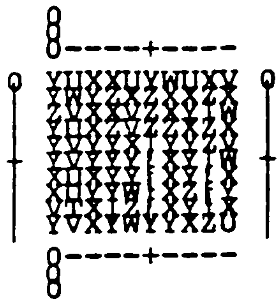

IDRISI image : 70043dnw

TTT	65	1	cells	=	1.00 %
UUU	66	7	cells	=	7.00 %
VVV	67	9	cells	=	9.00 %
WWW	68	6	cells	=	6.00 %
XXX	69	26	cells	=	26.00 %
YYY	70	27	cells	=	27.00 %
ZZZ	71	13	cells	=	13.00 %
|||	72	6	cells	=	6.00 %
[[[	73	5	cells	=	5.00 %

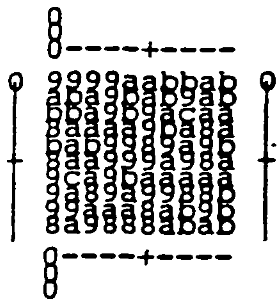

IDRISI image : 67045dnw

888	18	13	cells	=	13.00 %
999	19	27	cells	=	27.00 %
aaa	20	38	cells	=	38.00 %
bbb	21	20	cells	=	20.00 %
ccc	22	2	cells	=	2.00 %

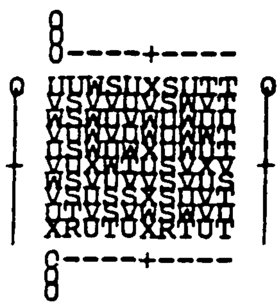

IDRISI image : 70045dnw

RRR	63	2	cells	=	2.00 %
SSS	64	16	cells	=	16.00 %
TTT	65	11	cells	=	11.00 %
UUU	66	27	cells	=	27.00 %
VVV	67	20	cells	=	20.00 %
WWW	68	17	cells	=	17.00 %
XXX	69	7	cells	=	7.00 %

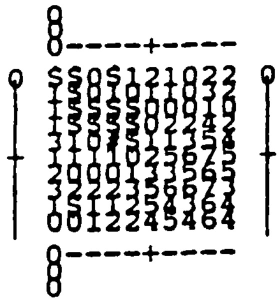

IDRISI image : 67046dnw

###	8	1	cells	=	1.00	%
$$$	9	14	cells	=	14.00	%
000	10	17	cells	=	17.00	%
111	11	21	cells	=	21.00	%
222	12	15	cells	=	15.00	%
333	13	9	cells	=	9.00	%
444	14	7	cells	=	7.00	%
555	15	8	cells	=	8.00	%
666	16	6	cells	=	6.00	%
777	17	2	cells	=	2.00	%

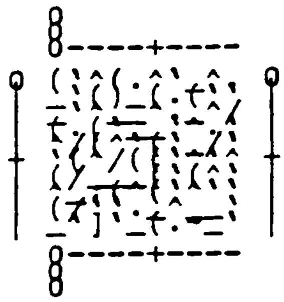

IDRISI image : 70046dnw

]]]	80	1	cells	=	1.00	%
;;;	82	1	cells	=	1.00	%
~~	83	1	cells	=	1.00	%
^^^	84	17	cells	=	17.00	%
(((	85	19	cells	=	19.00	%
___	86	20	cells	=	20.00	%
\\\	87	26	cells	=	26.00	%
///	88	6	cells	=	6.00	%
...	89	8	cells	=	8.00	%
)))	90	1	cells	=	1.00	%

```
   0
   0
   0----+----
0  9766775687  0
|  7565585576  |
|  7545467554  |
|  7529866655  |
|  7725475565  |
+  5555896655  +
|  8557675453  |
|  9768866767  |
|  7575475355  |
|  6875685676  |
   0----+----
   0
   0
```

IDRISI image : 67049dnw

333	13	2	cells	=	2.00 %
444	14	6	cells	=	6.00 %
555	15	34	cells	=	34.00 %
666	16	21	cells	=	21.00 %
777	17	24	cells	=	24.00 %
888	18	9	cells	=	9.00 %
999	19	4	cells	=	4.00 %

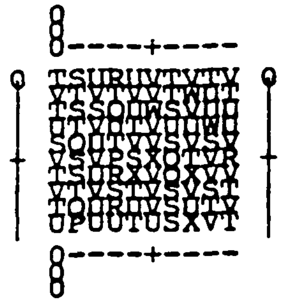

IDRISI image : 70049dnw

PPP	61	2	cells	=	2.00 %
QQQ	62	5	cells	=	5.00 %
RRR	63	4	cells	=	4.00 %
SSS	64	15	cells	=	15.00 %
TTT	65	20	cells	=	20.00 %
UUU	66	20	cells	=	20.00 %
VVV	67	27	cells	=	27.00 %
WWW	68	3	cells	=	3.00 %
XXX	69	4	cells	=	4.00 %

```
  0
  0
  0----+----
0 9a9aba9898 0
| 89bba9a889 |
| 899ba89889 |
| ab9ba8889a |
| aba9b889a8 |
+ 8a9998b89b +
| aa8ba9baa9 |
| 899aa999aa |
| 9a9a99aaba |
| 8999a9999a |
  0----+----
  0
  0
```

IDRISI image : 67050dnw

888	18	17	cells	=	17.00 %
999	19	38	cells	=	38.00 %
aaa	20	31	cells	=	31.00 %
bbb	21	14	cells	=	14.00 %

```
  0
  0
  0----+----
0 SSSUSSSQTR 0
| USPUTTWQUR |
| STSTRTVTUR |
| STSUTWYUWS |
| WUSWVZXUUR |
+ TTRTTUVSSQ +
| VSSUQTTTWS |
| TTSTRSTPSU |
| WUUUSUSRUR |
| SSQTSTUSUQ |
  0----+----
  0
  0
```

IDRISI image : 70050dnw

PPP	61	2	cells	=	2.00 %
QQQ	62	6	cells	=	6.00 %
RRR	63	9	cells	=	9.00 %
SSS	64	27	cells	=	27.00 %
TTT	65	23	cells	=	23.00 %
UUU	66	20	cells	=	20.00 %
VVV	67	4	cells	=	4.00 %
WWW	68	6	cells	=	6.00 %
XXX	69	1	cells	=	1.00 %
YYY	70	1	cells	=	1.00 %
ZZZ	71	1	cells	=	1.00 %

APPENDIX B

Digital Number, Radiance, and Reflectance Data

Appendix B1
Original Data

Reservoir	Chlorophyll (mg/m3)	Digital Counts 670 nm	Digital Counts 700 nm	Digital Counts 700-670 nm	Radiance (uW/cm2/sr) 670 nm	Radiance (uW/cm2/sr) 700 nm	Radiance (uW/cm2/sr) 700-670 nm	Irradiance (W/m2)	Reflectance 670 nm	Reflectance 700 nm	Reflectance 700-670 nm
1L	4.09	35.61	71.84	36.23	6.77	7.69	0.92	584.11	1.22E-02	1.70E-02	4.80E-03
1S	4.15	34.00	71.36	37.36	6.66	7.62	0.96	567.46	1.24E-02	1.73E-02	4.98E-03
2	5.24	35.33	79.75	44.42	6.75	8.91	2.16	611.40	1.16E-02	1.88E-02	7.19E-03
4	3.99	23.28	66.41	43.13	5.92	6.86	0.94	298.51	2.09E-02	2.97E-02	8.79E-03
6	24.52	17.93	69.87	51.94	5.55	7.39	1.84	238.00	2.46E-02	4.01E-02	1.55E-02
7	69.51	23.83	79.69	55.86	5.95	8.90	2.95	252.00	2.49E-02	4.56E-02	2.07E-02
8	8.22	7.70	69.36	61.66	4.84	7.31	2.47	727.20	7.01E-03	1.30E-02	5.97E-03
9	77.75	42.13	78.81	36.68	4.84	8.77	3.93	727.20	7.01E-03	1.56E-02	8.57E-03
11	8.12	7.81	67.75	59.94	4.85	7.06	2.21	729.40	7.00E-03	1.25E-02	5.50E-03
13	17.46	8.69	63.25	54.56	4.91	6.37	1.46	863.67	5.99E-03	9.52E-03	3.54E-03
16	1.57	8.69	60.52	51.83	4.91	5.95	1.04	802.33	6.44E-03	9.58E-03	3.13E-03
18	68.78	21.98	74.36	52.38	5.83	8.08	2.25	693.53	8.85E-03	1.50E-02	6.19E-03
19	11.91	19.41	67.74	48.33	5.65	7.06	1.41	282.00	2.11E-02	3.23E-02	1.12E-02
20	5.65	8.28	69.04	60.76	4.88	7.26	2.38	780.55	6.58E-03	1.20E-02	5.43E-03
21	206.28	25.03	87.88	62.85	6.04	10.16	4.12	490.80	1.30E-02	2.67E-02	1.38E-02
22	179.26	28.74	83.59	54.85	6.29	9.50	3.21	434.60	1.52E-02	2.82E-02	1.30E-02
23	56.66	26.90	78.17	51.27	6.17	8.67	2.5	768.00	8.46E-03	1.46E-02	6.12E-03
26	20.43	29.68	64.95	35.27	6.36	6.63	0.27	378.11	1.77E-02	2.26E-02	4.93E-03
27	3.78	10.52	62.94	52.42	5.04	6.32	1.28	427.00	1.24E-02	1.91E-02	6.68E-03
29	1.91	37.14	73.14	36.00	6.87	7.89	1.02	848.00	8.53E-03	1.20E-02	3.48E-03
30	7	9.34	70.76	61.42	4.95	7.53	2.58	838.28	6.22E-03	1.16E-02	5.38E-03
31	47.57	29.98	75.17	45.19	6.38	8.21	1.83	432.00	1.55E-02	2.45E-02	8.99E-03
32	116.99	27.64	80.47	52.83	6.22	9.02	2.8	296.41	2.21E-02	3.93E-02	1.72E-02
33	19.39	16.45	67.17	50.72	5.44	6.97	1.53	770.00	7.44E-03	1.17E-02	4.25E-03
34	53.11	26.58	80.78	54.20	6.14	9.07	2.93	412.73	1.57E-02	2.84E-02	1.27E-02
36	193.23	18.59	79.12	60.53	5.59	8.81	3.22	740.00	7.95E-03	1.54E-02	7.42E-03
38	1.97	18.21	61.74	43.53	5.57	6.14	0.57	808.00	7.26E-03	9.81E-03	2.55E-03
41	1.18	29.90	64.46	34.56	6.37	6.56	0.19	715.00	9.38E-03	1.18E-02	2.47E-03
42	32.08	22.55	67.54	44.99	5.87	7.03	1.16	440.00	1.40E-02	2.06E-02	6.59E-03
43	158.41	15.75	69.42	53.67	5.40	7.32	1.92	729.55	7.79E-03	1.30E-02	5.16E-03
45	9.05	19.71	66.26	46.55	5.67	6.83	1.16	304.33	1.96E-02	2.90E-02	9.36E-03
46	70.7	11.80	86.00	74.20	5.12	9.87	4.75	306.67	1.76E-02	4.16E-02	2.40E-02
49	30.19	16.02	65.53	49.51	5.42	6.72	1.3	444.00	1.29E-02	1.95E-02	6.69E-03
50	19.81	19.42	64.90	45.48	5.65	6.62	0.97	280.00	2.12E-02	3.05E-02	9.28E-03

Appendix B2
Final values used in data analysis

Reservoir	Chlorophyll (mg/m3)	DN 700-670 nm	Radiance 700-670 nm	Reflectance 700-670 nm
1L	4.09	36.23	0.92	0.004797
1S	4.15	37.36	0.96	0.004983
2	5.24	44.42	2.16	0.007194
4	3.99	43.13	0.94	0.008795
6	24.52	51.94	1.84	0.015543
7	69.51	55.86	2.95	0.020745
8	8.22	61.66	2.47	0.005973
9	77.75	36.68	3.93	0.008565
11	8.12	59.94	2.21	0.005498
13	17.46	54.56	1.46	0.003538
16	1.57	51.83	1.04	0.003133
18	68.78	52.38	2.25	0.006193
19	11.91	48.33	1.41	0.011233
20	5.65	60.76	2.38	0.005428
21	206.28	62.85	4.12	0.013774
22	179.26	54.85	3.21	0.012988
23	56.66	51.27	2.5	0.006119
26	20.43	35.27	0.27	0.004933
27	3.78	52.42	1.28	0.006685
29	1.91	36.00	1.02	0.003485
30	7	61.42	2.58	0.005382
31	47.57	45.19	1.83	0.008991
32	116.99	52.83	2.8	0.017201
33	19.39	50.72	1.53	0.00425
34	53.11	54.20	2.93	0.012714
36	193.23	60.53	3.22	0.00742
38	1.97	43.53	0.57	0.002555
41	1.18	34.56	0.19	0.002467
42	32.08	44.99	1.16	0.006585
43	158.41	53.67	1.92	0.005163
45	9.05	46.55	1.16	0.009364
46	70.7	74.20	4.75	0.023981
49	30.19	49.51	1.3	0.006691
50	19.81	45.48	0.97	0.009284

IMAGE EVALUATION TEST TARGET (QA-3)

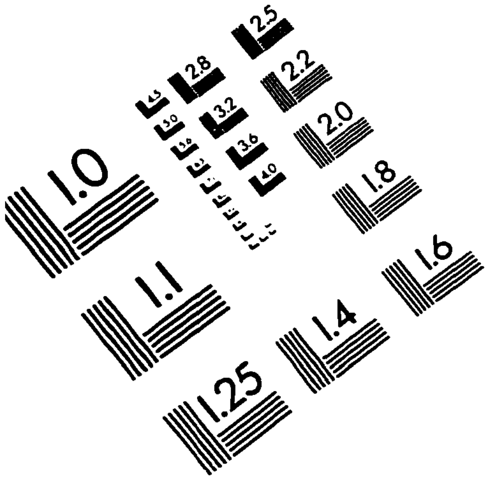

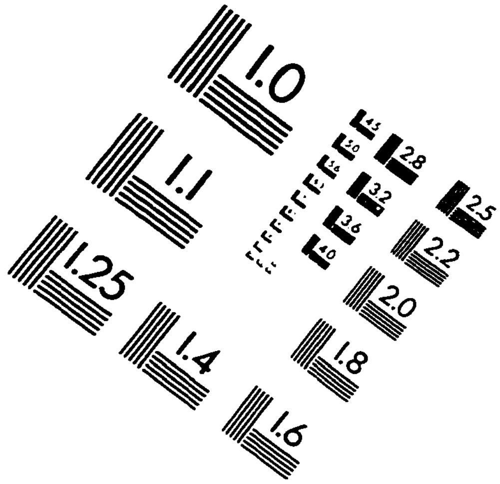

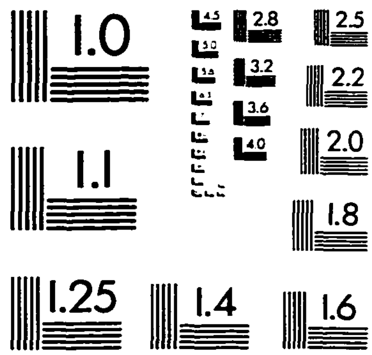

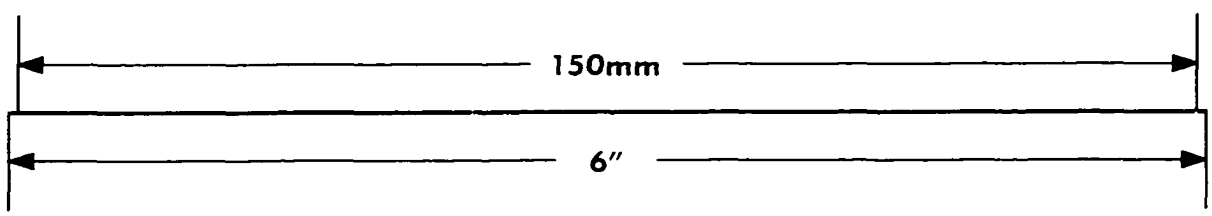

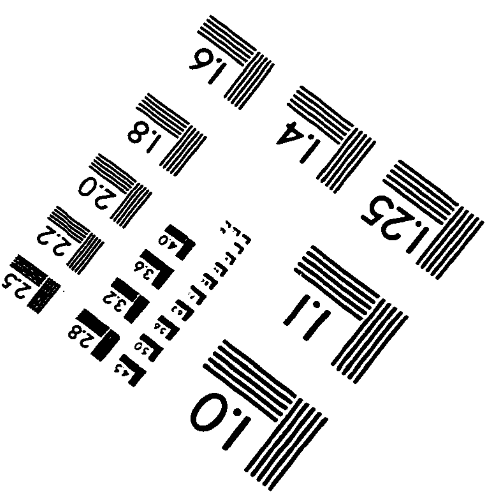

APPLIED IMAGE . Inc
1653 East Main Street
Rochester, NY 14609 USA
Phone: 716/482-0300
Fax: 716/288-5989